

Electronic Thesis and Dissertation Repository

11-26-2020 10:30 AM

Machine Learning Prediction of Shear Capacity of Steel Fiber Reinforced Concrete

Wassim Ben Chaabene, *The Univeristy of Western Ontario*

Supervisor: Moncef L. Nehdi, *The University of Western Ontario*

A thesis submitted in partial fulfillment of the requirements for the Master of Engineering Science degree in Civil and Environmental Engineering

© Wassim Ben Chaabene 2020

Follow this and additional works at: <https://ir.lib.uwo.ca/etd>



Part of the [Civil Engineering Commons](#), [Other Computer Engineering Commons](#), and the [Structural Engineering Commons](#)

Recommended Citation

Ben Chaabene, Wassim, "Machine Learning Prediction of Shear Capacity of Steel Fiber Reinforced Concrete" (2020). *Electronic Thesis and Dissertation Repository*. 7456.
<https://ir.lib.uwo.ca/etd/7456>

This Dissertation/Thesis is brought to you for free and open access by Scholarship@Western. It has been accepted for inclusion in Electronic Thesis and Dissertation Repository by an authorized administrator of Scholarship@Western. For more information, please contact wlsadmin@uwo.ca.

Abstract

The use of steel fibers for concrete reinforcement has been growing in recent years owing to the improved shear strength and post-cracking toughness imparted by fiber inclusion. Yet, there is still lack of design provisions for steel fiber-reinforced concrete (SFRC) in building codes. This is mainly due to the complex shear transfer mechanism in SFRC. Existing empirical equations for SFRC shear strength have been developed with relatively limited data examples, making their accuracy restricted to specific ranges. To overcome this drawback, the present study suggests novel machine learning models based on artificial neural network (ANN) and genetic programming (GP) to predict the shear strength of SFRC beams with great accuracy. Different statistical metrics were employed to assess the reliability of the proposed models. The suggested models have been benchmarked against various soft-computing models and existing empirical equations. Sensitivity analysis has also been conducted to identify the most influential parameters to the SFRC shear strength.

Keywords: *Machine learning; artificial neural network; genetic programming; steel fibers; concrete; shear strength; statistical metrics; sensitivity analysis*

Summary for Lay Audience

Shear failure of reinforced concrete (RC) beams has been a concern due to its brittle and sudden nature. The use of conventional stirrups to increase the shear capacity of RC beams has been effective in avoiding catastrophic failures. However, using conventional stirrups is laborious, costly, and can be challenging when the structure has a thin or irregular cross-section. The use of steel fiber-reinforced concrete has gained great momentum in recent years owing to the noteworthy increase in the shear capacity and possible replacement of minimum stirrups with steel fibers. Yet, the use of steel fibers remains limited due to the lack of design provisions in building codes. This is mainly associated with the complex shear transfer mechanism and random orientation of fibers inside the concrete matrix. Existing empirical equations for SFRC beams shear capacity have been developed with a relatively few data samples, which makes their accuracy over new samples that fall outside their range of validity uncertain.

To overcome such drawbacks, the research presented herein suggests two machine learning models developed from an extensive database to predict the shear capacity with high accuracy. The first hybrid model is a combination of artificial neural network (ANN) and atom search optimization (ASO). The second model, which is based on genetic programming (GP), is an alternative approach that aims to generate a transparent equation for estimating the SFRC shear strength. Appropriate tuning of the hyperparameters for each model has been conducted to achieve optimal accuracy. The performance of the suggested models was assessed via several statistical metrics. The accuracy of the models was also compared to that of other widely used machine learning models and empirical equations. Results reflected the superior accuracy of the proposed models in terms of correlation and error between predicted and actual values. In addition, sensitivity analyses were performed to identify the most important parameters affecting the shear strength. It was found that for both models, the shear span-to-depth ratio had the greatest influence on the shear capacity of SFRC beams without stirrups.

Co-Authorship Statement

The present thesis has been prepared with adherence to the integrated-article format stipulated by the Faculty of Graduate Studies at Western University. Chapters 2, 3 and 4 of the Thesis have been submitted for publication to journals. All programming tasks, data analysis, analytical work and writing of draft manuscripts for publication was carried out by the candidate under the direct supervision of Professor Moncef L. Nehdi. Any other co-author assisted in the development of the final version of the publications.

1. **Ben Chaabene, W.**, Flah, M., and Nehdi, M. L. (2020). Machine Learning Prediction of Mechanical Properties of Concrete: Critical review. *Construction and Building Materials*, 260, 119889. *Published*.
2. **Ben Chaabene, W.**, and Nehdi, M. L. Novel Soft Computing Hybrid Model for Predicting Shear Strength and Failure Mode of SFRC Beams with Superior Accuracy. *Composites Part C*, 3, 100070. *Published*
3. **Ben Chaabene, W.**, and Nehdi, M. L. Genetic Programming Based Symbolic Regression for Shear Capacity Prediction of SFRC Beams. *Construction and Building Materials*. *Under Review*.

Dedication

To:

My Father, Mustapha

My Mother, Mahbouba

My brothers and sisters

Acknowledgments

I would like to express my sincere gratitude to my supervisor Prof. Moncef L. Nehdi for giving me this opportunity and for his guidance, encouragement, and support throughout this amazing experience of research. I will be always grateful for that.

I would like to acknowledge the support of Mitacs for providing financial assistance during the first year of the research program. Their assistance was extremely helpful, and I am very grateful for that.

I would also like to express my deepest appreciation to the wonderful faculty and staff members at Western University for their support and for the great experience provided in this program.

I would like to extend my appreciation to all my friends and colleagues who provided support and encouragement throughout this journey. The valuable relationships that I have developed at Western University are priceless. I wish them all the best in the future.

Finally, I would like to express my endless appreciation and gratitude to my family and especially my parents. None of this would have been possible without the sacrifices they have made and the support they have provided throughout my life. Words are not enough to express my gratitude to them.

Table of Contents

Abstract.....	ii
Summary for Lay Audience.....	iii
Co-Authorship Statement.....	iv
Dedication.....	v
Acknowledgments.....	vi
Table of Contents.....	vii
List of Tables.....	x
List of Figures.....	xi
Nomenclature.....	xii
List of Acronyms.....	xiii
Chapter 1.....	1
Introduction.....	1
1.1 Background.....	1
1.2 Research Objectives.....	3
1.3 Original Contributions.....	3
1.4 Thesis Structure.....	4
1.5 References.....	5
Chapter 2.....	6
Machine Learning Prediction of Mechanical Properties of Concrete: Critical review.....	6
2.1 Introduction.....	6
2.2 Prediction of mechanical properties of concrete.....	7
2.2.1 Evaluation of machine learning models.....	7
2.2.2 Artificial Neural Network.....	8
2.2.3 Support vector machine.....	13
2.2.4 Decision tree models.....	23
2.2.5 Evolutionary algorithms.....	29
2.2.6 Selection of model inputs.....	33
2.3 Discussion and critical analysis.....	36
2.4 Practical recommendations and knowledge gaps.....	41
2.5 Conclusions.....	42
2.6 References.....	43

Chapter 3.....	53
Novel Soft Computing Hybrid Model for Predicting Shear Strength and Failure Mode of SFRC Beams with Superior Accuracy.....	53
3.1 Introduction	53
3.2 Experimental Database.....	54
3.3 Prediction of shear strength of SFRC beams	56
3.3.1 Atom search optimization.....	56
3.3.2 Artificial neural network.....	58
3.3.3 Hybrid ASO-ANN model	59
3.4 Classification of failure mode of SFRC beams	65
3.4.1 Decision tree	66
3.4.2 K-nearest neighbor.....	66
3.4.3 Naïve Bayes	67
3.4.4 Support vector machine	67
3.5 Results and discussion.....	67
3.5.1 Shear strength prediction	67
3.5.2 Prediction of failure mode	76
3.5.3 Improvement of developed models.....	81
3.6 Conclusions	82
3.7 References	83
Chapter 4.....	87
Genetic Programming Based Symbolic Regression for Shear Capacity Prediction of SFRC Beams.....	87
4.1 Introduction	87
4.2 Database Description.....	88
4.3 Feature Selection	92
4.4 Genetic Programming Based Symbolic Regression.....	94
4.5 Model Training through TGAN.....	96
4.6 Results and Discussion.....	98
4.6.1 Statistical metrics	98
4.6.2 Proposed new shear equation.....	99
4.6.3 Performance assessment of proposed equation.....	101
4.6.4 Sensitivity analysis.....	107
4.7 Verification of model applicability for reinforced concrete beams	110
4.8 Conclusions	111

4.9	References	112
Chapter 5	118
Conclusions and Recommendations	118
5.1	Summary and Conclusions.....	118
5.2	Model Limitations	120
5.3	Recommendations for Future Work.....	120
Appendix	122
Curriculum Vitae	145

List of Tables

Table 2.1: Statistical metrics	8
Table 2.2: Summary of used ANN-based models	14
Table 2.3: Summary of adopted SVM-based models.....	24
Table 2.4: Summary of employed decision tree models	30
Table 2.5: Summary of used evolutionary algorithms	34
Table 2.6: Comparison between ML models and empirical formulas over the same testing data	38
Table 2.7: Comparison between ML models over the same testing data	39
Table 3.1: Statistical characteristics of employed dataset	55
Table 3.2: Ranking system for ANN structure selection.....	62
Table 3.3: Final values of ASO-ANN parameters.....	65
Table 3.4: Empirical equations developed for estimating shear capacity of SFRC beams	68
Table 3.5: Parameters of various ML models	69
Table 3.6: Performance assessment of different ML models	70
Table 3.7: Performance assessment of empirical models.....	72
Table 3.8: Parameters of the classification models	77
Table 3.9: Performance evaluation of classification algorithms	79
Table 4.1: Database of SFRC beams without stirrups.....	89
Table 4.2: Descriptive statistics of the database.....	91
Table 4.3: Set of parameters used to develop GP-SR.....	96
Table 4.4: Existing equations for SFRC shear strength	103
Table 4.5: Performance evaluation of existing models	105
Table 4.6: Validation of proposed new equation.....	105
Table 4.7: Ranking of the different shear equations.....	106
Table A.1: Database used to develop ASO-ANN and the classification algorithms	122
Table A.2: Database used to develop the GP-SR model	137

List of Figures

Figure 2.1: Machine learning models.....	7
Figure 2.2: Structure of ANN model with m input variables and n hidden layers	9
Figure 2.3: Hyperplane classification.....	13
Figure 2.4: Nonlinear mapping in SVM.....	21
Figure 2.5: M5-tree process.....	27
Figure 2.6: General process of evolutionary algorithms.	29
Figure 2.7: BPNN searching mechanism.	41
Figure 3.1: Various forces affecting atomic population.	58
Figure 3.2: Structure of employed ANN model.	59
Figure 3.3: Flowchart of ASO-ANN model.	61
Figure 3.4: Performance assessment for different atom number.....	63
Figure 3.5: Performance assessment for depth weight values.....	64
Figure 3.6: Performance assessment for multiplier weight values.....	64
Figure 3.7: Four-point and three-point shear testing methods of SFRC beams.	66
Figure 3.8: Taylor Diagram visualization of model performance in SFRC shear strength prediction.....	73
Figure 3.9: Sensitivity indices of input variables.	76
Figure 3.10: Scatter plots of failure mode classification.	78
Figure 3.11: Confusion matrix of each classification model.....	80
Figure 4.1: Feature importance scores.....	92
Figure 4.2: Correlation matrix of input features.....	93
Figure 4.3: Crossover in GP-SR model.....	95
Figure 4.4: Mutation in GP-SR model.	95
Figure 4.5: Simplified process of TGAN.	97
Figure 4.6: Process of training and testing GP-SR.....	98
Figure 4.7: Effect of input features on the shear capacity	101
Figure 4.8: Taylor Diagram for SFRC shear strength prediction.	107
Figure 4.9: Sobol indices of different variables.	109
Figure 4.10: Correlation between predicted and experimental RC Shear strength	110

Nomenclature

N_F	total number of specimens that failed in flexural mode	MAE	mean absolute error
N_{FS}	total number of specimens that failed in flexural-shear mode	N	total number of atoms
N_S	total number of specimens that failed in shear mode	R	correlation coefficient
S_{Ti}	total order sensitivity index	$RMSE$	root mean square error
S_i	first-order sensitivity index	S	shear failure
V_f	steel fiber volume fraction	T	maximum number of iterations
b_w	beam width	V	variance
c_F	number of correctly predicted specimens failing in flexural mode	a	shear span
c_{FS}	number of correctly predicted specimens failing in flexural-shear mode	d	effective depth of beam
c_S	number of correctly predicted specimens failing in shear mode	d'	modified agreement index
d_f	fiber diameter	m	mass of the atom
f'_c	compressive strength of concrete.	r	random weight ranging from 0 to 1
f_{tf}	tensile strength of fibers	x	position of the atom
l_f	fiber length	y	actual value
\ddot{x}	acceleration of the atom	y'	predicted value
\dot{x}	velocity of the atom	α	depth weight
x_{best}	position of the best atom	β	multiplier weight
h	dimensionless factor depending on Euclidian distance and collision diameter	γ	classification accuracy metric
δ	Euclidian distance	ε	loss function
C	regularization parameter of SVR	η	depth function
E	expectation	λ	Lagrange multiplier.
COV	coefficient of variation	ρ	longitudinal steel ratio
FS	flexural-shear failure	μ	Mean
G	constraint force	φ	fitness value
I	interaction force	v_u	Shear capacity
K	subset of atomic population containing K atoms with the best value of fitness function	R_0	correlation coefficient through the origin

List of Acronyms

ABCP	Artificial Bee Colony Programming	LSSVR	Least-Square Support Vector Regression
ANFIS	Adaptive Neuro-Fuzzy Inference System	MARS	Multivariate Adaptive Regression Spline
ANN	Artificial Neural Network	MART	Multiple Additive Regression Trees
ASO	Atom Search Optimization	ML	Machine Learning
BAS	Beetle Antennae Search	MOGWO	Multi-Objective Grey Wolves Optimization
BBP	Biogeography-Based Programming	NB	Naïve Bayes
BPNN	Backpropagation Neural Network	NID	Neural Interpretation Diagram
CART	Classification and Regression Trees	PSO	Particle Swarm Optimization
CFRP	carbon fiber reinforced plastic	RAC	Recycled Aggregate Concrete
EA	Evolutionary Algorithms	RBF	Radial Basis Function
ECSO	Enhanced Cat Swarm Optimization	RC	Reinforced Concrete
ELM	Extreme Learning Machines	RF	Random Forest
FA	firefly algorithm	RSM	Response Surface Method
FL	Fuzzy Logic	SA	Sensitivity Analysis
GA	Genetic Algorithm	SCC	Self-Compacting Concrete
GEP	Gene Expression Programming	SDR	Standard Deviation Factor
GP	Genetic Programming	SFRC	Steel Fiber Reinforced Concrete
GP-SR	Genetic programming-based Symbolic Regression	SFS	Sequential Feature Selection
GSA	Global Sensitivity Analysis	SR	Symbolic Regression
HPC	High Performance Concrete	SVM	Support Vector Machine
HSC	High-Strength Concrete	SVR	Support Vector Regression
KNN	<i>k</i> -Nearest Neighbors	TGAN	Tabular Generative Adversarial Network
LHS	Latin Hypercube Sample	XGBoost	Extreme Gradient Boosting
LSSVM	Least-Square Support Vector Machine		

Chapter 1

Introduction

1.1 Background

The use of fibers to enhance the mechanical properties of brittle materials is not a new concept and dates back thousands of years. For instance, ancient civilizations of West Asia incorporated straw fibers to reinforce sunbaked bricks. In recent times, asbestos fibers had been widely used to reinforce cement paste matrices, but because of the health risks associated with such fibers, alternate fiber types were suggested throughout the 1960s and 1970s. Those fibers have been largely involved to enhance the mechanical properties of concrete.

In modern times, the most common types of fibers used in concrete enhancement include natural, glass, synthetic, and steel fibers. Natural fibers such as Sisal and Bamboo are the oldest type of fiber reinforcement, while the use of synthetic fibers such as carbon and nylon as well as glass fibers started in the 1960s. Even though these types of fibers impart to concrete better mechanical strength, they can also bring drawbacks. Natural fibers are vulnerable to degradation because of the high alkalinity of the pore-water in concrete (ACI Committee 544, 2009). Similarly, glass fibers are prone to durability issues engendered by concrete alkalinity. Regarding synthetic fibers, Greenough and Nehdi (2008) and Majdzadeh *et al.* (2006) stated that their ability to enhance the shear capacity of concrete is lower than that of steel fibers.

Currently, steel fibers are the most widely adopted and researched fiber type for concrete strength improvement (Slater *et al.* 2012). The use of steel fiber-reinforced concrete (SFRC) has been growing in recent years. SFRC was used in many construction projects including the floor slab of Chrysler Jefferson North Assembly Plant (Robinson *et al.* 1991) and the Gotthard Base Tunnel (Kronenberg, 2006). Steel fibers can impart to reinforced concrete several benefits including greater shear capacity and post-cracking toughness (Keshtegar *et al.* 2019). Such advantages on the shear strength encouraged the ACI

building code to allow the use of steel fibers as a replacement for minimum stirrups (ACI Committee 318, 2011). This can be effective when the placement of traditional stirrups is challenging, especially in some cases where the structure has a thin or irregular cross-section, such as in architectural panels (Khuntia *et al.* 1999). Placing concrete in closely spaced stirrups can be problematic, leading to voids in the concrete itself. In addition, stirrups are associated with significant labor input and consequently greater construction costs. The use of steel fibers can help overcome the aforementioned drawbacks.

Yet the adoption of SFRC in large-scale construction remains limited. This is essentially related to the lack of pertinent design provisions in building codes. The lack of shear design equations for SFRC beams is mainly linked to the complex shear transfer mechanism in SFRC beams without stirrups. The shear transfer in reinforced concrete is influenced by many factors including the aggregate interlock, which transfers shear stress across diagonal cracks. Moreover, shear resistance is also carried out via dowel resistance and compression block. Adding steel fibers was reported to enhance the shear strength because of the imparted post-cracking diagonal tension resistance across crack surfaces (Shoaib, 2012). Yet, the random orientation of the fibers as well as the intricate relationship between steel fibers and the concrete matrix make the accurate estimation of such contribution challenging. Such an intricacy has motivated researchers to develop accurate models for estimating the shear strength of SFRC beams. Conventional models for assessing the SFRC shear capacity have largely relied on empirical models, which are based on statistical analysis of experimental data (Ben Chaabene *et al.* 2020). However, these models have been developed with relatively few data examples, making their accuracy over new data that falls outside their range of validity uncertain. In addition, developing such models is associated with costly and time-consuming trial batches required to develop test specimens.

Recently, machine learning (ML) models have emerged as a strong contender for predicting the mechanical properties of concrete. Unlike empirical models, ML models are developed with relatively large datasets that make their accuracy over “unseen” data better than empirical equations.

1.2 Research Objectives

Even though ML models generally exhibit better accuracy than empirical and statistical models, the performance of each ML model can differ significantly from one problem to another. This is linked to the degree of complexity of the relationship between the inputs and the target variable along with the dataset size and number of features. Moreover, the performance of each ML algorithm depends on the hyperparameters, which require appropriate tuning before achieving optimal accuracy. Therefore, there is need to pursue more accurate algorithms that can acquire greater generalization capability to estimate the shear strength of SFRC beams. Therefore, the main objectives of the present thesis are:

- 1) To mitigate the limited availability of experimental data examples of SFRC beams that failed in shear by generating synthetic data using a generative adversarial network model (GAN) and exploiting it in “train-on-synthetic” “test-on-real” modeling approach.
- 2) To develop a novel hybrid machine learning model based on artificial neural network (ANN) to predict the shear capacity of SFRC beams without stirrups with accuracy and reliability that outperform that of existing models. The hyperparameters of the suggested model will be carefully tuned to achieve superior accuracy.
- 3) To train a classification algorithm for forecasting the failure mode of SFRC beams. Since ANN is a black-box model, an alternative method based on genetic programming will be proposed to generate a transparent SFRC shear strength equation. This should help non-programming experts to easily implement the constitutive equation in any computing language.

1.3 Original Contributions

The research presented in this thesis proposes novel soft-computing approaches to predicting the shear capacity of SFRC beams without stirrups. Due to the intricate shear transfer mechanism in such beams and the limitation of empirical equations, developing more accurate models to estimate the shear strength is of paramount importance. The present thesis helps address the problem through the following specific contributions:

1. Development of a novel machine learning model that hybridizes atom search optimization (ASO) and ANN to assess the shear strength of SFRC beams without stirrups.
2. Development of an accurate classification algorithm to forecast the failure mode of SFRC beams
3. Proposing a new shear equation for SFRC beams without stirrups via genetic programming based on symbolic regression (GP-SR) model.
4. For the first time in the open literature, an extensive synthetic database for SFRC beams without stirrups comprising 2000 data examples has been developed using a GAN model to cope with the limited number of experimental data samples.
5. Sensitivity analyses were conducted through the developed models to identify the most influential parameters affecting SFRC shear strength.

1.4 Thesis Structure

The current thesis has been structured and organized according to the integrated-article guidelines of the Faculty of Graduate Studies at Western University. It comprises five chapters that focus on the application of machine learning for SFRC shear strength prediction.

Chapter two provides a critical review of the different existing machine learning models used for forecasting the mechanical properties of concrete. Existing methods were categorized into four groups, highlighting the most commonly adopted soft-computing techniques.

Chapter three presents a novel hybrid machine learning model that combines ASO and ANN to predict the shear strength of SFRC beams without stirrups. Hyperparameters of the suggested model were carefully tuned to attain maximum accuracy. The performance of the model was benchmarked against other ML models and empirical equations using various statistical metrics. Sensitivity analyses were also conducted to identify the most important parameters affecting the shear strength. Moreover, a classification algorithm was implemented to predict the failure mode of SFRC beams.

Chapter four provides an alternative approach for assessing the shear strength of SFRC. Unlike the “black-box” model presented in chapter three; the genetic programming-based model involved in this chapter can generate an explicit mathematical equation for SFRC shear capacity. In addition, a tabular GAN algorithm was deployed to overcome the issue of the relatively limited number of data examples existing in the open literature.

Finally, Chapter five summarizes the research findings and conclusions, presents current knowledge gaps, and suggests future needed research.

1.5 References

- ACI committee 318. (2011). Building Code Requirements for Structural Concrete and Commentary. In *American Concrete Institute, Farmington Hills, MI*.
- ACI Committee 544. (2009). 544.1R-96: Report on Fiber Reinforced Concrete (Reapproved 2009). *American Concrete Institute*.
- Ben Chaabene, W., Flah, M., & Nehdi, M. L. (2020). Machine learning prediction of mechanical properties of concrete: Critical review. *Construction and Building Materials, 260*, 119889.
- Greenough, T., & Nehdi, M. (2008). Shear behavior of fiber-reinforced self-consolidating concrete slender beams. *ACI Materials Journal, 105*, 468–477.
- Keshtegar, B., Bagheri, M., & Yaseen, Z. M. (2019). Shear strength of steel fiber-unconfined reinforced concrete beam simulation: Application of novel intelligent model. *Composite Structures, 212*, 230–242.
- Khuntia, M., Stojadinovic, B., & Goel, S. C. (1999). Shear strength of normal and high-strength fiber reinforced concrete beams without stirrups. *ACI Structural Journal, 96*, 282–289.
- Kronenberg, J. (2006). *Sliding arch construction method used on the Gotthard Base Tunnel. 10*, 19–20.
- Majdzadeh, F., Soleimani, S. M., & Banthia, N. (2006). Shear strength of reinforced concrete beams with a fiber concrete matrix. *Canadian Journal of Civil Engineering, 33*, 726–734.
- Robinson, C., Colasanti, A., & Boyd, G. (1991). Steel Fibers Reinforce Auto Assembly Plant Floor. *Concrete International, 13*, 30–35.
- Shoaib, A. (2012). Shear in Steel Fiber Reinforced Concrete Members without Stirrups.
- Slater, E., Moni, M., & Alam, M. S. (2012). Predicting the shear strength of steel fiber reinforced concrete beams. *Construction and Building Materials, 26*, 423–436.

Chapter 2

Machine Learning Prediction of Mechanical Properties of Concrete: Critical review

2.1 Introduction

Accurate estimation of the mechanical properties of concrete has been a concern since such properties are often required by design codes. The conventional methods for predicting mechanical strength have largely relied on empirical methods that consist of statistical analysis of experimental data. However, those methods are associated with multiple drawbacks such as costly and time-consuming trial batches required to develop the test specimens. Moreover, empirical equations are developed using limited data examples, which makes their accuracy over new data uncertain.

Recently, machine learning (ML) methods have emerged as a strong contender for predicting the compressive, shear, and tensile strength of concrete along with its elastic modulus. ML models are developed via extensive databases, making their generalization capability and their accuracy over “unseen” data examples stronger than that of conventional techniques. Even though ML models can be employed to achieve the same goal, i.e. predicting mechanical strength, their process and accuracy can differ significantly from one problem to another. As shown in **Figure 2.1**, The most common ML models used to forecast concrete strength can be generally grouped into four major categories, namely artificial neural networks (ANN), support vector machine (SVM), decision trees, and evolutionary algorithms (EA). In this chapter, a comprehensive survey of the literature was carried out to examine the application of ML on the mechanical strength of concrete. The different ML models are critically reviewed and discussed, thus identifying current knowledge gaps and presenting practical recommendations that emanate from the current review.

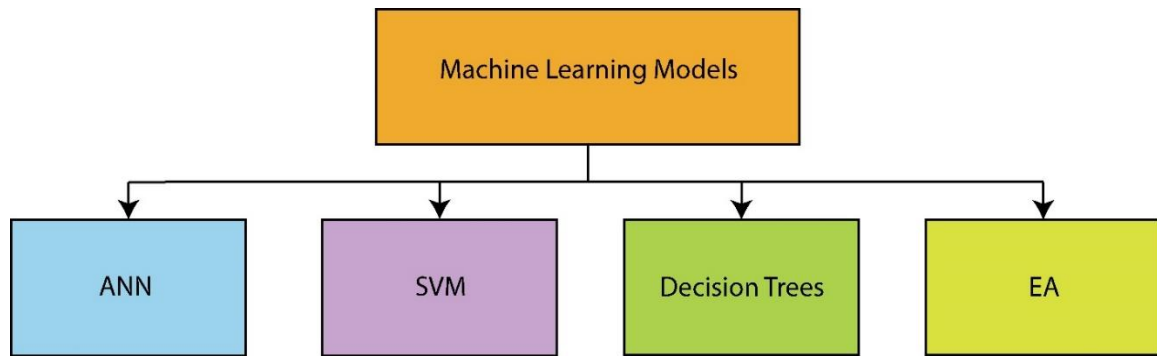


Figure 2.1: Machine learning models.

2.2 Prediction of mechanical properties of concrete

ML models have been extensively used as an effective tool for forecasting mechanical properties of concrete. Those models are typically applied to an extensive dataset, which is generally divided into training (TR), validation (VAL), and testing (TS) subsets. The training set is used for model training. Validation data provides unbiased evaluation of the model fit on training data and prevents model overfitting by stopping the training process when the error increases. The model is finally applied on the testing data to assess its predictive performance. The most commonly employed ML methods can be categorized into four major types, namely ANN, SVM, decision trees, and EA. The evaluation, process, and the application of these models are discussed below.

2.2.1 Evaluation of machine learning models

Performance assessment of ML algorithms has been carried out using several statistical methods that describe the model fitting. **Table 2.1** entails potential statistical metrics employed for evaluating ML models with their corresponding mathematical expressions. These methods indicate how well the predicted values fit with actual data. Moreover, they can be adopted in sensitivity analysis, pointing out the weight of each input variable in the prediction process (Belalia Douma et al., 2017; Sonebi et al., 2016; Van Dao et al., 2019; Xu, Zhao, et al., 2019). Not only can statistical metrics assess the performance of ML techniques, they may also be used as reference for comparing the effectiveness of several algorithms.

Table 2.1: Statistical metrics

Statistical parameter	Formula
Correlation coefficient (R)	$R = \frac{n \sum_{i=1}^n y'_i y_i - (\sum_{i=1}^n y'_i)(\sum_{i=1}^n y_i)}{\sqrt{n(\sum_{i=1}^n y_i'^2) - (\sum_{i=1}^n y'_i)^2} \sqrt{n(\sum_{i=1}^n y_i^2) - (\sum_{i=1}^n y_i)^2}}$
Coefficient of determination (R^2)	$R^2 = 1 - \frac{\sum_{i=1}^n (y'_i - y_i)^2}{\sum_{i=1}^n (y_i - \bar{y})^2}$
Mean square error (MSE)	$MSE = \frac{\sum_{i=1}^n (y'_i - y_i)^2}{n}$
Root mean square error ($RMSE$)	$RMSE = \sqrt{\frac{\sum_{i=1}^n (y'_i - y_i)^2}{n}}$
Mean absolute error (MAE)	$MAE = \frac{1}{n} \sum_{i=1}^n y'_i - y_i $
Mean absolute percentage error ($MAPE$)	$MAPE (\%) = \frac{1}{n} \sum_{i=1}^n \left \frac{y'_i - y_i}{y_i} \right \times 100$
Mean (μ)	$\mu = \frac{1}{n} \sum_{i=1}^n \frac{y_i}{y'_i}$
Standard deviation (σ)	$\sigma = \sqrt{\frac{1}{n} \sum_{i=1}^n \left(\frac{y_i}{y'_i} - \mu \right)^2}$
Coefficient of variation (COV)	$COV (\%) = \frac{\sigma}{\mu} \times 100$

2.2.2 Artificial Neural Network

Artificial neural network is a nonlinear model inspired by the basic framework of the human brain (Marugán et al., 2018; Mohandes et al., 2019; Nazemi et al., 2019; Sharifzadeh et al., 2019). In ANN models, information propagation is performed through links that receive the information from a processing element (neuron) to deliver it to the following neurons. Each information is affected by a weight, reflecting the significance of input variables to outputs (DeRousseau et al., 2018). Once a neuron receives an information, it merges with others coming from different neurons via a combination function. Then, the combined information is transported to the following nodes. This iterative process is repeated until the algorithm precisely fits the data, indicated by the convergence of the error rate, or when the maximum iteration number has been reached

(Bourdeau et al., 2019). The structure of ANN is generally composed of three types of layers: an input layer, a hidden layer(s), and an output layer (Fadaei et al., 2018). **Figure 2.2** illustrates the general structure of ANN. The input layer conveys input parameters for model training and testing. The hidden layer(s) is/are responsible for linking between the input layer and the output layer that delivers the result of the model. To produce the neuron output and ensure data transmission through hidden and output layers, activation functions are required (Hemmat Esfe et al., 2015; Mohandes et al., 2019). Furthermore, ANN training is achieved via learning algorithms, which enable the model to understand the concept of the problem. Hence, the general structure of ANN changes according to the type of learning algorithm. **Table 2.2** outlines the various ANN approaches employed for estimating concrete strength, which are discussed below.

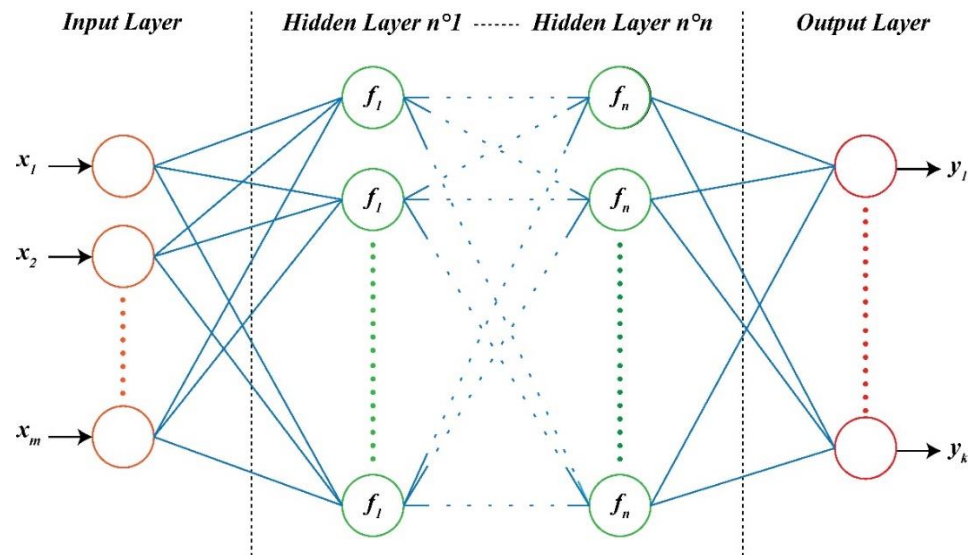


Figure 2.2: Structure of ANN model with m input variables and n hidden layers

2.2.2.1 Backpropagation neural network

It can be observed in **Table 2.2** that the backpropagation (BP) approach has been widely used by researchers to train ANN (Xu, Chen, et al., 2019). BP is a local search technique that employs learning algorithms, such as gradient descent and Levenberg-Marquardt, to

update the weights and biases of the ANN. Such an approach minimizes the cost function that generally expresses the error between actual and predicted strength. Backpropagation neural network (BPNN) was employed for instance to forecast the compressive strength of high-performance concrete (HPC) (Chithra et al., 2016; Chou et al., 2011; Deepa et al., 2010). The model incorporated concrete ingredients and age of testing as input parameters. Performance assessment revealed that BPNN exhibited good forecasting ability, outperforming regression models in terms of accuracy.

Other studies investigated the ability of BPNN in estimating the compressive strength of recycled aggregate concrete (RAC) (Deng et al., 2018; Duan et al., 2013a; Khademi et al., 2016; Hosein Naderpour et al., 2018; Topçu and Saridemir, 2008). For example, Topçu and Saridemir (2008) developed a BPNN based on gradient descent algorithm in addition to fuzzy logic (FL) model to forecast the compressive strength of RAC. Both methods showed good accuracy, but BPNN slightly outperformed FL in terms of R^2 , MAPE, and RMSE. Later research by Naderpour et al., (2018) evaluated the performance of BPNN and inspected the influence of each input parameter on the compressive strength of RAC through sensitivity analysis. Their model included six input variables and eighteen hidden nodes. Results demonstrated that BPNN accurately predicted the compressive strength of RAC, and that water absorption of aggregates along with water-to-total material ratio had the greatest impact on concrete strength. More recent studies examined the feasibility of forecasting the compressive strength of self-compacting concrete (SCC) via BPNN (P. G. Asteris et al., 2016; Panagiotis G Asteris and Kolovos, 2019; Belalia Douma et al., 2017; Siddique et al., 2011). For instance, Asteris and Kolovos (2019) developed an ANN model trained with Levenberg–Marquardt algorithm. Their results indicated that BPNN can successfully predict the compressive strength of SCC. Sensitivity analysis revealed that viscosity-modifying admixtures incorporated within SCC had the most important effect on compressive strength.

Moreover, several researchers have explored the applicability of BPNN to estimate the tensile strength of concrete (Behnood, Verian, et al., 2015; Topçu and Saridemir, 2008; Xu, Zhao, et al., 2019). For instance, Behnood et al., (2015) proposed a model to predict the tensile strength of steel fiber-reinforced concrete (SFRC). The model in which the

compressive strength of concrete was introduced as an input parameter, predicted the tensile strength of SFRC with satisfactory accuracy, showing better results than SVM. Furthermore, the elastic modulus of concrete has been estimated via BPNN (Duan et al., 2013b; Mohammadi and Behnood, 2018; Xu, Zhao, et al., 2019). Mohammadi and Behnood (2018) compared the effectiveness of BPNN and radial basis function neural network (RBFNN) in predicting the elastic modulus of RAC. The Levenberg-Marquart Learning algorithm was used in the BPNN model. Their results showed that BPNN had better predictive ability than that of RBFNN. Furthermore, multiple studies have explored BPNN forecasting of the shear capacity of reinforced concrete (RC) beams (Amani and Moeini, 2012; Mansour et al., 2004), concrete beams reinforced longitudinally with fiber-reinforced polymer (FRP) bars (Bashir and Ashour, 2012; Lee and Lee, 2014; H Naderpour et al., 2018), SFRC corbels (Kumar and Barai, 2010), and RC beams strengthened in shear with FRP (Perera et al., 2010; Tanarslan et al., 2012). Input parameters incorporated in these studies included the geometrical characteristics of beams along with the mechanical properties of concrete and reinforcing materials. Results indicated that BPNN successfully predicted the shear strength, demonstrating better accuracy than that of empirically developed equations (Lee and Lee, 2014).

2.2.2.2 Extreme Learning Machine

Extreme Learning Machine (ELM) is another potential approach used to train single hidden-layer feed-forward neural networks (J. Wang and Hu, 2015; Yaseen et al., 2018). In the ELM approach, hidden nodes are initiated in a random process and fixed without performing an iterative tuning. The model was adopted for instance by Al-Shamiri et al., (2019) to forecast the compressive strength of high-strength concrete (HSC). The number of hidden neurons in the model was gradually increased from 10 to 200, and the optimal obtained number was 110. Performance assessment of the model revealed the strong predictive ability of ELM, which was reflected by the value of the correlation coefficient. Earlier research by Yaseen et al., (2018) considered an ELM model to predict the compressive strength of foamed concrete. The model was benchmarked against three other ML algorithms namely M5 Tree, multivariate adaptive regression spline (MARS), and support vector regression (SVR). Performance assessment indicated that ELM had the best overall accuracy among the four models.

2.2.2.3 Hybrid ANN-based models

The idea behind hybrid approaches is to combine several algorithms so that the model performance and process can be noticeably improved. Owing to their ability in combining the advantages of more than one model, hybrid approaches have become of great interest among researchers. Thus, the performance of models like Adaptive Neuro-Fuzzy Inference System (ANFIS) has been widely examined (Ahmadi-Nedushan, 2012; Amani and Moeini, 2012; Khademi et al., 2016, 2017; Mohammadhassani et al., 2014; Van Dao et al., 2019; Yuan et al., 2014). ANFIS models are universal approximators that combine ANN and FL. This model uses ANN to enhance the membership capacities for decreasing the error rate in the output, while FL rules are responsible for providing expert knowledge (Jaafari et al., 2019; Van Dao et al., 2019). FL rules are used within the algorithm as fuzzy “if-then” rules to create the specified input-output sets. ANFIS was employed for instance to predict the compressive strength of geopolymers concrete along with concrete containing blast furnace slag and fly ash (Van Dao et al., 2019; Yuan et al., 2014). Results disclosed that ANFIS has a strong prediction ability, outperforming the BPNN model. ANFIS was also developed to predict the shear strength of RC and HSC beams (Amani and Moeini, 2012; Mohammadhassani et al., 2014). The model exhibited good predictions which outperformed those presented by design codes such as the American Concrete Institute and Canadian Standards Association. Another approach of optimizing ANN consisted of incorporating metaheuristic algorithms (Behnood and Golafshani, 2018; Bui et al., 2018; Yuan et al., 2014). Yuan et al., (2014) adopted the Genetic Algorithm (GA) model to optimize the weights and thresholds of BPNN. GA is a metaheuristic algorithm inspired by the natural evolution and selection concept (Kramer, 2017; Tsai et al., 2009). Its ability in acquiring a near global optimal solution while escaping local optima makes it a potential candidate for optimizing BPNN. The hybrid GA-ANN model was used to forecast the compressive strength of concrete containing slag and fly ash. Comparative study between GA-ANN and BPNN indicated that GA-ANN achieved the best performance. Behnood and Golafshani (2018) developed a multi-objective grey wolves optimization (MOGWO) algorithm for determining the most effective ANN structure. MOGWO is based on grey wolves optimization, which is a swarm intelligence optimization method based on the hunting strategies of grey wolves swarm. The hybrid MOGWO-ANN forecasted the

compressive strength of silica fume concrete with satisfactory accuracy. The maximum aggregate size was found to have significant impact on the compressive strength of concrete as indicated by sensitivity analysis. Bui et al., (2018) employed a modified firefly algorithm (MFA) to optimize the weights and biases of an ANN model for predicting the compressive and tensile strength of HPC. The firefly algorithm (FA) is a nature-inspired metaheuristics method based on the flashing characteristics and behavior of tropical fireflies (Yang, 2010). Study results showed that MFA-ANN model achieved accurate predictions and short computation time.

2.2.3 Support vector machine

Support Vector Machine is a ML classification model that aims to find an optimal hyperplane separating two different classes. As shown in **Figure 2.3**, the target of this method is maximizing the margin, which represents the distance from the hyperplane to the closest point of each class, to attain better classification performance on test data (DeRousseau et al., 2018). When the optimal hyperplane is found, the points located on its margin are called “support vectors”, and the solution proposed by this algorithm is based only on those points. However, some classes cannot be separated with a linear hyperplane, as illustrated in **Figure 2.4**.

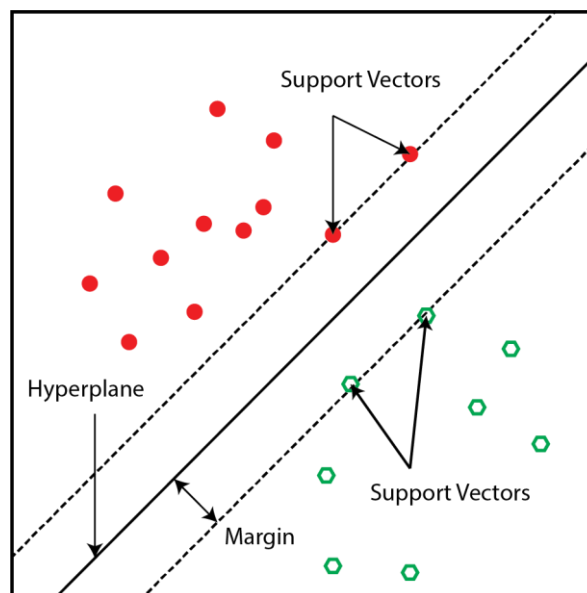


Figure 2.3: Hyperplane classification.

Table 2.2: Summary of used ANN-based models

Dataset size	TR (%)	VAL (%)	TS (%)	Concrete Type	Methods Used	Input Variables	Output	Statistical Index	Ref.
99	24	23	34	Cellular Concrete	BPNN	Cement, w/c ratio, sand to cement ratio, foam volume to cement ratio	Compressive strength	Absolute average error, Average algebraic error	(Nehdi et al., 2001)
1178	77.8	N/A	22.2	Concrete containing construction and demolition waste	BPNN	Cement, w/c ratio, mortar, aggregates, admixture, ratio of recycled materials, fineness modulus of fine and coarse aggregates, maximum aggregate size of fine and coarse aggregates, water absorption, age of testing	Compressive strength	R ² , Absolute Error	(Dantas et al., 2013)
135	70	15	15	Concrete containing FA and BFS	BPNN	Cement, BFS, curing age, ultrasonic pulse velocity, rebound number, fly ash	Compressive strength	R, MSE	(Atici, 2011)
180	83	N/A	17	Concrete containing FA and BFS	GA-BPNN ANFIS	Cement, BFS, coarse aggregate, fine aggregate, fly ash, water, superplasticizer	Compressive strength	RMSE, R ²	(Yuan et al., 2014)
144	10-fold cross-validation			Concrete containing FA, Haydite lightweight aggregate and Portland limestone cement	ANN	Cement type, curing age, water, cementitious material, fly ash, sand, pea gravel, Haydite lightweight aggregate, Micro Air	Compressive strength	R, RMSE, MAE	(Omran et al., 2016)
1030	70	15	15	Concrete containing silica fume	ANN combined with multi-objective grey wolves	Binder, water to binder ratio, silica fume to binder ratio, coarse aggregate to total aggregate ratio, coarse aggregate to binder ratio, superplasticizer to binder ratio, maximum aggregate size, concrete age	Compressive strength	RMSE, MAE, R	(Behnood and Golafshani, 2018)
91	N/A	N/A	N/A	Foamed Concrete	ELM	Cement, oven dry density, water/binder ratio, foamed volume	Compressive strength	R, RMSE, MAE, Relative RMSE, Relative MAE	(Yaseen et al., 2018)
210	70	15	15	GPC	ANFIS BPNN	Fly ash, sodium hydroxide, sodium silicate solution, water	Compressive strength	R ² , RMSE, MAE	(Van Dao et al., 2019)

Table 2.2 (continued)

Dataset size	TR (%)	VAL (%)	TS (%)	Concrete Type	Methods Used	Input Variables	Output	Statistical Index	Ref.
300	N/A	N/A	N/A	HPC	BPNN	Cement, BFS, fly ash, water, superplasticizer, coarse and fine aggregates, and curing age	Compressive strength	RMSE, MAE, R	(Deepa et al., 2010)
1030	10- fold cross-validation method			HPC	BPNN	Cement, BFS, fly ash, water, superplasticizer, coarse aggregate, fine aggregate, age of testing	Compressive strength	R ² , RMSE, MAPE	(Chou et al., 2011)
1030	90 80	N/A N/A	10 20	HPC	BPNN Bagged ANN Gradient boosted ANN Wavelet-bagged ANN Wavelet-gradient boosted ANN	Cement, BFS, fly ash, water, superplasticizer, coarse aggregate, fine aggregate, age of testing	Compressive strength	R ² , RMSE, MAE	(Ibrahim et al., 2013)
270	70	15	15	HPC	BPNN	Cement, nano silica, fine aggregate, copper slag, age of specimen, superplasticizer	Compressive strength	R, R ² , RMSE, MAPE	(Chithra et al., 2016)
1133	10- fold cross-validation method			HPC	MFA-BPNN	Water, cement, BFS, fly ash, superplasticizer, coarse and fine aggregates, age of testing	Compressive strength	R, RMSE, MAE, MAPE	(Bui et al., 2018)
324	75	N/A	25	HSC	ELM BPANN	Water, cement, fine aggregate, coarse aggregate, superplasticizer	Compressive strength	RMSE, MAE, MAPE, R, Nash-Sutcliffe efficiency	(Al-Shamiri et al., 2019)
173	70	15	15	Normal concrete	BPNN ANFIS	Cement, w/c ratio, maximum size of aggregate, gravel, sand 3/4, sand 3/8, fineness modulus of sand	Compressive strength	R ²	(Khademi et al., 2017)
210	67	N/A	33	RAC	BPNN	Age of the specimen, cement, water, sand, aggregate, recycled aggregate, superplasticizer and silica fume	Compressive strength	RMSE, R ² , MAPE	(Topçu and Saridemir, 2008)
139	N/A	N/A	N/A	RAC	BPNN	Water absorption, w/c ratio, fine aggregate, natural coarse aggregate, recycled coarse aggregate, water to total material ratio	Compressive strength	R, MSE	(Hosein Naderpour et al., 2018)

Table 2.2 (continued)

Dataset size	TR (%)	VAL (%)	TS (%)	Concrete Type	Methods Used	Input Variables	Output	Statistical Index	Ref.
168	N/A	N/A	N/A	RAC	BPNN	Water, cement, sand, natural coarse aggregate, recycled coarse aggregate, w/c ratio, fineness modulus of sand, water absorption of the aggregates, saturated surface-dried, density, maximum size of aggregates, impurity content and replacement ratio of recycled coarse aggregate, conversion coefficient of different concrete specimen	Compressive strength	R ² , RMSE, MAPE	(Duan et al., 2013a)
257	70	15	15	RAC	BPNN ANFIS	Cement, natural fine aggregate, recycled fine aggregate, natural coarse aggregates 10 mm, natural coarse aggregates 20 mm, recycled coarse aggregates 10 mm, recycled coarse aggregates 20 mm, admixture, water, w/c ratio, sand to aggregate ratio, water to total materials ratio, replacement ratio of recycled aggregate to natural aggregate, aggregate/cement ratio	Compressive strength	R ² , Sum of squared errors, MSE	(Khademi et al., 2016)
74	68	N/A	32	RAC	BPNN Convolutional Neural Network	Recycled coarse aggregate replacement ratio, recycled fine aggregate replacement ratio, fly ash replacement ratio, w/c ratio	Compressive strength	Relative error	(Deng et al., 2018)
112	70	15	15	Rubberized Concrete	BPNN	W/C ratio, superplasticizer, coarse aggregates, fine aggregates, crumb rubber, tire chips	Compressive strength	R, MAE, MSE	(Bachir et al., 2018)
324	70	15	15	Rubberized concrete	BPNN	Temperature, exposure duration, fiber content, w/c ratio	Compressive strength	MSE, RMSE, R, average absolute deviation, COV, Sum of squared errors	(Gupta et al., 2019)
145	78 83	N/A N/A	28 17	HSC Normal concrete	ANFIS	Compressive strength of concrete	Elastic Modulus	RMSE, MAPE	(Ahmadi-Nedushan, 2012)

Table 2.2 (continued)

Dataset size	TR (%)	VAL (%)	TS (%)	Concrete Type	Methods Used	Input Variables	Output	Statistical Index	Ref.
169	67	16.5	16.5	SCC	BPNN	Cement, coarse aggregate, fine aggregate, water, limestone powder, fly ash, ground granulated BFS, silica fume, rice husk ash, superplasticizer, viscosity modifying admixtures	Compressive strength	R	(P. G. Asteris et al., 2016)
114	80	N/A	20	SCC	BPNN	Binder, fly ash replacement percentage, water/binder ratio, fine aggregate, coarse aggregate, superplasticizer	Compressive strength	R, Relative error	(Belalia Douma et al., 2017)
205	67	16.5	16.5	SCC	BPNN	Cement, coarse aggregate, fine aggregate, water, limestone powder, fly ash, ground granulated BFS, silica fume, rice husk ash, superplasticizers, viscosity modifying admixtures	Compressive strength	R, MSE	(Panagiotis G Asteris and Kolovos, 2019)
126	83		17	Steel fiber added lightweight concrete	BPNN	The amounts of steel fiber, water, w/c ratio, cement, pumice sand, pumice gravel, and superplasticizer	Compressive strength	MSE, MARE, R	(Altun et al., 2008)
421	N/A	N/A	N/A	RAC	BPNN	Recycled aggregate replacement ratio, w/c ratio, aggregate to cement ratio, ratio of recycled aggregate maximum particle size to natural aggregate maximum particle size	Elastic Modulus	Mean, SD, RMSE, MAPE	(Xu, Zhao, et al., 2019)
400	80	N/A	20	RAC	BPNN RBFNN	w/c ratio, volume replacement of natural aggregate by recycled aggregate, coarse aggregate to cement ratio, fine aggregate to total aggregate ratio, saturated surface dry specific gravity of the mixed (i.e., natural and recycled) coarse aggregates, water absorption of the mixed coarse aggregates, 28-day cube compressive strength of the mixture	Elastic Modulus	RMSE, MAE, MAPE	(Mohammadi and Behnood, 2018)
324	70	15	15	RAC	BPNN	Cement, water to cement ratio, total aggregate to cement ratio, fine aggregate percentage, mass substitution rate of natural aggregate by recycled aggregate, characteristic of coarse aggregate, constituents of recycled coarse aggregate, type and preparation methods of coarse aggregate, cement type, specimen size	Elastic Modulus	R ² , RMSE, MAPE	(Duan et al., 2013b)

Table 2.2 (continued)

Dataset size	TR (%)	VAL (%)	TS (%)	Concrete Type	Methods Used	Input Variables	Output	Statistical Index	Ref.
87	80	N/A	20	FRP reinforced	BPNN	Effective depth, web width, compressive strength of concrete, shear span to depth ratio, modulus of elasticity of FRP, reinforcement ratio	Shear strength	MAE, COV, σ , μ	(Bashir and Ashour, 2012)
106	73	N/A	27	FRP reinforced	BPNN	Effective depth, web width, shear span to depth ratio, modulus of elasticity and ratio of FRP flexural reinforcement, compressive strength of concrete	Shear strength	μ , σ , COV, RMSE, R^2	(Lee and Lee, 2014)
177	60	20	20	FRP reinforced	BPNN	Width of web, effective depth of tensile reinforcement, shear span to depth ratio, compressive strength of concrete, FRP reinforcement ratio, modulus of elasticity of FRP	Shear strength	MAE, MSE, R, COV	(H Naderpour et al., 2018)
122	80	N/A	20	High Strength Concrete	ANFIS	Tensile reinforcement ratio, concrete compressive strength, shear span to depth ratio	Shear strength	COV, MSE, R	(Mohammadhassani et al., 2014)
176	80	N/A	20	RC	BPNN	Cylinder concrete compressive strength, yield strength of longitudinal and transverse reinforcing bars, shear span to effective depth ratio, cross-sectional dimensions of the beam, longitudinal and transverse reinforcement ratios	Shear strength	μ , COV	(Mansour et al., 2004)
123	81	N/A	19	RC	BPNN ANFIS	Compressive strength, longitudinal reinforcement volume, shear span to depth ratio, transverse reinforcement, effective depth, beam width	Shear strength	R^2 , RMSE, MAE	(Amani and Moeini, 2012)
98	81	N/A	19	RC strengthened in shear with FRP	BPNN	Breadth of the beam, height of the beam section, ratio of the FRP transversal reinforcement, angle between principal fiber orientation and longitudinal axis of the member, elastic modulus of FRP reinforcement, longitudinal steel reinforcement ratio, cross sectional area of transverse steel per length unit, yielding stress of the shear steel reinforcement, compressive strength of concrete, shear span to depth ratio, strengthening configuration	Shear strength	R, μ , COV, σ	(Perera et al., 2010)

Table 2.2 (continued)

Dataset size	TR (%)	VAL (%)	TS (%)	Concrete Type	Methods Used	Input Variables	Output	Statistical Index	Ref.
84	61	N/A	39	RC strengthened in shear with FRP	BPNN	Beam width, effective height of the beam, concrete compressive strength, type of wrapping scheme, the angle between the principal fiber orientation and the longitudinal axis of the member, elastic modulus of the FRP reinforcement, rupture strain of FRP reinforcement, total fabric design thickness, shear span to depth ratio	Shear strength	RMSE, R ²	(Tanarslan et al., 2012)
730	90	N/A	10	SFRC	BPNN	Concrete cylinder compressive strength, effective depth, beam width, shear span to depth ratio, longitudinal steel ratio, fiber volume fraction, fiber aspect ratio	Shear strength	MAE, RMSE, Pearson's coefficient	(Kumar and Barai, 2010)
714	10-fold cross-validation			HPC	MFA-BPNN	Curing age, cubic compressive strength	Tensile strength	R, RMSE, MAE, MAPE	(Bui et al., 2018)
346	N/A	N/A	N/A	RAC	BPNN	Recycled aggregate replacement ratio, w/c ratio, aggregate to cement ratio, ratio of recycled aggregate maximum particle size to natural aggregate maximum particle size	Tensile strength	Mean, SD, RMSE, MAPE	(Xu, Zhao, et al., 2019)
210	67	N/A	33	RAC	BPNN	Age of the specimen, cement, water, sand, aggregate, recycled aggregate, superplasticizer, silica fume	Tensile strength	RMS, R ² , MAPE	(Topçu and Saridemir, 2008)
980	70	15	15	SFRC	BPNN	Water to binder ratio, concrete compressive strength, age of the specimen, fiber reinforcing index	Tensile strength	R, R ² , MAPE, MAE, RMSE	(Behnood, Verian, et al., 2015)
187	90	N/A	10	HSC	BPNN	Water to binder ratio, water content, fine aggregate ratio, fly ash replacement ratio, air-entraining agent, ratio, silica fume replacement ratio and superplasticizer content.	Compressive strength	RMSE, R ² , MAPE, sum of squares error	(Öztaş et al., 2006)
225	50	N/A	50	Ground granulated blast furnace slag concrete	BPNN	Cement, blast furnace slag, superplasticizer, aggregates, water and age of samples	Compressive strength	R ²	(Bilim et al., 2009)

Table 2.2 (continued)

Dataset size	TR (%)	VAL (%)	TS (%)	Concrete Type	Methods Used	Input Variables	Output	Statistical Index	Ref.
2817	70	15	15	Normal and high-performance concrete	Grey wolf optimized ANN Grey wolf optimized ANFIS	Coarse aggregate, sand, water, cement, BFS, fly ash, superplasticizer, age of specimens	Compressive strength	RMSE, scatter index, MAE, R ² , uncertainty with 95% confidence level, MBE	(Golafshani et al., 2020)
240	56	21	23	Silica fume concrete	BPNN	Cement, amount of silica fume replacement, water content, amount of aggregate, plasticizer content, and age of samples	Compressive strength	Mean absolute relative error, MSE	(Özcan et al., 2009)

In such cases, the input space has to be mapped into higher dimensional feature space in order to make the linear separation of classes possible (Zheng et al., 2015). Nonlinear mapping process is generally performed through nonlinear function. Then, the output of the algorithm is obtained from nonlinear space through kernel functions (Kisi, 2015; Moraes et al., 2013; Raghavendra and Deka, 2014). These functions can be classified into five types; polynomial, sigmoid, radial basis, exponential radial basis, and linear (Zendehboudi et al., 2018). They help determine a nonlinear decision boundary without the need for computing the optimal hyperplane parameters in the feature space.

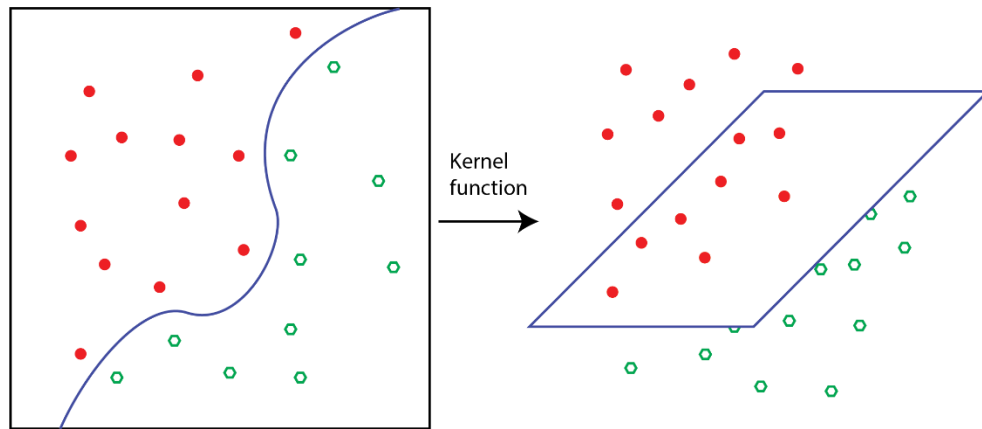


Figure 2.4: Nonlinear mapping in SVM.

Thus, the solution can be expressed as a combination of the weighted values of kernel functions at support vectors (Moraes et al., 2013). When SVM is mainly applied for regression analysis, the model is generally called support vector regression (SVR) (Chou et al., 2011; Zendehboudi et al., 2018). It deals with regression problems as a set of linear equations, leading to faster training process and better accuracy (Sadri and Burn, 2012; Yaseen et al., 2018). Several studies have examined the predictive ability of SVM **Table 2.3** outlines the different SVM-based models used for estimating concrete strength. It can be observed that SVM algorithms have been employed as standalone models in some studies and optimized with metaheuristic algorithms in others.

2.2.3.1 Standalone SVM models

The application of individual SVM models to predict the mechanical strength of concrete has been extensively investigated. For instance, Chou et al., (2011) used SVM to predict the compressive strength of HPC. The model was developed using a radial basis kernel function. Results indicated that SVM had high prediction accuracy based on the value of MAPE. Omran et al., (2016) employed SVM based on sequential minimal optimization to forecast the compressive strength of concrete containing Haydite lightweight aggregate and Portland limestone cement. Deng et al., (2018) used SVM for predicting the compressive strength of recycled aggregate concrete (RAC). Performance evaluation showed that the model achieved acceptable predictive accuracy. In another study conducted by Behnood et al., (2015), SVM was employed to forecast the tensile strength of SFRC and revealed better performance than that of nonlinear regression analysis. The elastic modulus of HSC and RAC was also predicted via SVM (Mohammadi and Behnood, 2018; Yan and Shi, 2010) and satisfactory results were reported. The least-square support vector machine (LSSVM) is another variation of SVM in which the least-squares loss function is used to build the optimization problem and achieve better accuracy (Kaytez et al., 2015). Several studies evaluated the performance of this model in predicting the mechanical strength of concrete. For instance, Yaseen et al., (2018) proposed the least square support vector regression (LSSVR) to predict the compressive strength of foamed concrete and this model achieved reliable accuracy.

2.2.3.2 Hybrid SVM-based models

The application of SVM within hybrid approaches aims to optimize the process and the performance of standalone SVM models. Several studies have used FA, for instance, as an optimization approach to estimate the compressive strength and the shear strength of concrete. For example, Pham et al., (2016) adopted the FA-LSSVR hybrid model to estimate the compressive strength of HPC. FA was mainly incorporated to evaluate the hyperparameters of LSSVM. Two experiments were conducted: the first consisted of splitting data into training and testing sets, while the second one was based on 10-fold cross-validation. Results uncovered the strong ability of FA-LSSVR in forecasting the compressive strength of concrete, which was reflected by MAPE. More recent studies investigated the prediction of the shear strength of RC and SFRC beams along with FRP

reinforced slabs through FA-LSSVM algorithm (Al-Musawi et al., 2020; Chou et al., 2016; Vu and Hoang, 2016). The model comprised input parameters including geometrical characteristics of beams and slabs, as well as the mechanical properties of reinforcing components. Results showed that FA-LSSVM achieved accurate forecasting of the shear strength of concrete structures. In another study conducted by Yu et al., (2018), an enhanced version of a swarm-based algorithm named cat swarm optimization was used to forecast the compressive strength of HPC. The enhanced cat swarm optimization (ECSO) model was employed to optimize the key parameters of SVM. The probabilistic Akaike information criterion was adopted as the objective function for the optimization problem. ECSO-SVM model exhibited high predictive ability, as evidenced by statistical metrics. Keshtegar et al., (2019) developed a new model that hybridizes the response surface method (RSM) and SVM. The model forecasted the shear strength of SFRC beams with satisfactory results. The hybrid RSM-SVM model was also compared to other standalone intelligent models such as RSM, SVR, and classical neural network in addition to eight empirical formulations. It was reported that RSM-SVR model had better accuracy compared to the other models. Cheng et al., (2012) developed an evolutionary fuzzy SVM inference model for time series data, which combines FL, SVM, and GA to estimate the compressive strength of HPC. Results indicated that the developed model performed better than SVM and BPNN as depicted in scatter diagrams presenting actual and predicted values.

2.2.4 Decision tree models

Decision tree models are ML techniques in which formal rules are created through patterns in the data (DeRousseau et al., 2018). As outlined in **Table 2.4**, three decision tree-based models, namely M5P-tree, Multiple Additive Regression Trees (MART) and Random Forest (RF) have mostly been used to predict the mechanical properties of concrete. The process and application of each model are discussed below.

Table 2.3: Summary of adopted SVM-based models

Dataset size	TR (%)	VAL (%)	TS (%)	Concrete Type	Methods Used	Input Variables	Output	Statistical Index	Ref.
1030	10-fold cross-validation			HPC	SVM	Cement, BFS, fly ash, water, superplasticizer, coarse aggregate, fine aggregate, age of testing	Compressive strength	R ² , RMSE, MAPE	(Chou et al., 2011)
1030	90	N/A	10	HPC	Evolutionary fuzzy SVM inference model for time series data	Cement, BFS, fly ash, water, superplasticizer, coarse aggregate, fine aggregate, age of testing	Compressive strength	R, R ² , RMSE, MAE	(Cheng et al., 2012)
144	10-fold cross-validation			Concrete containing fly ash, Haydite lightweight aggregate and Portland limestone cement	SVM	Cement type, curing age, water, cementitious material, fly ash, sand, pea gravel, Haydite lightweight aggregate, Micro Air	Compressive strength	R, RMSE, MAE	(Omran et al., 2016)
239	10-fold cross-validation			HPC	FA-LSSVR	Cement, fine aggregate, small coarse aggregate, medium coarse aggregate, water, superplasticizer, concrete age	Compressive strength	RMSE, MAPE, R ²	(Pham et al., 2016)
91	N/A	N/A	N/A	Foamed concrete	LSSVR	Cement, oven dry density, water/binder ratio, foamed volume	Compressive strength	R, RMSE, MAE, Relative RMSE, Relative MAE	(Yaseen et al., 2018)
1761	70	N/A	30	HPC	ECISO-SVM	Water, cement, BFS, fly ash, superplasticizer, coarse, aggregate, fine aggregate, curing age	Compressive strength	Squared correlation coefficient, σ , Relative RMSE, R ² MAPE, Index of agreement, MAE, SRL, Error to signal ratio	(Yu et al., 2018)
74	68	N/A	32	RAC	SVM	Recycled coarse aggregate replacement ratio, recycled fine aggregate replacement ratio, fly ash replacement ratio, w/c ratio	Compressive strength	Relative error	(Deng et al., 2018)

Table 2.3 (continued)

Dataset size	TR (%)	VAL (%)	TS (%)	Concrete Type	Methods Used	Input Variables	Output	Statistical Index	Ref.
82	88	N/A	12	FRP reinforced (slabs)	Firefly algorithm combined with LSSVM	Types of column section, section area of column, effective flexural depth of slab, compressive strength of concrete, Young's modulus of the FRP slab, reinforcement ratio	Shear strength	RMSE, MAPE, R ²	(Vu and Hoang, 2016)
	10-fold cross-validation								
214	10-fold cross-validation			RC	Smart artificial firefly algorithm based LSSVR	Ratio of effective depth to breadth of beam, yield strength of horizontal reinforcement, yield strength of vertical web reinforcement, ratio of shear span to effective depth, ratio of effective span to effective depth, main reinforcement ratio, horizontal and vertical shear reinforcement ratio	Shear strength	R, RMSE, MAE, MAPE	(Chou et al., 2016)
139	70	N/A	30	SFRC	Firefly algorithm Combined with SVR	Concrete strength, longitudinal steel strength, shear span to depth ratio, effective depth of beam, beam width, maximum aggregate size, longitudinal steel ratio, steel fiber volume fraction, fiber length, the equivalent fiber diameter	Shear strength	Scatter index, MAPE, RMSE, MAE, Root mean square relative error, mean relative error, BIAS	(Al-Musawi et al., 2020)
139	75	N/A	25	SFRC	Response surface method combined with SVR	Concrete strength, longitudinal steel strength, shear span to depth ratio, effective depth of beam, beam width, maximum aggregate size, longitudinal steel ratio, steel fiber volume fraction, fiber length, equivalent fiber diameter	Shear strength	MAE, RMSE, modified agreement index, modified Nash and Sutcliffe efficiency	(Keshtegar et al., 2019)
980	70	15	15	SFRC	SVM	Water to binder ratio, concrete compressive strength, age of the specimen, fiber reinforcing index	Tensile strength	R, R ² , MAPE, MAE, RMSE	(Behnood, Verian, et al., 2015)

Table 2.3 (continued)

Dataset size	TR (%)	VAL (%)	TS (%)	Concrete Type	Methods Used	Input Variables	Output	Statistical Index	Ref.
400	80	N/A	20	RAC	SVR	w/c ratio, volume replacement of natural aggregate by recycled aggregate, coarse aggregate to cement ratio, fine aggregate to total aggregate ratio, saturated surface dry specific gravity of the mixed (i.e., natural and recycled) coarse aggregates, water absorption of the mixed coarse aggregates, 28-day cube compressive strength of the mixture	Elastic modulus	RMSE MAE MAPE	(Mohammadi and Behnood, 2018)
159	78 81	N/A N/A	22 19	HSC Normal concrete	SVM	Compressive strength of concrete	Elastic modulus	RMSE, MAPE	(Yan and Shi, 2010)
650	50	N/A	50	Concrete containing coarse recycled concrete aggregates	LSSVR	Coarse recycled concrete aggregate replacement ratio, aggregate to cement ratio, bulk density of recycled concrete aggregate, water absorption of coarse recycled concrete aggregate, water-to-cement ratio	Compressive strength	RMSE, MAE, MAPE	(Gholampour et al., 2020)
421	47	N/A	53	Concrete containing coarse recycled concrete aggregates	LSSVR	Coarse recycled concrete aggregate replacement ratio, aggregate to cement ratio, bulk density of recycled concrete aggregate, water absorption of coarse recycled concrete aggregate, water-to-cement ratio	Elastic modulus	RMSE, MAE, MAPE	(Gholampour et al., 2020)
346	51	N/A	49	Concrete containing coarse recycled concrete aggregates	LSSVR	Coarse recycled concrete aggregate replacement ratio, aggregate to cement ratio, bulk density of recycled concrete aggregate, water absorption of coarse recycled concrete aggregate, water-to-cement ratio	Tensile strength	RMSE, MAE, MAPE	(Gholampour et al., 2020)

2.2.4.1 M5P-tree

M5P is an expanded version of Quinlan's M5 algorithm, where a conventional decision tree is combined with linear regression functions at the nodes. The construction of the M5 model is performed through three main steps (Behnood, Olek, et al., 2015; Zhan et al., 2011). First, a tree model is built using a splitting criterion that divides the data into subsets. Then, tree pruning is performed to remove or merge unwanted subtrees in order to overcome data overfitting that appeared during tree construction. Finally, a smoothing process is performed to compensate for the sharp discontinuities occurring between adjacent linear models at the pruned tree leaves. This process is schematically represented in **Figure 2.5**.

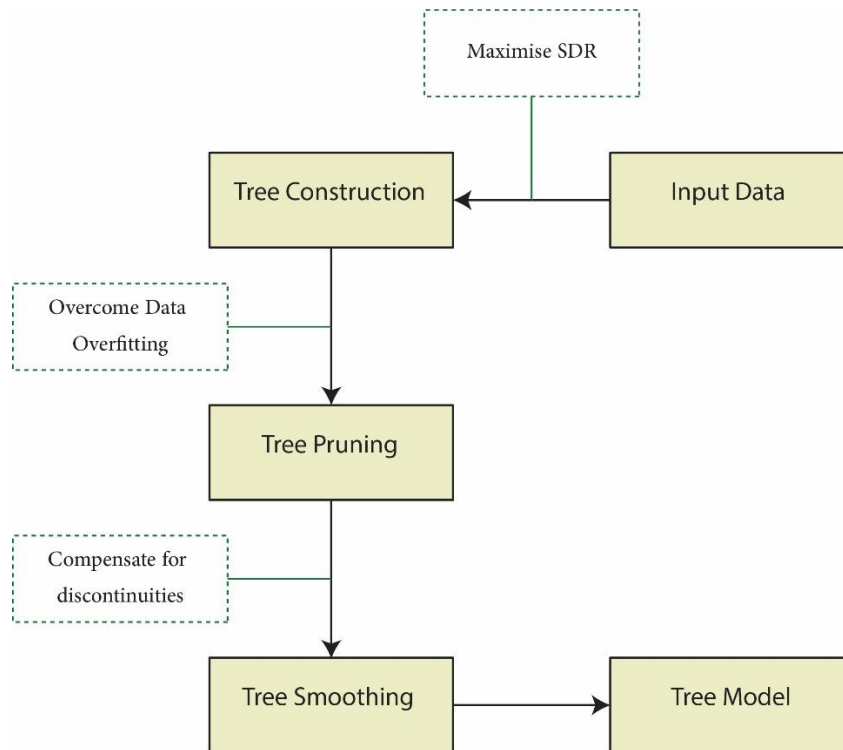


Figure 2.5: M5-tree process.

In order to split the input space and generate the regression tree in this model, a measure called the standard deviation factor (SDR), which is the maximum reduction in output errors after branching, is considered (Behnood et al., 2017; Behnood, Verian, et al., 2015). M5 algorithm was modified to M5P to deal with enumerated attributes as well as attribute

missing values. In the M5P tree algorithm, all enumerated attributes are transformed into binary variables before tree construction (Almasi et al., 2017). M5P has been used in several studies to predict the mechanical properties of concrete (Behnood et al., 2017; Deepa et al., 2010; Omran et al., 2016). The application of this model included forecasting the compressive strength of HPC and foamed concrete, along with concrete fabricated with fly ash, Haydite lightweight aggregate, and Portland limestone cement (Deepa et al., 2010; Omran et al., 2016; Yaseen et al., 2018). The model comprised various input variables including concrete mixture ingredients, age of testing, and other dimensionless ratios. It was concluded that the M5P model predicted the compressive strength accurately, as evidenced by statistical metrics.

2.2.4.2 MART

MART is a powerful meta classifier that involves the conventional classification and regression trees (CART) enhanced with stochastic gradient boosting that tends to improve the accuracy of learning algorithms by combining and fitting a series of models with low error rates, forming an ensemble model that has better performance (Elish, 2009; Friedman, 2002). MART has been used by Chou et al., (2011) to predict the compressive strength of HPC. The model achieved adequate predictive accuracy and outperformed both ANN and SVM in terms of R^2 .

2.2.4.3 Random forest

Random forest (RF) has also been adopted in multiple studies as a forecasting tool. RF combines multiple decision trees, each of which is built from a new training set based on the bagging method (Chehreh Chelgani et al., 2016; Han et al., 2019). The bagging method, which is also known as bootstrap aggregation, is an ensemble training method that consists of two steps: bootstrap and aggregation. In the first step, identically distributed and independent datasets are created by randomly resampling the original set of data. During the second step, the new datasets are used for training the base predictors independently. Results are obtained by averaging the predictions of each tree predictor through the aggregation method. The RF has been used by several researchers for predicting the mechanical strength of concrete. For instance, Han et al., (2019) employed RF to forecast the compressive strength of HPC. Earlier study by Mangalathu and Jeon (2018) adopted

the same model for predicting the shear strength of RC beam-column joints. Results of both studies were in good agreement, affirming the ability of RF in producing reliable predictions. Another research conducted by J. Zhang et al., (2019) consisted of applying RF to estimate the uniaxial compressive strength of SCC. The RF model was enhanced with a beetle antennae search (BAS) algorithm which was developed from the behavior of the beetle that tunes to a position with a higher concentration of odor when searching nearby areas using its two antennae (Jiang and Li, 2017). The authors concluded that BAS demonstrated great capacity in finding optimum hyper-parameters of RF and that the hybrid BAS-RF algorithm showed good forecasting ability.

2.2.5 Evolutionary algorithms

Evolutionary algorithms form a category of heuristic search methods in which the process of finding a solution in the search space is based on the mechanism of biological evolution including selection, mutation, recombination, reproduction, and recombination (Eiben and Smit, 2011; Vikhar, 2017). The general process of evolutionary algorithms is illustrated in **Figure 2.6**. First, an initial population representing a set of candidate solutions is randomly generated. Then, the evaluation of this population is performed via the fitness function. The next generation which comprises a better set of candidates is then generated through recombination and mutation. Recombination consists of generating new candidates via a binary operator applied on the previous generation (parents). Mutation only modifies one candidate from the previous set. After both operators, i.e. recombination and mutation, are applied, a new generation is created based on the fitness function. This iterative process stops when the desired value of fitness function is achieved or when the maximum number of generations is reached.

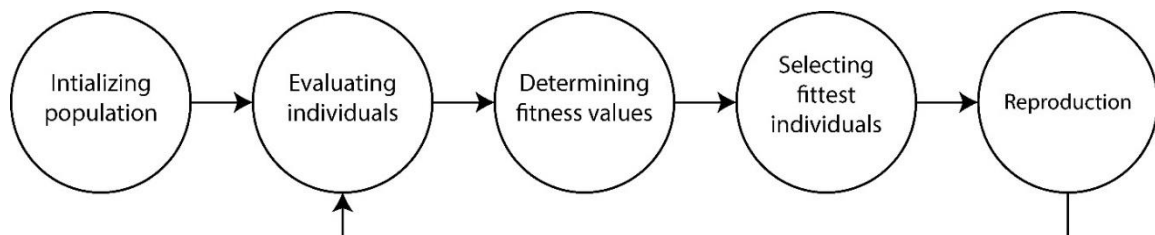


Figure 2.6: General process of evolutionary algorithms.

Table 2.4: Summary of employed decision tree models

Dataset size	TR (%)	VAL (%)	TS (%)	Concrete Type	Methods Used	Input Variables	Output	Statistical Index	Ref.
300	N/A	N/A	N/A	HPC	M5P-tree	Cement, BFS, fly ash, water, superplasticizer, coarse and fine aggregates, and curing age	Compressive strength	RMSE, MAE, R	(Deepa et al., 2010)
1030	10- fold cross-validation			HPC	MART Bagging regression trees	Cement, BFS, fly ash, water, superplasticizer, coarse aggregate, fine aggregate, age of testing	Compressive strength	R ² , RMSE, MAPE	(Chou et al., 2011)
144	10- fold cross-validation			Concrete containing FA, Haydite lightweight aggregate and Portland limestone cement	M5P-tree M5-rules REPTree	Cement type, curing age, water, cementitious material, fly ash, sand, pea gravel, Haydite lightweight aggregate, Micro Air	Compressive strength	R, RMSE, MAE	(Omran et al., 2016)
1030	5- fold cross-validation			HPC	Genetic weighted pyramid operation tree	Cement, fly ash, slag, water, superplasticizer, coarse aggregate, fine aggregate, age of testing	Compressive strength	RMSE, MAE, MAPE, Reference index	(Cheng et al., 2014)
1912	85	N/A	15	Normal concrete HPC	M5P-tree	Cement, water, fly ash, BFS, superplasticizer, coarse aggregate, fine aggregate, age of concrete	Compressive strength	Slope of regression line (SRL), R, R ² , MAPE, MAE, RMSE	(Behnood et al., 2017)
91	N/A	N/A	N/A	Foamed concrete	M5-Tree	Cement, oven dry density, water to binder ratio, foamed volume	Compressive strength	R, RMSE, MAE, Relative RMSE, Relative MAE	(Yaseen et al., 2018)
1030	90		10	HPC	Random Forest	Water to binder ratio, BFS to water ratio, fly ash to water ratio, coarse aggregate to binder ratio, coarse aggregate to fine aggregate ratio	Compressive strength	R, MAE, RMSE, MAPE	(Han et al., 2019)
131	10- fold cross-validation			SCC	Beetle antennae search based random forest	Water to binder ratio, macro-synthetic polypropylene fiber, steel fiber, scoria, crumb rubber, natural fine aggregate, natural coarse aggregate	Compressive strength	RMSE, R	(J. Zhang et al., 2019)

Table 2.4 (continued)

Dataset size	TR (%)	VAL (%)	TS (%)	Concrete Type	Methods Used	Input Variables	Output	Statistical Index	Ref.
536	70	N/A	30	RC	Random Forest	Concrete compressive strength, joint transverse reinforcement, joint shear stress, in-plane joint geometry, out-of-plane joint geometry, ratio of beam depth to column depth, joint eccentricity parameter, ratio of beam width to column width, column axial load ratio, beam bar bond parameter, column to beam flexural moment strength ratio, column intermediate longitudinal reinforcement factor	Shear Strength	μ , Covariance, COV, MSE, ABS, R^2	(Mangalathu and Jeon, 2018)
454	80	N/A	20	RAC	M5 Tree	Compressive strength, w/c ratio, coarse aggregate to cement ratio, fine aggregate to total aggregate ratio, volume fraction of recycled aggregate in RAC, saturated surface dry specific gravity, water absorption of the mixed coarse aggregates (natural aggregate + recycled aggregate)	Elastic Modulus	R, R^2	(Behnood, Olek, et al., 2015)
470	80	N/A	20	Concrete containing waste foundry sand	M5P-Tree	Waste foundry sand to cement ratio, water to cement ratio, coarse aggregate to cement ratio, fine aggregate to total aggregate ratio, waste foundry sand to fine aggregate ratio, superplasticizer to cement ratio multiplied by 1000, and age of concrete	Compressive strength	RMSE, MAE, MAPE, R^2 , R	(Behnood and Golafshani, 2020)
172	80	N/A	20	Concrete containing waste foundry sand	M5P-Tree	Waste foundry sand to cement ratio, water to cement ratio, coarse aggregate to cement ratio, fine aggregate to total aggregate ratio, waste foundry sand to fine aggregate ratio, superplasticizer to cement ratio multiplied by 1000, and age of concrete	Elastic modulus	RMSE, MAE, MAPE, R^2 , R	(Behnood and Golafshani, 2020)
295	80	N/A	20	Concrete containing waste foundry sand	M5P-Tree	Waste foundry sand to cement ratio, water to cement ratio, coarse aggregate to cement ratio, fine aggregate to total aggregate ratio, waste foundry sand to fine aggregate ratio, superplasticizer to cement ratio multiplied by 1000, and age of concrete	Tensile strength	RMSE, MAE, MAPE, R^2 , R	(Behnood and Golafshani, 2020)
40	15-fold cross validation 20-fold cross validation			high-volume mineral admixture concrete	M5 M5P	Age of testing, cement, fly ash, slag content	Compressive strength	R^2 , MAE	(Ayaz et al., 2015)

Table 2.4 (continued)

Dataset size	TR (%)	VAL (%)	TS (%)	Concrete Type	Methods Used	Input Variables	Output	Statistical Index	Ref.
650	50	N/A	50	Concrete containing coarse recycled concrete aggregates	M5	Coarse recycled concrete aggregate replacement ratio, aggregate to cement ratio, bulk density of recycled concrete aggregate, water absorption of coarse recycled concrete aggregate, water-to-cement ratio	Compressive strength	RMSE, MAE, MAPE	(Gholampour et al., 2020)
650	50	N/A	50	Concrete containing coarse recycled concrete aggregates	M5	Coarse recycled concrete aggregate replacement ratio, aggregate to cement ratio, bulk density of recycled concrete aggregate, water absorption of coarse recycled concrete aggregate, water-to-cement ratio	Compressive strength	RMSE, MAE, MAPE	(Gholampour et al., 2020)
421	47	N/A	53	Concrete containing coarse recycled concrete aggregates	M5	Coarse recycled concrete aggregate replacement ratio, aggregate to cement ratio, bulk density of recycled concrete aggregate, water absorption of coarse recycled concrete aggregate, water-to-cement ratio	Elastic modulus	RMSE, MAE, MAPE	(Gholampour et al., 2020)
346	51	N/A	49	Concrete containing coarse recycled concrete aggregates	M5	Coarse recycled concrete aggregate replacement ratio, aggregate to cement ratio, bulk density of recycled concrete aggregate, water absorption of coarse recycled concrete aggregate, water-to-cement ratio	Tensile strength	RMSE, MAE, MAPE	(Gholampour et al., 2020)

Evolutionary algorithms have been widely adopted for predicting concrete strength. **Table 2.5** entails some recent studies that adopted evolutionary algorithms for assessing concrete strength. Gandomi et al., (2014, 2017) employed gene expression programming (GEP) to predict the shear strength of slender RC beams. Minimizing the objective function that comprises the values of statistical indexes corresponding to learning, validation, and testing data has been performed to get the best GEP algorithm. The model achieved good predictive accuracy, and a comparative study revealed the superiority of GEP over design codes such as the ACI and Eurocode 2. Linear genetic programming is another evolutionary algorithm that has been used for instance in predicting the compressive strength of carbon fiber reinforced plastic (CFRP) confined concrete (Amir Hossein Gandomi, Alavi, and Sahab, 2010). Four different formulations have been developed through LGP model. Results showed that the formulations can provide strong accuracy. Parametric analysis was also conducted to figure out the impact of influencing parameters. The obtained results were in good agreement with those presented from experimental studies of other researchers. Golafshani and Behnood (2018) adopted three models, namely genetic programming (GP), artificial bee colony programming (ABCP), and biogeography-based programming (BBP) to forecast the elastic modulus of RAC. The developed models achieved reliable accuracy. Also, water absorption along with fine aggregate-to-total aggregate ratio and compressive strength of concrete had significant effect on the elastic modulus of RAC.

2.2.6 Selection of model inputs

Selection of the most relevant features needed for training and testing the different ML models is key to simplifying the models and improving their performance. Beside computational efforts, human intelligence and experience are needed to select the most suitable parameters for running ML models. This leads to an accurate selection of the inputs that have noteworthy impact on concrete strength and avoiding parameters with low influence, which can save computation time. Several studies adopted common features for predicting concrete strength. For example, binder content, aggregates, and mineral additions such as fly ash and blast furnace slag have been extensively integrated (P. G. Asteris et al., 2016; Panagiotis G Asteris and Kolovos, 2019; Bui et al., 2018; Cheng et al., 2012; Chou et al., 2011; Deepa et al., 2010; Han et al., 2019; Yu et al., 2018).

Table 2.5: Summary of used evolutionary algorithms

Dataset size	TR (%)	VAL (%)	TS (%)	Concrete Type	Methods Used	Input Variables	Output	Statistical Index	Ref.
1942	70	15	15	RC	GEP	Beam width, effective depth, shear span to depth ratio, compressive strength, longitudinal reinforcement ratio	Shear strength	R, MAE, RMSE	(Amir H. Gandomi et al., 2014)
466	70	15	15	RC	GEP	Beam width, effective depth, shear span to depth ratio, compressive strength, longitudinal reinforcement ratio, amount of shear reinforcement	Shear strength	R, MAE, RMSE	(Amir H. Gandomi et al., 2017)
1938	70	15	15	RC	Linear genetic programming	Compressive strength, mechanic arm, longitudinal reinforcement ratio, maximum size of coarse aggregate, shear span to depth ratio	Shear strength	R, MAE, RMSE	(A H Gandomi et al., 2011)
208	67	14	19	SFRC	Multi expression programming (MEP)	shear span to depth ratio, average fiber matrix interfacial bond stress, fiber factor, splitting tensile strength, split-cylinder strength of fiber concrete, compressive strength of concrete, longitudinal reinforcement ratio	Shear strength	R ² , MAE, RMSE	(Sarveghadi et al., 2019)
83	53	22	25	RC	GEP	the axial force, the width of the cross-section, 28-day compressive strength of concrete, the ratio of shear span to the effective depth of the cross-section, the percentage of longitudinal reinforcement, the cross-sectional area, the transverse reinforcement ratio, and the yield stress of the transverse reinforcement,	Shear strength	R, MAE, RMSE	(Aval et al., 2017)
1028	70	N/A	30	HPC	Geometric Semantic Genetic Programming	Cement, Fly ash, Blast furnace slag, Water, Superplasticizer, Coarse aggregate, Fine aggregate, Age of testing.	Compressive strength	RMSE	(Castelli et al., 2013)
70	81	N/A	19	Normal concrete	Linear genetic programming	Compressive strength	Elastic Modulus	R, MAE	(Amir Hossein Gandomi, Alavi, Sahab, et al., 2010)
89	78	N/A	22	HSC					
104	54	19	27	FRP-Reinforced concrete	GEP	Compressive strength, beam width, effective depth, shear span to depth ratio, longitudinal reinforcement ratio, modulus of elasticity of steel and FRP longitudinal bars	Shear strength	Average absolute error	(Kara, 2011)

Table 2.5 (continued)

Dataset size	TR (%)	VAL (%)	TS (%)	Concrete Type	Methods Used	Input Variables	Output	Statistical Index	Ref.
101	90	N/A	10	CFRP confined concrete	Linear genetic programming	Diameter of the concrete cylinder, thickness of the CFRP layer, ultimate tensile strength of the CFRP laminate, unconfined ultimate concrete strength	Compressive strength	R, MAPE	(Amir Hossein Gandomi, Alavi, and Sahab, 2010)
400	80	N/A	20	RAC	GP ABCP BBP	Water to cement ratio, volume fraction of coarse RA in RAC, coarse aggregate to cement ratio, fine aggregate to total aggregate ratio, saturated surface dry specific gravity of the mixed coarse aggregates, water absorption of the mixed coarse aggregates, and 28-day cube compressive strength of the mixture.	Elastic modulus	MAE, RMSE, MAPE, OBJ	(Golafshani and Behnood, 2018)

Aggregates are also an important parameter affecting the mechanical strength of concrete. Appropriate hardness, granular size distribution, and cleanness of aggregates have a significant effect on the strength of concrete materials. Supplementary cementitious materials such as fly ash, blast furnace slag, and silica fume are amongst the most commonly incorporated materials in concrete owing to the beneficial effect of their pozzolanic properties and microfiller effect on the compressive strength of concrete (Ayaz et al., 2015; Nath and Sarker, 2014). For instance, fly ash can increase the workability resulting in less mixing water needed for concrete, which in turn can improve the strength of concrete. Ultrafine silica fume particles densify the cement paste-aggregate interfacial zone, dramatically enhancing compressive strength. Moreover, the water-to-binder (w/b) ratio, curing conditions and age, and chemical admixtures have been considered as crucial input parameters for assessing concrete strength. For instance, increasing the w/b ratio decreases the proportion of hydrated products and increases the porous structure in concrete, leading to lower mechanical strength.

2.3 Discussion and critical analysis

ML techniques have been adopted by several researchers as a new approach to forecast the mechanical strength of concrete materials. As entailed in **Table 2.6**, statistical metrics retrieved from a non-exhaustive list of studies reflects the noteworthy advantage of ML techniques over empirical formulas for the same testing data.

This can be explained by the ability of ML techniques in accurately predicting the properties of complex concrete materials, where the relationship between concrete mixture ingredients and the corresponding compressive strength is highly nonlinear. Also, it can be observed in Tables 2, 3, 4, and 5 that ML models were developed based on extensive databases, implying that the number of data examples used for developing those models is significantly higher than that of empirically developed equations. Accordingly, the applicability of empirical models is limited to few examples, leading to higher error when forecasting “unseen” data. Furthermore, a potential problem associated with empirical and statistical formulas is their inability to provide an accurate estimation of the mechanical strength of concrete incorporating new admixtures, thus ignoring the effect of the new ingredients on the final output. Conversely, ML models offer the advantage of updating

the predictive mechanism by controlling the number of inputs (features) and ingredients considered within the model. Moreover, the impact of each input variable on concrete strength can be determined through ML techniques via sensitivity analysis. These advantages of ML models make the application of statistical and empirical models limited to some problems in which the studied concrete has a simple structure since conventional methods are convenient in providing explicit mathematical formulas.

In addition to the difference between statistical approaches and ML models, there are contrasts between ML algorithms in terms of process and performance. Thus, each ML technique has several advantages and drawbacks compared to other models. This can be supported by the values of statistical metrics shown in **Table 2.7**, which reveals the performance of multiple ML models over the same testing data. As mentioned previously, several studies adopted ANN because of their inherent advantages. An explicit vector of weights and biases along with a fixed number of hidden layers and hidden neurons achieved after several trials can lead to a well-defined structure of ANN model. However, such repetitive trial and error-tuning process is time-consuming. Another major weakness of the ANN model is associated with the BP approach, where the training process is performed through a gradient descent algorithm on the error space that includes local minima (Jafrasteh and Fathianpour, 2017; L. Wang et al., 2015). As outlined in **Figure 2.7**, convergence of BP to local minima and avoidance of global solutions has been a concern (Chandwani et al., 2015; O. Akande et al., 2014; Yuan et al., 2014). Using ELM as an alternative method can mitigate the problem of convergence to local optima and provide more simplicity since no learning rate and stopping criteria are required (Christou et al., 2019). Al-Shamiri et al., (2019) compared ELM to BPNN and recorded better performance with ELM model. However, the adopted model could require more hidden neurons than the BP approach due to the random determination of the input weights and hidden biases (L. Zhang and Zhang, 2017; Zhu et al., 2005). An excessive number of hidden neurons used in complex models leads to overfitting, which means that the complexity of concrete properties can be overestimated by ANN (Behnood and Golafshani, 2018). To overcome the aforementioned drawbacks, various metaheuristic and ensemble models have been proposed to enhance ANN performance and process.

Table 2.6: Comparison between ML models and empirical formulas over the same testing data

Ref.	Output	Model	Statistical metrics					
(Keshtegar et al., 2019)	Shear strength	(Kwak et al., 2002) RSM-SVR	MAE	0.508 0.186	RMSE	0.699 0.233		
(Sarveghadi et al., 2019)	Shear strength	(Kwak et al., 2002) MEP	R	0.950 0.952	MAE	0.804 0.520	RMSE	1.680 0.733
(Al-Musawi et al., 2020)	Shear strength	(Kwak et al., 2002) SVR-FFA	MAE	0.524 0.176	RMSE	0.717 0.277		
(Vu and Hoang, 2016)	Shear strength	(Ospina et al., 2003) ANN	R ²	0.91 0.96	RMSE	117.51 53.190	MAPE	15.48 10.48
(Xu, Zhao, et al., 2019)	Compressive strength	(Pereira et al., 2012) ANN	RMSE	28.15 7.71	MAPE	54.22 15.13		
(Xu, Zhao, et al., 2019)	Elastic modulus	(Sri Ravindrarajah and Tam, 1985) ANN	RMSE	5749.73 4425.89	MAPE	17.85 11.21		
(Xu, Zhao, et al., 2019)	Tensile strength	(Pereira et al., 2012) ANN	RMSE	0.720 0.480	MAPE	14.650 11.890		

Table 2.7: Comparison between ML models over the same testing data

Ref.	Dataset size	Output	Models	Statistical metrics					
(Chou et al., 2011)	1030	Compressive strength	ANN	R ²	0.909	RMSE	5.030	MAPE	10.903
			SVM		0.885		5.619		12.773
			MART		0.911		4.949		13.886
(Bui et al., 2018)	1133	Compressive strength	GEP	R	0.910	MAE	5.200		
			FA-LSSVR		0.940		3.860		
			MFA-ANN		0.950		3.410		
(Van Dao et al., 2019)	210	Compressive strength	ANN	R ²	0.851	MAE	1.989	RMSE	2.423
			ANFIS		0.879		1.655		2.265
(Yu et al., 2018)	1761	Compressive strength	BPNN	R ²	0.960	MAE	5.038		
			ELM		0.934		4.278		
			ANFIS		0.906		4.183		
			SVM		0.793		5.950		
			M5		0.937		4.028		
			ECSO-SVM		0.942		3.980		
(Pham et al., 2016)	239	Compressive strength	ANN	R ²	0.760	RMSE	6.740	MAPE	13.410
			SVM		0.790		6.070		12.020
			FA-LSSVR		0.870		4.860		9.810
(Al-Shamiri et al., 2019)	324	Compressive strength	ELM	R	0.9965	MAE	0.6049	RMSE	0.7998
			BP		0.9949		0.7372		0.9498
(Yuan et al., 2014)	180	Compressive strength	ANN	R ²	0.680	RMSE	3.21		
			GA-ANN		0.813		2.22		
			ANFIS		0.950		1.46		
(Behnood, Verian, et al., 2015)	980	Tensile strength	ANN	R ²	0.874	MAE	0.408	RMSE	0.526
			SVM		0.890		0.400		0.524
			M5 Tree		0.866		0.412		0.598
(Keshtegar et al., 2019)	139	Shear strength	ANN	MAE	0.322	RMSE	0.461		
			SVR		0.622		1.040		
			RSM		0.347		0.444		
			RSM-SVR		0.186		0.233		

For instance, using GA and ensemble algorithms such as bagging and gradient boosting to optimize the predictive accuracy of ANN has proven to be effective (Ibrahim et al., 2013; Yuan et al., 2014). However, GA-ANN model adopted by Yuan et al., (2014) tended to increase model complexity and computation time. Another alternative consists of using ANFIS models, which combine the learning abilities of ANN and the reasoning capabilities of FL (Yuan et al., 2014). Şahin and Erol (2017) reported that ANFIS could detect the nonlinear structure process with rapid learning capability. This is further supported by a comparative study conducted by Van Dao et al., (2019). However, ANFIS may suffer from issues related to fuzzy rule selection that affect its performance along with inability to generate more than one output variable (Yu et al., 2018).

Regarding SVM models, they have shown powerful nonlinear mapping and generalization abilities (Yu et al., 2018). They also have the ability to identify and integrate support vectors during the training process, which prevents non-support vectors from affecting the performance of the model. However, this technique has multiple disadvantages, such as the time-consuming and heuristic approach of selecting the appropriate kernel function, which depends on the trial and error process. In addition, the performance of the nonlinear SVR technique cannot be easily interpreted because the process of mapping a nonlinear input space to a high dimensional feature space can be complex (Dibike et al., 2014).

The aforementioned techniques, i.e. ANN and SVM, are considered as “black-box” models due to massive node sizes and internal connections (Cheng et al., 2014; Farquad et al., 2014; Yadav and Chandel, 2014). Thus, generating a transparent mathematical formula that describes the functional relationship between input variables and outputs through those models is difficult. To overcome this common problem, decision trees and EA can be deployed. Those models have the ability of generating explicit mathematical formulations that describe the relationships between features and corresponding outputs. However, decision tree algorithms can lead to overfitting issues. In addition, the accuracy of both decision trees and EA is typically lower than that of hybrid and standalone SVM and ANN models, as evidenced by statistical metrics retrieved from different previous studies (Behnood, Verian, et al., 2015; Bui et al., 2018; Yu et al., 2018). Shortcomings of decision tree models can be mitigated through tree-based ensemble models such as RF and MART (Chou et al., 2011). Chou et al., (2011) for instance recorded better results from MART model than those obtained from standalone ANN and SVM. Still, ensemble models bring more complexity to the model and increase computation time. In addition, it can be noticed that the size of the dataset used for developing the models varies from one study to another. Studies that considered fewer data examples may record accurate results. However, the model can exhibit higher error when exposed to new data compared to those developed from more extensive databases.

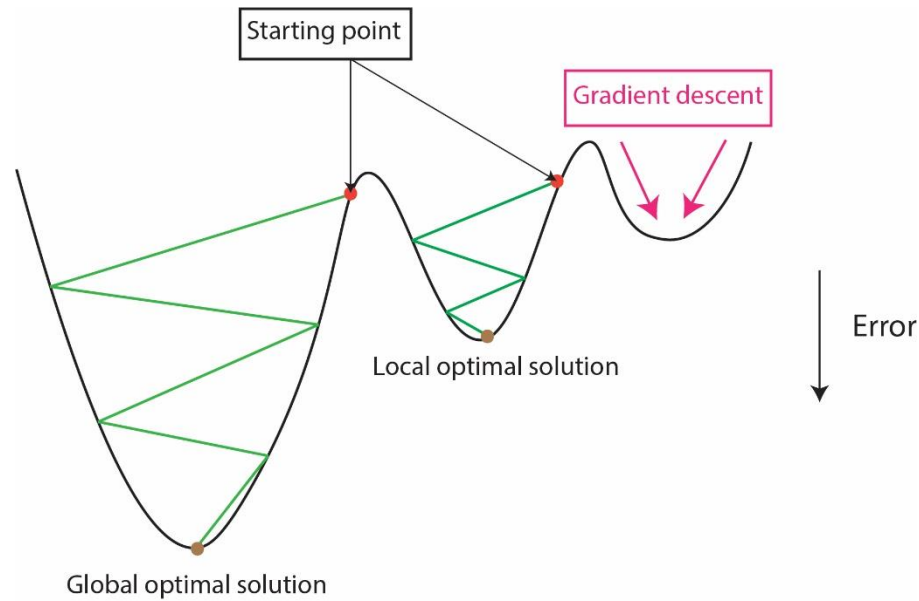


Figure 2.7: BPNN searching mechanism.

2.4 Practical recommendations and knowledge gaps

Since all ML approaches discussed above have various advantages and drawbacks, the selection of the most suitable model is based on different criteria. The nature of the relationship between concrete mixture ingredients and its mechanical strength is a major factor that influences the model choice. If this relationship is highly nonlinear and affected by several features, employing models such as ANN and SVM would be a good choice owing to their great ability in solving problems in non-linear environment with lower error. For more accurate results and better process, optimizing those models with metaheuristic algorithms is effective. However, when model transparency is required, decision trees and evolutionary algorithms can be employed because they can generate explicit mathematical formulas that better describe the physical relationship between inputs and output. Still, the accuracy of both models is lower than that of hybrid and standalone ANN and SVM models as indicated by statistical metrics shown in **Table 2.7**. Adopting ensemble models can increase the accuracy of decision trees but leads to higher computation time and model complexity.

According to the current study, hybrid ANN and SVM models have shown the best ability to predict concrete strength in terms of accuracy and process. Although they increase computation time, applying those models on extensive databases with appropriate feature selection would generate the most accurate results. However, the only way to select the most suitable metaheuristic model is based on a trial and error process. Thus, no accurate method exists to select the best optimization algorithm since they can provide different results from one problem to another.

We stand at the brink of a fourth industrial revolution, where data driven intelligent systems, additive manufacturing, robotics, the internet of things, cloud computing, and other emerging technologies are fusing the digital, biological, and physical worlds. The construction field is lagging in capturing the opportunities in this rapidly changing world. Machine learning prediction of the engineering properties of construction materials and structures are a contribution towards generative intelligent design. Yet, diverse knowledge gaps still remain before structural engineers can emulate processes used in robotics, mechatronics and other advanced fields.

2.5 Conclusions

Several recent studies have been conducted to predict the mechanical strength of concrete, exploring the benefits of some approaches and presenting drawbacks of others. In particular, forecasting the strength of complex concrete mixtures by conventional statistical and empirical models has been a fundamental challenge since these models are generally inaccurate, and their development is costly and time-consuming. Thus, researchers have suggested ML models to overcome such drawbacks. In this study, ML models have been grouped into four major types, namely ANN, SVM, decision trees, and EA. The application of those models to predict the compressive strength, shear strength, tensile strength, and elastic modulus of concrete has been reviewed. Also, the advantages and drawbacks of the presented techniques have been critically discussed and compared. It has been realized that the performance of the models is influenced by various factors, such as the nature of the relationship between concrete mixture ingredients and its strength, the size of the training data set, and the number of features adopted in the model. The review of the performance of ML techniques along with their benefits and drawbacks presented in this study should

help engineers in choosing the suitable models for predicting the mechanical strength of concrete. Owing to their ability in providing accurate estimation of concrete strength, further research shall be conducted to examine the reliability of ML models in forecasting the properties of more innovative concrete types such as self-healing concrete, geopolymer concrete, nano-modified, bio-inspired, and other emerging binder systems.

2.6 References

- Ahmadi-Nedushan, B. (2012). Prediction of elastic modulus of normal and high strength concrete using ANFIS and optimal nonlinear regression models. *Construction and Building Materials*, 36, 665–673.
- Al-Musawi, A. A., Alwanas, A. A. H., Salih, S. Q., Ali, Z. H., Tran, M. T., and Yaseen, Z. M. (2020). Shear strength of SFRCB without stirrups simulation: implementation of hybrid artificial intelligence model. *Engineering with Computers*, 36(1), 0.
- Al-Shamiri, A. K., Kim, J. H., Yuan, T. F., and Yoon, Y. S. (2019). Modeling the compressive strength of high-strength concrete: An extreme learning approach. *Construction and Building Materials*, 208, 204–219.
- Almasi, S. N., Bagherpour, R., Mikaeil, R., Ozcelik, Y., and Kalhori, H. (2017). Predicting the Building Stone Cutting Rate Based on Rock Properties and Device Pullback Amperage in Quarries Using M5P Model Tree. *Geotechnical and Geological Engineering*, 35(4), 1311–1326.
- Altun, F., Kişi, Ö., and Aydin, K. (2008). Predicting the compressive strength of steel fiber added lightweight concrete using neural network. *Computational Materials Science*, 42(2), 259–265.
- Amani, J., and Moeini, R. (2012). Prediction of shear strength of reinforced concrete beams using adaptive neuro-fuzzy inference system and artificial neural network. *Scientia Iranica*, 19(2), 242–248.
- Asteris, P. G., Kolovos, K. G., Douvika, M. G., and Roinos, K. (2016). Prediction of self-compacting concrete strength using artificial neural networks. *European Journal of Environmental and Civil Engineering*, 20, s102–s122.
- Asteris, Panagiotis G, and Kolovos, K. G. (2019). Self-compacting concrete strength prediction using surrogate models. *Neural Computing and Applications*, 31, 409–424.
- Atici, U. (2011). Expert Systems with Applications Prediction of the strength of mineral admixture concrete using multivariable regression analysis and an artificial neural network. *Expert Systems With Applications*, 38(8), 9609–9618.
- Aval, S. B. B., Ketabdari, H., and Gharebaghi, S. A. (2017). Estimating Shear Strength of Short Rectangular Reinforced Concrete Columns Using Nonlinear Regression and Gene Expression Programming. *Structures*, 12(July), 13–23.

- Ayaz, Y., Kocamaz, A. F., and Karakoç, M. B. (2015). Modeling of compressive strength and UPV of high-volume mineral-admixed concrete using rule-based M5 rule and tree model M5P classifiers. *Construction and Building Materials*, 94, 235–240.
- Bachir, R., Mohammed, A. M. S., and Habib, T. (2018). Using artificial neural networks approach to estimate compressive strength for rubberized concrete. *Periodica Polytechnica Civil Engineering*, 62(4), 858–865.
- Bashir, R., and Ashour, A. (2012). Neural network modelling for shear strength of concrete members reinforced with FRP bars. *Composites Part B: Engineering*, 43(8), 3198–3207.
- Behnood, A., Behnood, V., Modiri, M., and Esat, K. (2017). Prediction of the compressive strength of normal and high-performance concretes using M5P model tree algorithm. *Construction and Building Materials*, 142, 199–207.
- Behnood, A., and Golafshani, E. M. (2018). Predicting the compressive strength of silica fume concrete using hybrid artificial neural network with multi-objective grey wolves. *Journal of Cleaner Production*, 202, 54–64.
- Behnood, A., and Golafshani, E. M. (2020). Machine learning study of the mechanical properties of concretes containing waste foundry sand. *Construction and Building Materials*, 243, 118152.
- Behnood, A., Olek, J., and Glinicki, M. A. (2015). Predicting modulus elasticity of recycled aggregate concrete using M5' model tree algorithm. *Construction and Building Materials*, 94, 137–147.
- Behnood, A., Verian, K. P., and Gharehveran, M. M. (2015). Evaluation of the splitting tensile strength in plain and steel fiber-reinforced concrete based on the compressive strength. *Construction and Building Materials*, 98, 519–529.
- Belalia Douma, O., Boukhatem, B., Ghrici, M., and Tagnit-Hamou, A. (2017). Prediction of properties of self-compacting concrete containing fly ash using artificial neural network. *Neural Computing and Applications*, 28(s1), 707–718.
- Bilim, C., Atiş, C. D., Tanyildizi, H., and Karahan, O. (2009). Predicting the compressive strength of ground granulated blast furnace slag concrete using artificial neural network. *Advances in Engineering Software*, 40(5), 334–340.
- Bourdeau, M., Nefzaoui, E., Guo, X., and Chatellier, P. (2019). Modeling and forecasting building energy consumption : A review of data- driven techniques. *Sustainable Cities and Society*, 48(April), 101533.
- Bui, D. K., Nguyen, T., Chou, J. S., Nguyen-Xuan, H., and Ngo, T. D. (2018). A modified firefly algorithm-artificial neural network expert system for predicting compressive and tensile strength of high-performance concrete. *Construction and Building Materials*, 180, 320–333.
- Castelli, M., Vanneschi, L., and Silva, S. (2013). Prediction of high performance concrete strength using Genetic Programming with geometric semantic genetic operators. *Expert Systems with Applications*, 40(17), 6856–6862.

- Chandwani, V., Agrawal, V., and Nagar, R. (2015). Modeling slump of ready mix concrete using genetic algorithms assisted training of Artificial Neural Networks. *Expert Systems with Applications*, 42(2), 885–893.
- Chehreh Chelgani, S., Matin, S. S., and Makaremi, S. (2016). Modeling of free swelling index based on variable importance measurements of parent coal properties by random forest method. *Measurement: Journal of the International Measurement Confederation*, 94, 416–422.
- Cheng, M. Y., Chou, J. S., Roy, A. F. V., and Wu, Y. W. (2012). High-performance Concrete Compressive Strength Prediction using Time-Weighted Evolutionary Fuzzy Support Vector Machines Inference Model. *Automation in Construction*, 28, 106–115.
- Cheng, M. Y., Firdausi, P. M., and Prayogo, D. (2014). High-performance concrete compressive strength prediction using Genetic Weighted Pyramid Operation Tree (GWPOT). *Engineering Applications of Artificial Intelligence*, 29, 104–113.
- Chithra, S., Kumar, S. R. R. S., Chinnaraju, K., and Ashmita, F. A. (2016). A comparative study on the compressive strength prediction models for High Performance Concrete containing nano silica and copper slag using regression analysis and Artificial Neural Networks. *Construction and Building Materials*, 114, 528–535.
- Chou, J., Ph, D., Chiu, C., Ph, D., Farfoura, M., and Al-taharwa, I. (2011). *Optimizing the Prediction Accuracy of Concrete Compressive Strength Based on a Comparison of Data-Mining Techniques*. 25(June), 242–253.
- Chou, J., Ph, D., Ngo, N., Pham, A., and Ph, D. (2016). *Shear Strength Prediction in Reinforced Concrete Deep Beams Using Nature-Inspired Metaheuristic Support Vector Regression*. 30(1), 1–9.
- Christou, V., Tspouras, M. G., Giannakeas, N., Tzallas, A. T., and Brown, G. (2019). Hybrid extreme learning machine approach for heterogeneous neural networks. *Neurocomputing*, 361, 137–150.
- Dantas, A. T. A., Batista Leite, M., and De Jesus Nagahama, K. (2013). Prediction of compressive strength of concrete containing construction and demolition waste using artificial neural networks. *Construction and Building Materials*, 38, 717–722.
- Deepa, C., Sathiyakumari, K., and Sudha, V. P. (2010). Prediction of the Compressive Strength of High Performance Concrete Mix using Tree Based Modeling. *International Journal of Computer Applications*, 6(5), 18–24.
- Deng, F., He, Y., Zhou, S., Yu, Y., Cheng, H., and Wu, X. (2018). Compressive strength prediction of recycled concrete based on deep learning. *Construction and Building Materials*, 175, 562–569.
- DeRousseau, M. A., Kasprzyk, J. R., and Srubar, W. V. (2018). Computational design optimization of concrete mixtures: A review. In *Cement and Concrete Research* (Vol. 109, Issue December 2017, pp. 42–53). Elsevier.
- Dibike, Y. B., Velickov, S., and Solomatine, D. (2014). *Support Vector Machines : Review*

and Applications in Civil Engineering. October.

- Duan, Z. H., Kou, S. C., and Poon, C. S. (2013a). Prediction of compressive strength of recycled aggregate concrete using artificial neural networks. *Construction and Building Materials*, 40, 1200–1206.
- Duan, Z. H., Kou, S. C., and Poon, C. S. (2013b). Using artificial neural networks for predicting the elastic modulus of recycled aggregate concrete. *Construction and Building Materials*, 44, 524–532.
- Eiben, A. E., and Smit, S. K. (2011). Parameter tuning for configuring and analyzing evolutionary algorithms. In *Swarm and Evolutionary Computation* (Vol. 1, Issue 1, pp. 19–31). Elsevier B.V.
- Elish, M. O. (2009). Improved estimation of software project effort using multiple additive regression trees. *Expert Systems with Applications*, 36(7), 10774–10778.
- Fadaei, N., Yan, W. M., Mahdi Tafarroj, M., and Kasaeian, A. (2018). The application of artificial neural networks to predict the performance of solar chimney filled with phase change materials. *Energy Conversion and Management*, 171, 1255–1262.
- Farquad, M. A. H., Ravi, V., and Raju, S. B. (2014). Churn prediction using comprehensible support vector machine: An analytical CRM application. *Applied Soft Computing Journal*, 19, 31–40.
- Friedman, J. H. (2002). Stochastic gradient boosting. *Computational Statistics and Data Analysis*, 38(4), 367–378.
- Gandomi, A H, Alavi, A. H., and Yun, G. J. (2011). Nonlinear modeling of shear strength of SFRC beams using linear genetic programming. *Structural Engineering and Mechanics*, 38(1), 1–25.
- Gandomi, Amir H., Alavi, A. H., Gandomi, M., and Kazemi, S. (2017). Formulation of shear strength of slender RC beams using gene expression programming, part II: With shear reinforcement. *Measurement: Journal of the International Measurement Confederation*, 95, 367–376.
- Gandomi, Amir H., Alavi, A. H., Kazemi, S., and Gandomi, M. (2014). Formulation of shear strength of slender RC beams using gene expression programming, part I: Without shear reinforcement. *Automation in Construction*, 42, 112–121.
- Gandomi, Amir Hossein, Alavi, A. H., and Sahab, M. G. (2010). New formulation for compressive strength of CFRP confined concrete cylinders using linear genetic programming. *Materials and Structures/Materiaux et Constructions*, 43(7), 963–983.
- Gandomi, Amir Hossein, Alavi, A. H., Sahab, M. G., and Arjmandi, P. (2010). *Formulation of elastic modulus of concrete using linear genetic programming †*. 24(6), 1273–1278.
- Gholampour, A., Mansouri, I., Kisi, O., and Ozbakkaloglu, T. (2020). Evaluation of mechanical properties of concretes containing coarse recycled concrete aggregates using multivariate adaptive regression splines (MARS), M5 model tree (M5Tree), and

- least squares support vector regression (LSSVR) models. *Neural Computing and Applications*, 32(1), 295–308.
- Golafshani, E. M., and Behnood, A. (2018). Automatic regression methods for formulation of elastic modulus of recycled aggregate concrete. *Applied Soft Computing Journal*, 64, 377–400.
- Golafshani, E. M., Behnood, A., and Arashpour, M. (2020). Predicting the compressive strength of normal and High-Performance Concretes using ANN and ANFIS hybridized with Grey Wolf Optimizer. *Construction and Building Materials*, 232, 117266.
- Gupta, T., Patel, K. A., Siddique, S., Sharma, R. K., and Chaudhary, S. (2019). Prediction of mechanical properties of rubberised concrete exposed to elevated temperature using ANN. *Measurement: Journal of the International Measurement Confederation*, 147.
- Han, Q., Gui, C., Xu, J., and Lacidogna, G. (2019). A generalized method to predict the compressive strength of high-performance concrete by improved random forest algorithm. *Construction and Building Materials*, 226, 734–742.
- Hemmat Esfe, M., Wongwises, S., Naderi, A., Asadi, A., Safaei, M. R., Rostamian, H., Dahari, M., and Karimipour, A. (2015). Thermal conductivity of Cu/TiO₂-water/EG hybrid nanofluid: Experimental data and modeling using artificial neural network and correlation. *International Communications in Heat and Mass Transfer*, 66, 100–104.
- Ibrahim, H., Karakurt, O., and Namli, E. (2013). Engineering Applications of Artificial Intelligence High performance concrete compressive strength forecasting using ensemble models based on discrete wavelet transform. *Engineering Applications of Artificial Intelligence*, 26(4), 1246–1254.
- Jaafari, A., Panahi, M., Pham, B. T., Shahabi, H., Bui, D. T., Rezaie, F., and Lee, S. (2019). Meta optimization of an adaptive neuro-fuzzy inference system with grey wolf optimizer and biogeography-based optimization algorithms for spatial prediction of landslide susceptibility. *Catena*, 175, 430–445.
- Jafrasteh, B., and Fathianpour, N. (2017). A hybrid simultaneous perturbation artificial bee colony and back-propagation algorithm for training a local linear radial basis neural network on ore grade estimation. *Neurocomputing*, 235, 217–227.
- Jiang, X., and Li, S. (2017). BAS: Beetle Antennae Search Algorithm for Optimization Problems. *International Journal of Robotics and Control*, 1(1), 1.
- Kara, I. F. (2011). Prediction of shear strength of FRP-reinforced concrete beams without stirrups based on genetic programming. *Advances in Engineering Software*, 42(6), 295–304.
- Kaytez, F., Taplamacioglu, M. C., Cam, E., and Hardalac, F. (2015). Forecasting electricity consumption: A comparison of regression analysis, neural networks and least squares support vector machines. *International Journal of Electrical Power and Energy Systems*, 67, 431–438.

- Keshtegar, B., Bagheri, M., and Yaseen, Z. M. (2019). Shear strength of steel fiber-unconfined reinforced concrete beam simulation: Application of novel intelligent model. *Composite Structures*, 212, 230–242.
- Khademi, F., Akbari, M., Jamal, S. M., and Nikoo, M. (2017). Multiple linear regression, artificial neural network, and fuzzy logic prediction of 28 days compressive strength of concrete. *Frontiers of Structural and Civil Engineering*, 11(1), 90–99.
- Khademi, F., Mohammadmehdi, S., and Deshpande, N. (2016). Predicting strength of recycled aggregate concrete using Artificial Neural Network, Adaptive Neuro-Fuzzy Inference System and Multiple Linear Regression. *International Journal of Sustainable Built Environment*, 5(2), 355–369.
- Kisi, O. (2015). Pan evaporation modeling using least square support vector machine, multivariate adaptive regression splines and M5 model tree. *Journal of Hydrology*, 528, 312–320.
- Kramer, O. (2017). Genetic Algorithm Essentials. *Springer International Publishing AG*, 679, 11–20.
- Kumar, S., and Barai, S. V. (2010). Neural networks modeling of shear strength of SFRC corbels without stirrups. *Applied Soft Computing Journal*, 10(1), 135–148.
- Kwak, Y.-K. K., Eberhard, M. O., Kim, W.-S. S., and Kim, J. (2002). Shear Strength of Steel Fiber-Reinforced Concrete Beams without Stirrups. *ACI Structural Journal*, 99(4), 530–538.
- Lee, S., and Lee, C. (2014). Prediction of shear strength of FRP-reinforced concrete flexural members without stirrups using artificial neural networks. *Engineering Structures*, 61, 99–112.
- Mangalathu, S., and Jeon, J. S. (2018). Classification of failure mode and prediction of shear strength for reinforced concrete beam-column joints using machine learning techniques. *Engineering Structures*, 160(September 2017), 85–94.
- Mansour, M. Y., Dicleli, M., Lee, J. Y., and Zhang, J. (2004). Predicting the shear strength of reinforced concrete beams using artificial neural networks. *Engineering Structures*, 26(6), 781–799.
- Marugán, A. P., Márquez, F. P. G., Perez, J. M. P., and Ruiz-Hernández, D. (2018). A survey of artificial neural network in wind energy systems. In *Applied Energy* (Vol. 228, Issue April, pp. 1822–1836). Elsevier.
- Mohammadhassani, M., Nezamabadi-pour, H., Suhatri, M., and Shariati, M. (2014). An evolutionary fuzzy modelling approach and comparison of different methods for shear strength prediction of high-strength concrete beams without stirrups. In *Smart Structures and Systems* (Vol. 14, Issue 5, pp. 785–809).
- Mohammadi, E., and Behnood, A. (2018). Application of soft computing methods for predicting the elastic modulus of recycled aggregate concrete Input layer Output layer. *Journal of Cleaner Production*, 176, 1163–1176.

- Mohandes, S. R., Zhang, X., and Mahdiyar, A. (2019). A comprehensive review on the application of artificial neural networks in building energy analysis. *Neurocomputing*, 340, 55–75.
- Moraes, R., Valiati, J. F., and Gavião Neto, W. P. (2013). Document-level sentiment classification: An empirical comparison between SVM and ANN. *Expert Systems with Applications*, 40(2), 621–633.
- Naderpour, H, Poursaeidi, O., and Ahmadi, M. (2018). Shear resistance prediction of concrete beams reinforced by FRP bars using artificial neural networks. *Measurement: Journal of the International Measurement Confederation*, 126(May), 299–308.
- Naderpour, Hosein, Rafiean, A. H., and Fakharian, P. (2018). Compressive strength prediction of environmentally friendly concrete using artificial neural networks. *Journal of Building Engineering*, 16(October 2017), 213–219.
- Nath, P., and Sarker, P. K. (2014). Effect of GGBFS on setting, workability and early strength properties of fly ash geopolymer concrete cured in ambient condition. *Construction and Building Materials*, 66, 163–171.
- Nazemi, E., Dinca, M., Movafeghi, A., Rokrok, B., and Choopan Dastjerdi, M. H. (2019). Estimation of volumetric water content during imbibition in porous building material using real time neutron radiography and artificial neural network. *Nuclear Instruments and Methods in Physics Research, Section A: Accelerators, Spectrometers, Detectors and Associated Equipment*, 940, 344–350.
- Nehdi, M., Djebbar, Y., and Khan, A. (2001). Neural network model for preformed-foam cellular concrete. *ACI Materials Journal*, 98(5), 402–409.
- O. Akande, K., O. Owolabi, T., Twaha, S., and Olatunji, S. O. (2014). Performance Comparison of SVM and ANN in Predicting Compressive Strength of Concrete. *IOSR Journal of Computer Engineering*, 16(5), 88–94.
- Omran, B. A., Chen, Q., and Jin, R. (2016). Comparison of Data Mining Techniques for Predicting Compressive Strength of Environmentally Friendly Concrete. *Journal of Computing in Civil Engineering*, 30(6), 1–13.
- Ospina, C. E., Alexander, S. D. B., and Roger Cheng, J. J. (2003). Punching of Two-Way Concrete Slabs with Fiber-Reinforced Polymer Reinforcing Bars or Grids. *ACI Structural Journal*, 100(5), 589–598.
- Özcan, F., Atış, C. D., Karahan, O., Uncuoğlu, E., and Tanyildizi, H. (2009). Comparison of artificial neural network and fuzzy logic models for prediction of long-term compressive strength of silica fume concrete. *Advances in Engineering Software*, 40(9), 856–863.
- Öztaş, A., Pala, M., Özbay, E., Kanca, E., Çağlar, N., and Bhatti, M. A. (2006). Predicting the compressive strength and slump of high strength concrete using neural network. *Construction and Building Materials*, 20(9), 769–775.
- Pereira, P., Evangelista, L., and De Brito, J. (2012). The effect of superplasticisers on the

- workability and compressive strength of concrete made with fine recycled concrete aggregates. *Construction and Building Materials*, 28(1), 722–729.
- Perera, R., Barchín, M., Arteaga, A., and Diego, A. De. (2010). Prediction of the ultimate strength of reinforced concrete beams FRP-strengthened in shear using neural networks. *Composites Part B: Engineering*, 41(4), 287–298.
- Pham, A. D., Hoang, N. D., and Nguyen, Q. T. (2016). Predicting Compressive Strength of High-Performance Concrete Using Metaheuristic-Optimized Least Squares Support Vector Regression. *Journal of Computing in Civil Engineering*, 30(3), 28–31.
- Raghavendra, S., and Deka, P. C. (2014). Support vector machine applications in the field of hydrology: A review. In *Applied Soft Computing Journal* (Vol. 19, pp. 372–386).
- Sadri, S., and Burn, D. H. (2012). Nonparametric methods for drought severity estimation at ungauged sites. *Water Resources Research*, 48(12).
- Şahin, M., and Erol, R. (2017). A Comparative Study of Neural Networks and ANFIS for Forecasting Attendance Rate of Soccer Games. *Mathematical and Computational Applications*, 22(4), 43.
- Sarveghadi, M., Gandomi, A. H., Bolandi, H., and Alavi, A. H. (2019). Development of prediction models for shear strength of SFRCB using a machine learning approach. *Neural Computing and Applications*, 31(7), 2085–2094.
- Sharifzadeh, M., Sikinioti-Lock, A., and Shah, N. (2019). Machine-learning methods for integrated renewable power generation: A comparative study of artificial neural networks, support vector regression, and Gaussian Process Regression. *Renewable and Sustainable Energy Reviews*, 513–538.
- Siddique, R., Aggarwal, P., and Aggarwal, Y. (2011). Prediction of compressive strength of self-compacting concrete containing bottom ash using artificial neural networks. *Advances in Engineering Software*, 42(10), 780–786.
- Sonebi, M., Cevik, A., Grünewald, S., and Walraven, J. (2016). Modelling the fresh properties of self-compacting concrete using support vector machine approach. *Construction and Building Materials*, 106, 55–64.
- Sri Ravindrarajah, R., and Tam, C. T. (1985). Properties of concrete made with crushed concrete as coarse aggregate. *Magazine of Concrete Research*, 37(130), 29–38.
- Tanarslan, H. M., Secer, M., and Kumanlioglu, A. (2012). An approach for estimating the capacity of RC beams strengthened in shear with FRP reinforcements using artificial neural networks. *Construction and Building Materials*, 30, 556–568.
- Topçu, I. B., and Saridemir, M. (2008). Prediction of mechanical properties of recycled aggregate concretes containing silica fume using artificial neural networks and fuzzy logic. *Computational Materials Science*, 42(1), 74–82.
- Tsai, C. F., Hsu, Y. F., Lin, C. Y., and Lin, W. Y. (2009). Intrusion detection by machine learning: A review. In *Expert Systems with Applications* (Vol. 36, Issue 10, pp.

11994–12000).

- Van Dao, D., Ly, H. B., Trinh, S. H., Le, T. T., and Pham, B. T. (2019). Artificial intelligence approaches for prediction of compressive strength of geopolymer concrete. *Materials*, 12(6).
- Vikhar, P. A. (2017). Evolutionary algorithms: A critical review and its future prospects. *Proceedings - International Conference on Global Trends in Signal Processing, Information Computing and Communication, ICGTSPICC 2016*, 261–265.
- Vu, D., and Hoang, N. (2016). Punching shear capacity estimation of FRP-reinforced concrete slabs using a hybrid machine learning approach. *Structure and Infrastructure Engineering*, 12(9), 1153–1161.
- Wang, J., and Hu, J. (2015). A robust combination approach for short-term wind speed forecasting and analysis - Combination of the ARIMA (Autoregressive Integrated Moving Average), ELM (Extreme Learning Machine), SVM (Support Vector Machine) and LSSVM (Least Square SVM) forecasts. *Energy*, 93, 41–56.
- Wang, L., Zeng, Y., and Chen, T. (2015). Back propagation neural network with adaptive differential evolution algorithm for time series forecasting. *Expert Systems with Applications*, 42(2), 855–863.
- Xu, J., Chen, Y., Xie, T., Zhao, X., Xiong, B., and Chen, Z. (2019). Prediction of triaxial behavior of recycled aggregate concrete using multivariable regression and artificial neural network techniques. *Construction and Building Materials*, 226, 534–554.
- Xu, J., Zhao, X., Yu, Y., Xie, T., Yang, G., and Xue, J. (2019). Parametric sensitivity analysis and modelling of mechanical properties of normal- and high-strength recycled aggregate concrete using grey theory, multiple nonlinear regression and artificial neural networks. *Construction and Building Materials*, 211, 479–491.
- Yadav, A. K., and Chandel, S. S. (2014). Solar radiation prediction using Artificial Neural Network techniques: A review. In *Renewable and Sustainable Energy Reviews* (Vol. 33, pp. 772–781). Elsevier Ltd.
- Yan, K., and Shi, C. (2010). Prediction of elastic modulus of normal and high strength concrete by support vector machine. *Construction and Building Materials*, 24(8), 1479–1485.
- Yang, X.-S. (2010). Nature-Inspired Metaheuristic Algorithms. In *Nature-Inspired Metaheuristic Algorithms Second Edition*. Luniver Press.
- Yaseen, Z. M., Deo, R. C., Hilal, A., Abd, A. M., Bueno, L. C., Salcedo-Sanz, S., and Nehdi, M. L. (2018). Predicting compressive strength of lightweight foamed concrete using extreme learning machine model. *Advances in Engineering Software*, 115(April 2017), 112–125.
- Yu, Y., Li, W., Li, J., and Nguyen, T. N. (2018). A novel optimised self-learning method for compressive strength prediction of high performance concrete. *Construction and Building Materials*, 184, 229–247.

- Yuan, Z., Wang, L. N., and Ji, X. (2014). Prediction of concrete compressive strength: Research on hybrid models genetic based algorithms and ANFIS. *Advances in Engineering Software*, 67, 156–163.
- Zendehboudi, A., Baseer, M. A., and Saidur, R. (2018). Application of support vector machine models for forecasting solar and wind energy resources: A review. In *Journal of Cleaner Production* (Vol. 199, pp. 272–285).
- Zhan, C., Gan, A., and Hadi, M. (2011). Prediction of lane clearance time of freeway incidents using the M5P tree algorithm. *IEEE Transactions on Intelligent Transportation Systems*, 12(4), 1549–1557.
- Zhang, J., Ma, G., Huang, Y., sun, J., Aslani, F., and Nener, B. (2019). Modelling uniaxial compressive strength of lightweight self-compacting concrete using random forest regression. *Construction and Building Materials*, 210, 713–719.
- Zhang, L., and Zhang, D. (2017). Evolutionary Cost-Sensitive Extreme Learning Machine. *IEEE Transactions on Neural Networks and Learning Systems*, 28(12), 3045–3060.
- Zheng, B., Myint, S. W., Thenkabail, P. S., and Aggarwal, R. M. (2015). A support vector machine to identify irrigated crop types using time-series Landsat NDVI data. *International Journal of Applied Earth Observation and Geoinformation*, 34(1), 103–112.
- Zhu, Q. Y., Qin, A. K., Suganthan, P. N., and Huang, G. Bin. (2005). Evolutionary extreme learning machine. *Pattern Recognition*, 38(10), 1759–1763.

Chapter 3

Novel Soft Computing Hybrid Model for Predicting Shear Strength and Failure Mode of SFRC Beams with Superior Accuracy

3.1 Introduction

The ability of steel fibers to enhance the post-cracking toughness and shear strength of concrete stimulated noteworthy increase in the use of steel fiber-reinforced concrete in the construction industry. However, steel fibers impart complexity to concrete and make accurate assessment of shear strength challenging. The empirical shear strength models usually suffer from multiple drawbacks including the costly and time-consuming experimental work associated with their development, and the limited number of samples used to develop such models. Emergence of machine learning (ML) models have motivated researchers to develop more accurate models and save the required experimental work. Yet, the performance of ML models can differ significantly from one problem to another. There is, therefore, a need to explore more powerful algorithms that can achieve superior accuracy for a specific problem.

In the present chapter, a novel hybrid soft computing model that combines atom search optimization (ASO) and artificial neural network (ANN) has been implemented to predict the shear capacity of SFRC beams without stirrups. The ASO model was deployed to optimize the weights and biases of ANN and avoid local minima in which the standalone ANN model might fall. Hyperparameters of the suggested model have been carefully tuned via a trial and error process to select the most accurate algorithm. In addition, the performance of the proposed model was benchmarked against other ML models and empirical equations. Sensitivity analysis was also carried out to find out the most influential parameters. The current chapter also suggests four different ML classification approaches to forecast the failure mode of SFRC beams, which is not achievable by the model described earlier. This allows the estimation of the ductility degree and informs engineers of the likelihood of shear failure, which could avert sudden structural shear failures.

3.2 Experimental Database

The comprehensive database retrieved from the open literature entails results of experimental tests performed on 573 SFRC beams without stirrups that failed in shear, flexural-shear, or flexural mode. Amongst the total number of specimens, 484 data examples have been selected from the published database of Lantsoght (Lantsoght, 2019). However, this database comprises specimens that only failed in shear mode or flexural-shear mode. To create an appropriate dataset for failure mode classification of SFRC beams subjected to three-point and four-point shear testing method, 89 data examples which exhibited flexural failure were added to the database from the open literature (Amin and Foster, 2016; Batson et al., 1972; Cho and Kim, 2003; Kang et al., 2011; Kwak et al., 2002; Lim et al., 1987; Mansur et al., 1986; Narayanan and Darwish, 1987; Sahoo et al., 2016; Sahoo and Sharma, 2014; Shoaib et al., 2015; Tahenni et al., 2016). Accordingly, two different sets of data have been used to handle the regression and classification problems separately. The first set involves 484 specimens that failed in shear mode and flexural-shear mode. The set is used for developing the regression model which predicts the shear capacity of SFRC beams, thus the 89 specimens that failed in flexural mode were discounted. The second set comprises 475 specimens that failed in three different modes namely, shear failure, flexural-shear failure, and flexural failure. This set is created by combining the additional 89 specimens with those data examples in Lantsoght's dataset for which the failure mode is reported (386 specimens).

The input variables considered for model training and testing include the beam width (b_w), effective depth of beam (d), longitudinal steel ratio (ρ), shear span-to-depth ratio (a/d), steel fiber volume fraction (V_f), fiber aspect ratio (l_f/d_f), compressive strength of concrete (f'_c) and tensile strength of fibers (f_{tf}). Statistical characteristics of the input variables are given in **Table 3.1**. The adopted features, however, have different ranges. This can affect the analysis by making features with significantly wider ranges more influential even though they can be less important predictors. This can be solved through data normalization. Scaling the data is crucial for ensuring the same treatment of all input features and to avoid biasing the model.

Table 3.1: Statistical characteristics of employed dataset

Input variables	Geometric properties of the beam			Steel properties	Concrete properties	Fiber properties			Output variable	Shear capacity
	b_w (mm)	d (mm)	a/d	ρ	$f'c$ (MPa)	V_f (%)	l_f/d_f	f_{tf} (MPa)		v_u (MPa)
Minimum	50.000	85.250	0.460	0.004	9.770	0.200	25.000	260.000		0.558
Maximum	610.000	923.000	6.000	0.057	215.000	4.500	191.000	4913.000		13.916
Mean	145.816	258.595	2.919	0.025	48.933	0.890	71.607	1252.083		3.601
Mode	200.000	127.000	3.500	0.031	33.220	1.000	60.000	1100.000		2.105
Standard deviation	59.371	147.736	0.980	0.010	25.268	0.552	24.448	461.467		2.148
Skewness	1.679	1.941	0.013	0.780	2.227	2.544	1.613	1.765		2.045
Kurtosis	10.690	7.836	3.332	3.958	10.663	14.791	7.954	11.495		7.605

The formula adopted for data normalization is expressed as follows:

$$w_{i,norm} = \frac{w_i - w_{max}}{w_{max} - w_{min}} \quad (3.1)$$

where w_{max} and w_{min} are the maximum and minimum values of the selected feature, respectively. Furthermore, before the training process, data were randomly permuted to expose the model to more diverse data and exclude similarity of features from the same reference. Data visualization and pre-processing which consisted of removing possible outliers was conducted to ensure better model training accuracy.

3.3 Prediction of shear strength of SFRC beams

3.3.1 Atom search optimization

Atom search optimization (ASO) is a novel population-based heuristic algorithm that was first introduced by Zhao et al., (2019). ASO is inspired by molecular dynamics, in which positions and velocities of an atomic population are iteratively updated to converge to the near global solution of the search space. This atomic motion is generally governed by two types of forces, namely interaction forces and constraint forces (Ryckaert et al., 1977). The former type, which is approximated by the Lennard-Jones (L-J) potential, reflects the interaction force between a pair of atoms that can be repulsive or attractive (Stone, 2013; Zhao et al., 2019). The mathematical expression of the interaction force (I) applied to the i^{th} atom from the j^{th} atom at the t^{th} iteration is given by:

$$I_{ij}(t) = -\eta(t) \left[2 \left(h_{ij}(t) \right)^{13} - \left(h_{ij}(t) \right)^7 \right] \quad (3.2)$$

where h_{ij} is a dimensionless number that depends on the Euclidian distance between i^{th} atom and j^{th} atom along with the collision diameter, while $\eta(t)$ is the depth function which adjusts regions of attraction and repulsion and has the following formula:

$$\eta(t) = \alpha \left(1 - \frac{t-1}{T} \right)^3 e^{-20 \left(\frac{t}{T} \right)} \quad (3.3)$$

with T and α defined as the maximum number of iteration and the depth weight, respectively. Thus, the total force applied to the i^{th} atom can be expressed as follows:

$$I_i(t) = \sum_{j \in K_{Best}} r_j I_{ij}(t) \quad (3.4)$$

where r_j represents a random weight ranging in $[0,1]$ and K_{Best} is a subset of the atomic population that contains the first K atoms with the best values of the fitness function. As provided in **Eq. (3.5)**, this subset, which is a function of the total number of atoms (N), is updated in each iteration to allow the transition of the algorithm from exploration behavior, defined as the capacity to look for new solutions throughout the entire search space, to exploitation, which means the ability to find the best solution within a local region.

$$K(t) = N - (N - 2)\sqrt{(t/T)} \quad (3.5)$$

Regarding applied forces, each atom of the population is subjected to a constraint force caused by the atom holding the best position in the search space. This force is given by:

$$G_i(t) = \lambda(t)(x_{best}(t) - x_i(t)) \quad (3.6)$$

where $x_{best}(t)$ and $x_i(t)$ are the position of the best and i^{th} atom, respectively. The term $\lambda(t)$, defined in **Eq. (3.7)** and affected by a multiplier weight (β), denotes the Lagrange multiplier.

$$\lambda(t) = \beta e^{-\frac{20t}{T}} \quad (3.7)$$

Given the interaction forces and the constraint forces, the acceleration of each atom described in **Eq. (3.8)** can be determined to update positions and velocities of the atomic population. Therefore, the mass of each atom needs to be introduced. The mass of each atom (m) reflects the reliability of the solution defined by the position of the atom, indicating better solutions with higher mass values. Accordingly, the mass can be determined through the value of the fitness function as expressed in **Eqs. (3.9) and (3.10)**.

$$\ddot{x}_i(t) = \frac{I_i(t) + G_i(t)}{m_i(t)} \quad (3.8)$$

$$m_i(t) = \frac{M_i(t)}{\sum_{j=1}^N M_j(t)} \quad (3.9)$$

where $M_i(t)$ is defined by:

$$M_i(t) = e^{-\frac{\varphi_i(t) - \varphi_{Best}(t)}{\varphi_{Worst}(t) - \varphi_{Best}(t)}} \quad (10)$$

with $\varphi_{Best}(t)$, $\varphi_{Worst}(t)$ and $\varphi_i(t)$ are the fitness values of the best, worst and i^{th} atom, respectively at t^{th} iteration. Hence, updating the velocity and position of the i^{th} atom at $(t + 1)^{th}$ iteration can be achieved via the following formulas:

$$\dot{x}_i(t + 1) = r_i \dot{x}_i(t) + \ddot{x}_i(t) \quad (3.11)$$

$$x_i(t + 1) = x_i(t) + \dot{x}_i(t + 1) \quad (3.12)$$

The different forces that govern the motion of an atomic population within the search space are depicted in **Figure 3.1**.

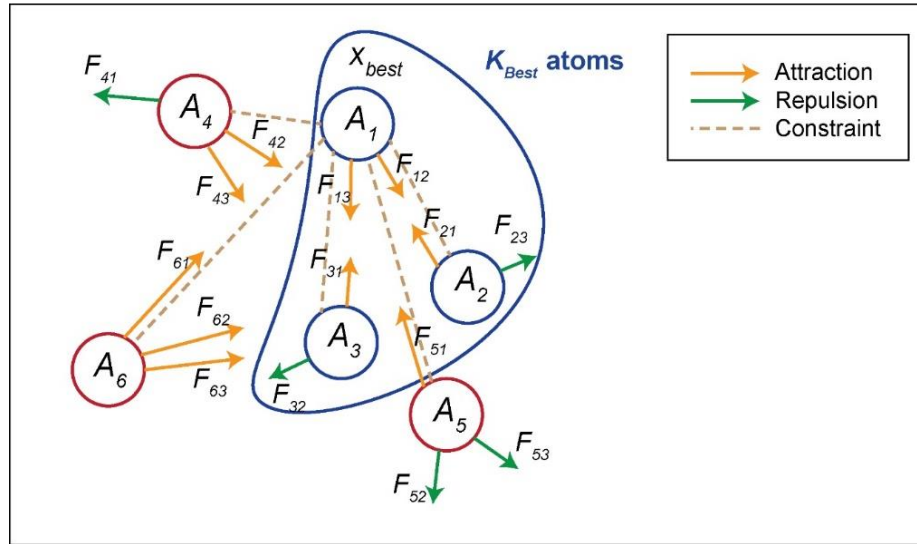


Figure 3.1: Various forces affecting atomic population.

3.3.2 Artificial neural network

Artificial neural network (ANN) is a machine learning technique inspired by the basic framework of the human brain (Marugán et al., 2018; Mohandes et al., 2019; Nazemi et al., 2019; Sharifzadeh et al., 2019). In the present study, a shallow neural network with one hidden layer and eight hidden neurons was employed. The adopted ANN structure is fixed after multiple simulations are performed based on a trial and error process as described below. A schematic of the model structure is given in **Figure 3.2**. The reason for selecting

a shallow network is the simplicity of its structure compared to deep neural networks. Simple structures are computationally less expensive and less vulnerable to overfitting that might occur in complex architectures. Having more than one hidden layer for this problem will significantly increase the number of network connections and consequently the number of weights and biases that need to be optimized. In addition, the convergence of ASO to near global optima will be more challenging with the increase of the number of such parameters.

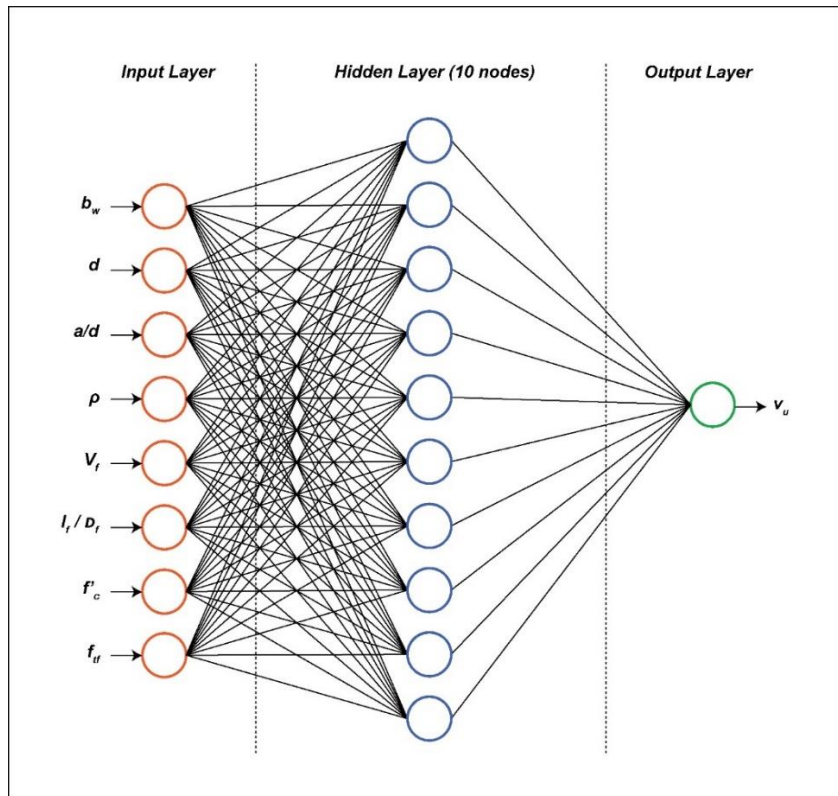


Figure 3.2: Structure of employed ANN model.

3.3.3 Hybrid ASO-ANN model

The process of the hybrid atom search optimized artificial neural network (ASO-ANN) consists of optimizing the neural network weights and biases through ASO search abilities to minimize the fitness function that expresses the error between actual and predicted values. For this specific problem, the atom positions in the search space represent a vector of weights and biases of ANN. The atom positions, i.e. the vector of weights and biases,

will be updated through an iterative process until the best accuracy reflected by the fitness function value is achieved. In the present study, the adopted fitness function is the root mean squared error, which can be expressed by **equation 3.13**, where y'_i is the predicted value, y_i is the actual value and n is the number of data examples.

$$RMSE = \sqrt{\frac{\sum_{i=1}^n (y'_i - y_i)^2}{n}} \quad (3.13)$$

The model training was conducted using 75% of data examples (363 specimens), which were randomly selected from the dataset. The other 25% (121 specimens) were used for the testing process. The flowchart of the hybrid ASO-ANN model is presented in **Figure 3.3**. The process set out in the flowchart has been replicated many times. Each time a different structure of ANN is selected by changing the number of hidden units. After setting the ANN structure, the number of atoms along with their positions and velocities are initialized. The neural network is then trained using the positions of the atoms in the search space. The fitness value of each atom is generated by running the ANN; hence the location of the best atom is defined. Also, the fitness value of the worst atom is recorded for future calculations. Two stopping criteria are subsequently applied to check whether further iterations shall be performed. The first criterion is the maximum number of iterations, which is initially set at $T = 200$. The second criterion is the number of consecutive iterations in which the fitness value remains unchanged. This value was fixed at twenty. If the algorithm meets one of those criteria, the iterative process is halted. Otherwise, the atom positions and velocities are updated to retrain the ANN model as per the process outlined in Section 3.3. As indicated earlier, the entire mechanism shown in the flowchart is repeated several times to determine the ANN structure that generates the best fitness value. This trial and error approach is implemented since there are no agreed upon methods to establish a properly predefined ANN structure. For each iteration, the values for depth and multiplier weights were set at 50 and 0.2, respectively. Three different computations are carried out and average values are considered for selecting the most suitable structure. As outlined in **Table 3.2**, a ranking system based on the average *RMSE* values over the training and testing phase was suggested to define the best ANN structure (Moayedi et al., 2019).

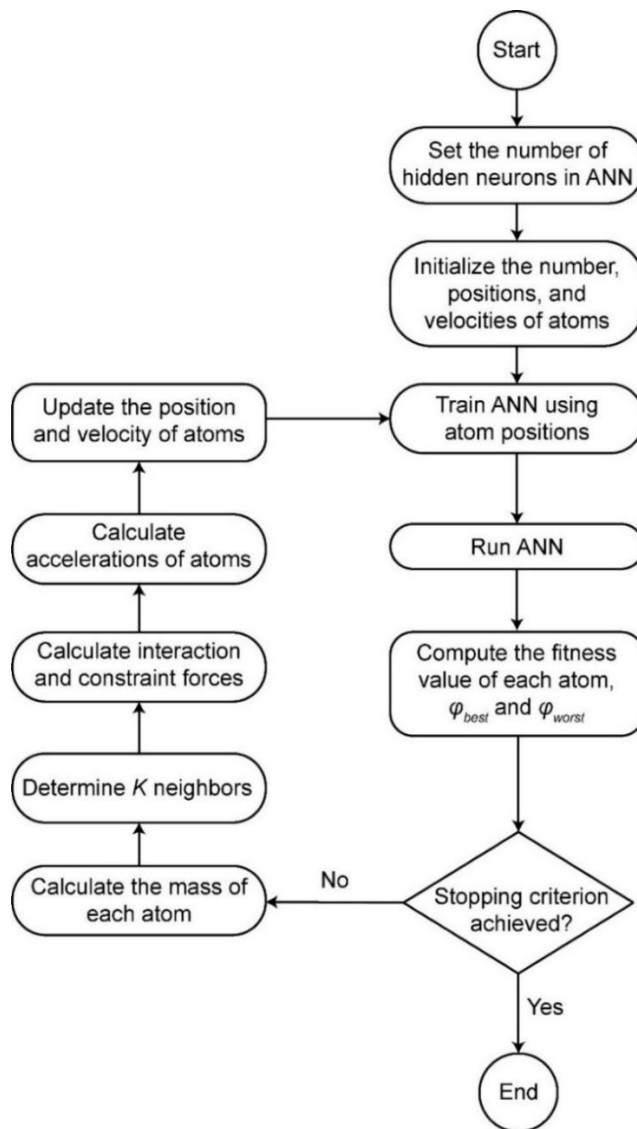


Figure 3.3: Flowchart of ASO-ANN model.

Higher ranks reflect better performance of the model. It can be observed that ANN with 10 hidden nodes displayed the best accuracy over the training and testing phases. Hence, this structure was adopted for future simulations. After fixing the ANN structure, the number of atoms is another important factor that needs to be determined for optimal results. The same constant values of hyperparameters, i.e. $\alpha = 50$ and $\beta = 0.2$, were used to determine the best atoms number for the model. The results of the different simulations are depicted in **Figure 3.4**. It can be observed that an atomic population of 125 atoms achieved the best accuracy in terms of *RMSE* after multiple iterations. It was also found that after 150 iterations, the value of *RMSE* remained constant for the different atomic populations.

Table 3.2: Ranking system for ANN structure selection

Model number	Number of Hidden layer nodes	RMSE								Ranking		Total Ranking
		First Computation		Second Computation		Third Computation		Average		Training	Testing	
		Training	Testing	Training	Testing	Training	Testing	Training	Testing			
1	1	0.769	0.871	0.989	1.050	0.790	0.888	0.849	0.936	1	1	2
2	2	0.799	0.871	0.781	0.852	0.802	0.860	0.794	0.861	2	3	5
3	3	0.727	0.872	0.783	0.842	0.732	0.867	0.747	0.861	3	4	7
4	4	0.704	0.866	0.756	0.886	0.739	0.834	0.733	0.862	4	2	6
5	5	0.738	0.841	0.709	0.769	0.721	0.821	0.723	0.810	5	5	10
6	6	0.693	0.816	0.704	0.858	0.663	0.756	0.687	0.810	6	6	12
7	7	0.684	0.784	0.683	0.765	0.678	0.743	0.681	0.764	7	7	14
8	8	0.642	0.811	0.598	0.723	0.602	0.725	0.614	0.753	8	8	16
9	9	0.559	0.707	0.591	0.721	0.603	0.717	0.584	0.715	10	10	20
10	10	0.507	0.614	0.624	0.669	0.578	0.689	0.570	0.658	15	15	30
11	11	0.567	0.643	0.566	0.650	0.598	0.682	0.577	0.658	12	14	26
12	12	0.532	0.666	0.647	0.762	0.596	0.702	0.592	0.710	9	11	20
13	13	0.562	0.726	0.573	0.721	0.595	0.704	0.577	0.717	13	9	22
14	14	0.594	0.637	0.550	0.688	0.569	0.664	0.571	0.663	14	13	27
15	15	0.598	0.752	0.579	0.616	0.575	0.713	0.584	0.694	11	12	23

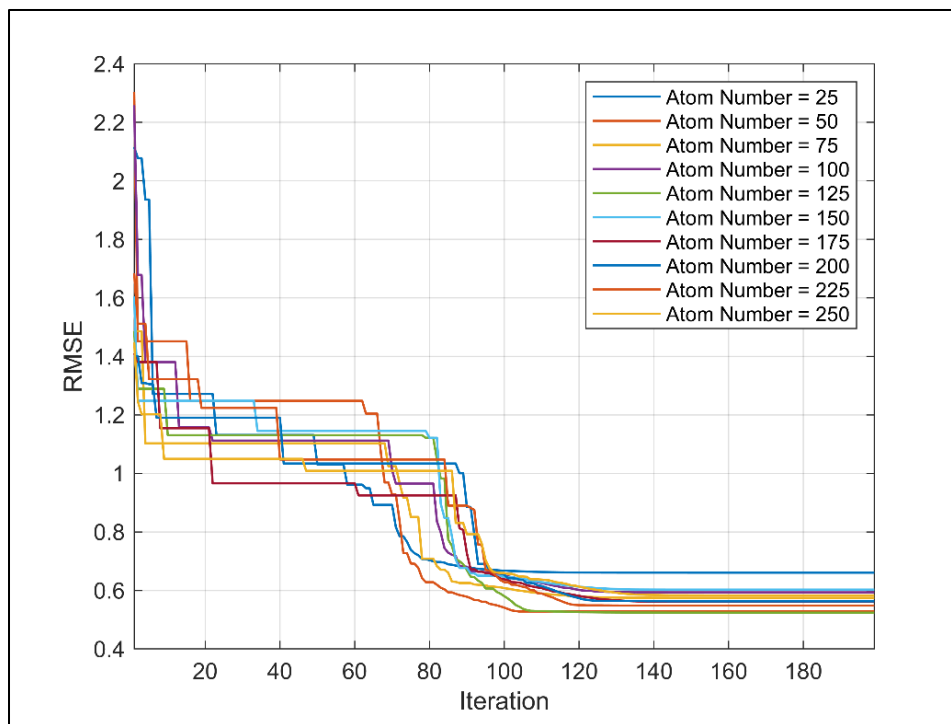


Figure 3.4: Performance assessment for different atom number.

Therefore, the maximum number of iterations selected for model development is 150. This will save computational time for future calculations while maintaining similar accuracy. The next step consists of fixing the depth and multiplier weight values. Empirically, the values should be in the range from 0 to 100 and from 0 to 1 for the depth and multiplier weight, respectively (Zhao et al., 2019). Accordingly, different values of α and β were used to determine the model having best accuracy. One of the two parameters remained constant in each analysis. Results of the simulations are illustrated in **Figure 3.5** and **Figure 3.6**. It was determined that the best values of α and β are 80 and 0.6, respectively. The final values of the model parameters used in the subsequent section are entailed in **Table 3.3**. The reason for adopting a single-variate approach for determining the structure and hyperparameters is the associated computational time. Trying possible combinations by the integration of several for loops in the same script led to unusual computational time.

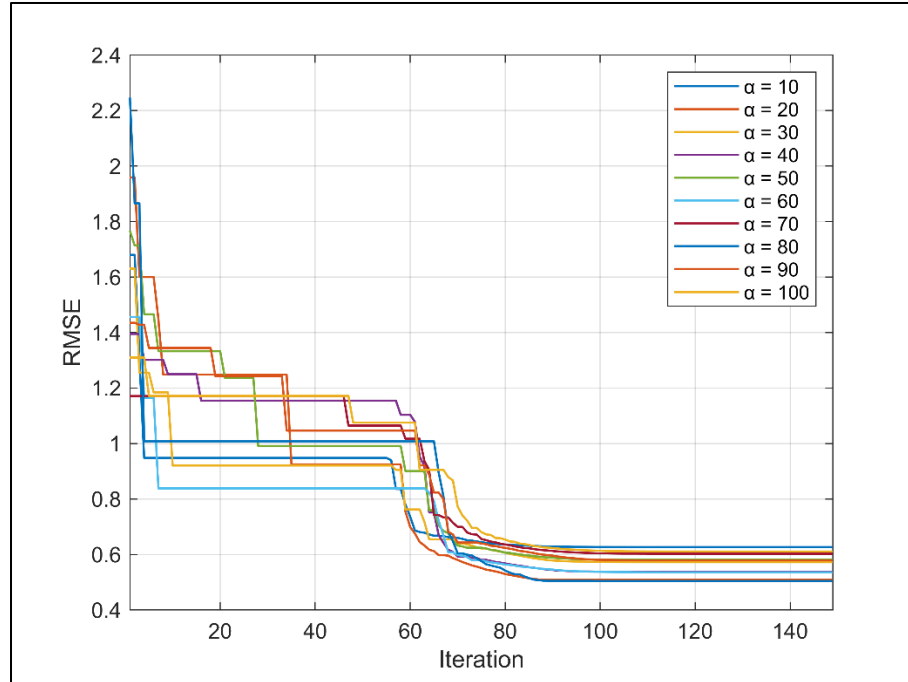


Figure 3.5: Performance assessment for depth weight values.

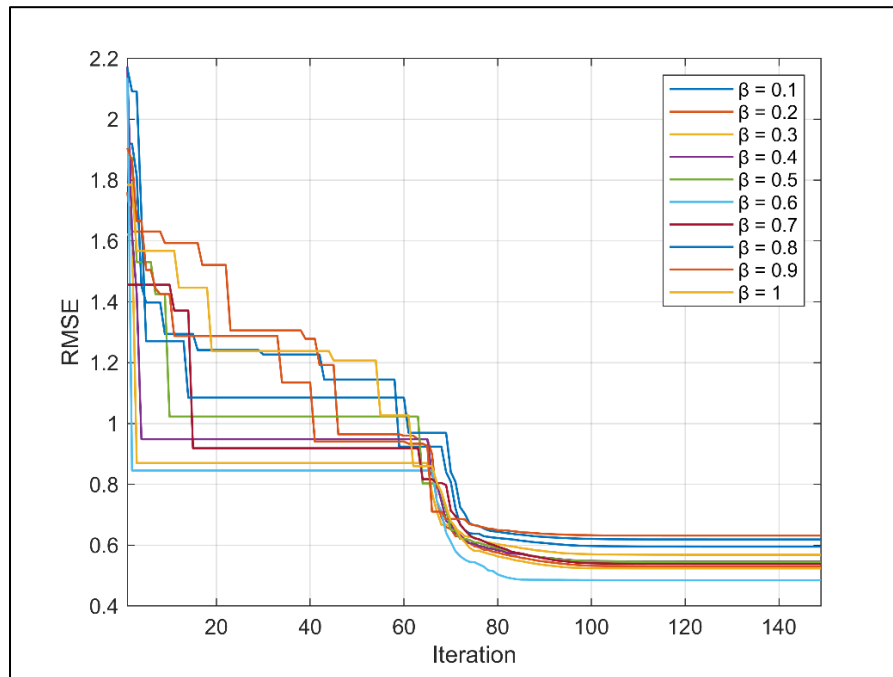


Figure 3.6: Performance assessment for multiplier weight values.

Table 3.3: Final values of ASO-ANN parameters

Parameter	Value
Number of hidden nodes in ANN	10
Number of atoms	125
Depth weight	80
Multiplier weight	0.6
Maximum number of iterations	150

3.4 Classification of failure mode of SFRC beams

For simply supported beams loaded at midspan, it is important to estimate the failure mode since it reflects ductility. Regression models like ASO-ANN can provide a numerical estimation of the load capacity of the beam. However, they cannot depict the likelihood of shear failure. Therefore, a classification model is needed to predict the failure mode of SFRC beams without stirrups undergoing three- and four-point shear testing. Such beams can fail in three distinct modes, namely shear failure (*S*), flexural-shear failure (*FS*) and flexural failure (*F*) (Huang et al., 2015; Kang et al., 2011). As illustrated in **Figure 3.7**, flexural failure is associated with the development of flexural cracks, while flexural-shear failure is initiated by the formation of flexural cracks ending with failure in shear. Conversely, shear failure is stimulated by shear cracks that propagate inclined to the beam's main axis. Shear failure is more brittle compared to other modes, while flexural failure reflects desired ductile behavior (Kang et al., 2011). Four classification models named decision tree, *k*-Nearest Neighbors (KNN), SVM, and naïve Bayes were implemented to forecast the failure mode of SFRC. Training these models was conducted with 75% of data examples (356 specimens), while 119 specimens were used for the testing phase. Prior to training, data were normalized using the z-score method. A brief description of each model is discussed below.

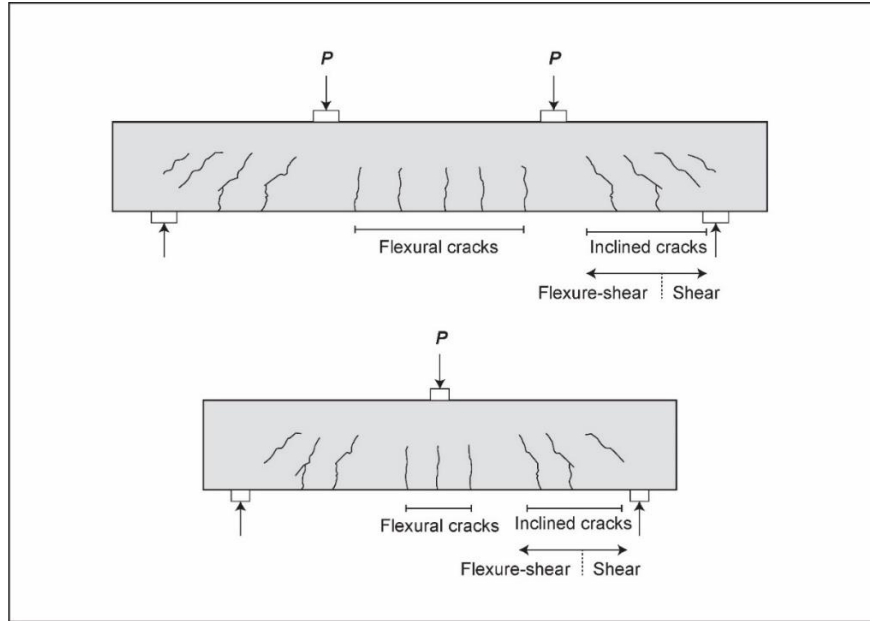


Figure 3.7: Four-point and three-point shear testing methods of SFRC beams.

3.4.1 Decision tree

Decision tree models are non-parametric machine learning techniques in which formal rules are created via patterns in the data (DeRousseau et al., 2018). The output of this model is obtained through various decisions described by test functions at tree nodes (Karbassi et al., 2014).

3.4.2 K-nearest neighbor

k -nearest neighbor (KNN) is a non-parametric classifier that aims to assign uncategorized samples to the group of its nearest samples (Ahmadi-Nedushan, 2012). Generally, the k neighboring samples are determined through Euclidian distance, which can be expressed as follows:

$$\delta(p_1, p_2) = \sqrt{\sum_{i=1}^n (p_{1i} - p_{2i})^2} \quad (3.14)$$

where p_{1i} and p_{2i} represent the coordinates of two points p_1 and p_2 in n dimensional space, respectively. Appropriate selection of the parameter k is crucial because the risk of model overfitting and instability can increase when high values of the parameter are selected (Cracknell and Reading, 2014).

3.4.3 Naïve Bayes

Naïve Bayes (NB) is a probabilistic model that adopts the Bayes theory for classifying data. Estimation of class probabilities through NB is based on “naïve” assumption of feature independence (Mangalathu and Jeon, 2018). Thus, the probability that an output variable $y = (y_1, \dots, y_n)$ is associated with a class C is given by:

$$P(C|y) = \frac{P(C) \prod_{i=1}^n P(y_i|C)}{P(y)} \quad (3.15)$$

3.4.4 Support vector machine

Support vector machine is a classification algorithm that is based on the concept of “margins”. This model aims to find the optimal hyperplane that classifies the data through maximizing the margin representing the distance between the hyperplane and the closest points of each class (Omran et al., 2016; Raghavendra and Deka, 2014). This classification process is performed using a subset of training examples called support vectors. When linear separation of classes cannot be performed in complex problems, kernel functions are needed to make such a separation achievable (Zheng et al., 2015). Quadratic kernel function was used in the current study.

3.5 Results and discussion

3.5.1 Shear strength prediction

The performance of the ASO-ANN model was benchmarked against six empirical equations, which are outlined in **Table 3.4**. In addition, the performance of the model was compared to that of several hybrid and standalone machine learning techniques including ANN, genetic algorithm optimized neural network (GA-ANN), particle swarm optimized neural network (PSO-ANN), support vector regression (SVR), and particle swarm optimized SVR (PSO-SVR). Genetic algorithm and particle swarm optimization are both metaheuristic algorithms that can enhance the accuracy of ANN and SVR (Safarzaghan Gilan et al., 2012; Yuan et al., 2014). The parameters of the various ML models are outlined in **Table 3.5**. Several statistical metrics were used for validating and comparing the above models as discussed below

Table 3.4: Empirical equations developed for estimating shear capacity of SFRC beams

Reference	Suggested model
(Sharma, 1986)	$v_u = kf_t(d/a)^{\frac{1}{4}}$ $k = 1 \text{ if } f_t \text{ is obtained by direct tension test; } (2/3) \text{ if obtained by indirect tension test; } (4/9) \text{ if obtained via modulus of rupture}$
(Narayanan and Darwish, 1987)	$v_u = e(0.24f_{spfc} + 80\rho(d/a)) + v_b$ $v_b = 0.41\tau F; F = (l_f/d_f)V_f\rho_f; \tau = 4.15 \text{ MPa}$ $e = \begin{cases} 1 & \text{if } (a/d) \geq 2.8 \\ 2.8(d/a) & \text{if } (a/d) < 2.8 \end{cases}$ $f_{spfc} = +0.7 + \sqrt{F}$
(Ashour et al., 1992)	$v_u = \begin{cases} (2.11^3\sqrt{f'_c} + 7F)(\rho(d/a))^{\frac{1}{3}} & \text{if } (a/d) \geq 2.5 \\ (2.11^3\sqrt{f'_c} + 7F)(\rho(d/a))^{\frac{1}{3}}(5d/2a) + v_b(2.5 - a/d) & \text{if } (a/d) < 2.5 \end{cases}$ $v_u = (0.7\sqrt{f'_c} + 7F)(d/a) + 17.2\rho(d/a)$
(Khuntia et al., 1999)	$v_u = (0.167\alpha + 0.25F)\sqrt{f'_c}$ $\alpha = \begin{cases} 1 & \text{if } (a/d) \geq 2.5 \\ 2.5(d/a) & \text{if } (a/d) < 2.5 \end{cases}$
(Kwak et al., 2002)	$v_u = 3.7ef_{spfc}^{\frac{2}{3}}(\rho(d/a))^{\frac{1}{3}} + 0.8v_b$ $e = \begin{cases} 1 & \text{if } (a/d) > 3.4 \\ 3.4(d/a) & \text{if } (a/d) \leq 3.4 \end{cases}$
(Shahnewaz and Alam, 2014)	$v_u = 0.2 + 0.034f'_c + 19\rho^{0.087} - 5.8(a/d)^{\frac{1}{2}} + 3.4V_f^{0.4} - 800(l_f/d_f)^{-1.6} - 12((a/d)V_f)^{0.05} - 197((a/d)(l_f/d_f))^{-1.4}$ $+ 105(V_f(l_f/d_f))^{-2.12} \text{ if } (a/d) \leq 2.5$ $v_u = 0.2 + 0.072(f'_c)^{0.85} + 12.5\rho^{0.084} - 24(a/d)^{0.07} + 13.5V_f^{0.07} + 450(l_f/d_f)^{-2} - 0.0002((a/d)V_f)^{3.9} - 27.69((a/d)(l_f/d_f))^{-0.84}$ $+ 1181(V_f(l_f/d_f))^{-2.69} - 21.89((a/d)V_f)(l_f/d_f)^{-0.9} \text{ if } (a/d) > 2.5$

Table 3.5: Parameters of various ML models

Model	Optimized parameters	Algorithm properties	Value / Type
ASO-ANN	Weight and biases vector of ANN	Atom Population	125
		Depth weight	80
		Multiplier weight	0.6
		Maximum iteration number	150
		Number of ANN hidden neuron	10
		Hidden layer activation function	Hyperbolic tangent sigmoid transfer function
		Output layer activation function	Linear transfer function
PSO-SVR	Regularization parameter (C) Loss function (ϵ) RBF parameter (σ)	Particles number	125
		Acceleration constant (c_1)	2
		Acceleration constant (c_2)	2
		Inertia weight	Linearly decreasing from 0.9 to 0.3
		Maximum iteration number	150
		Kernel function	RBF kernel
GA-ANN	Weight and biases vector of ANN	Population size	150
		Selection	Roulette wheel
		Crossover	0.7
		Mutation	0.3
		Maximum generation number	175
		Number of ANN hidden neuron	12
		Hidden layer activation function	Hyperbolic tangent sigmoid transfer function
		Output layer activation function	Linear transfer function
PSO-ANN	Weight and biases vector of ANN	Particles number	125
		Acceleration constant (c_1)	2
		Acceleration constant (c_2)	2
		Inertia weight	Linearly decreasing from 0.9 to 0.3
		Maximum iteration number	150
		Number of ANN hidden neuron	10
		Hidden layer activation function	Hyperbolic tangent sigmoid transfer function
		Output layer activation function	Linear transfer function
ANN	Weight and biases vector of ANN	Training function	Levenberg-Marquardt
		Hidden layer activation function	Hyperbolic tangent sigmoid transfer function
		Output layer activation function	Linear transfer function
SVR	Regularization parameter (C) Loss function (ϵ) RBF parameter (σ)	Kernel function	RBF kernel

3.5.1.1 Statistical metrics

Performance assessment of the proposed algorithms was conducted through several statistical metrics that denote the model fitting. Beside *RMSE* that was described earlier,

the correlation coefficient (R), mean absolute error (MAE), and modified agreement index (d') are adopted as expressed below:

$$R = \frac{n \sum_{i=1}^n y'_i y_i - (\sum_{i=1}^n y'_i)(\sum_{i=1}^n y_i)}{\sqrt{n(\sum_{i=1}^n y_i'^2) - (\sum_{i=1}^n y'_i)^2} \sqrt{n(\sum_{i=1}^n y_i^2) - (\sum_{i=1}^n y_i)^2}} \quad (3.16)$$

$$MAE = \frac{1}{n} \sum_{i=1}^n |y'_i - y_i| \quad (3.17)$$

$$d' = 1 - \frac{\sum_{i=1}^n |y_i - y'_i|}{\sum_{i=1}^n |y_i - \bar{y}| + |y'_i - \bar{y}|} \quad (3.18)$$

with \bar{y} is the mean of actual data. These metrics are widely used in the AI field to evaluate the predictive accuracy of machine learning models (Chai and Draxler, 2014).

3.5.1.2 Prediction results

The performance of the different empirical models, as well as the adopted machine learning algorithms, is reflected by the values of statistical models. The accuracy of each model in the training and testing phases is outlined in **Table 3.6**. The closer the R and d' values to 1 the better the model accuracy is. Conversely, smaller values of MAE and $RMSE$ reflect better precision of the model. It can be observed that the proposed ASO-ANN achieved the highest predictive accuracy amongst all ML models in terms of correlation with $R = 0.974$ for the training phase and $R = 0.951$ for the testing phase.

Table 3.6: Performance assessment of different ML models

Model	Training phase				Testing phase			
	R	MAE	$RMSE$	d'	R	MAE	$RMSE$	d'
ANN	0.890	0.573	0.894	0.812	0.878	0.622	0.993	0.789
SVR	0.904	0.625	0.852	0.821	0.894	0.676	1.037	0.807
PSO-ANN	0.930	0.428	0.663	0.859	0.905	0.472	0.802	0.846
GA-ANN	0.931	0.421	0.649	0.863	0.912	0.466	0.783	0.861
PSO-SVR	0.953	0.354	0.562	0.881	0.929	0.424	0.734	0.870
ASO-ANN	0.974	0.239	0.461	0.928	0.951	0.304	0.601	0.909

Furthermore, the model presented minimum error between actual and predicted values with $MAE = 0.239$ and $RMSE = 0.461$ for the training phase and $MAE = 0.304$ and $RMSE = 0.601$ for the testing phase.

Such superior performance of ASO-ANN can be explained by several factors. The search mechanism in ASO-ANN is based on the concept of attraction and repulsion forces applied between atoms. Atoms holding heavier mass, i.e. better fitness value, have small acceleration, thus they look for better positions in a local search zone. Contrarily, atoms with lighter mass will be attracted by heavy atoms, but their acceleration is much more important and makes them seek for new promising areas quickly. Repulsive forces are the key difference between ASO and other metaheuristic algorithms. Those forces prevent convergence of the algorithm at an early stage of the search process. Usually, the direction of particles or individuals in nature-inspired optimization algorithms is significantly affected by the particle holding the best fitness value in each iteration. Incorporating repulsive forces can provide particles of an optimization algorithm with better chance to explore the search space. This can also avoid premature convergence of the model and ensure the discovery of new promising regions. As iterations progress, repulsion becomes weaker to allow the concentration of the atomic population in local regions and ensure the convergence of the algorithm.

Estimating the shear strength of SFRC beams is a complex problem characterized by an intricate relationship with input variables. Such intricacy can make any optimization algorithm face problems when seeking near global optima, especially that the search space might involve multiple local solutions. Adopting a metaheuristic algorithm with better capacity in seeking new regions in the search space, i.e. better exploration capability, is key to alleviating this challenging problem and increasing chances of convergence toward near global solutions.

Contrarily to ASO-ANN, the standalone ANN model exhibited the lowest accuracy amongst the ML techniques with $R = 0.890$ for the training and $R = 0.878$ for the testing phases, respectively. The adopted ANN model was trained by the Levenberg–Marquardt algorithm, which can be trapped in local minima and lead to lower accuracy. Similarly, the standalone SVR model showed lower accuracy than that of hybrid ML models, which is

mainly due to lack of optimization of the RBF kernel function hyperparameters as well as the regularization parameter and loss function. When these standalone models are combined with metaheuristic algorithms, the accuracy of the latter is significantly improved via enhancement of the process and optimization of hyperparameters (M. Nehdi et al., 2007; Moncef Nehdi and Nikopour, 2011). However, implementing these optimization techniques can affect model transparency and speed, leading to longer simulations and intricate structures. Thus, hybrid models should be avoided when fast simulations and model transparency are favored. Moreover, it can be observed that ML models performed better on training data compared to testing data. This is mainly because they have been established through training data, which leads to lower accuracy when such models are exposed to new data in the testing phase.

Analysis of results also reveals the superiority of ML models over empirical formulations in the testing phase in terms of R , MAE , $RMSE$, and d . The equation proposed by Kwak et al., (2002) exhibited the best accuracy amongst empirically developed equations with $R = 0.873$ in the testing phase. Yet, the accuracy of the suggested formula is lower than that of data-driven models as outlined in **Table 3.7**.

Table 3.7: Performance assessment of empirical models

Model	Testing phase			
	R	MAE	$RMSE$	d'
(Sharma, 1986)	0.672	1.249	1.942	0.614
(Narayanan and Darwish, 1987)	0.806	0.953	1.678	0.745
(Ashour et al., 1992)	0.713	1.294	2.528	0.623
(Khuntia et al., 1999)	0.737	1.431	1.943	0.647
(Kwak et al., 2002)	0.873	0.823	1.433	0.758
(Shahnewaz and Alam, 2014)	0.863	1.576	1.856	0.712

Empirical models were generally established through limited number of data examples, leading to higher error when forecasting the shear capacity of “unseen” data compared to ML techniques. It can also be observed in **Table 3.7** that the Kwak et al., (2002) model

performed better than the Narayanan and Darwish (1987) model, even though both models were reported to have similar performance in the literature. This is mainly due to the limited number of data examples used to validate and compare the models. Expanding the dataset revealed remarkable contrast in the performance of the two models.

Another visual metric that can be explored to compare the performance of different models is the Taylor diagram illustrated in **Figure 3.8** (Taylor, 2001). Taylor diagram provides a graphical illustration of the accuracy of each model based on the correlation coefficient, the root mean-square-centered difference, and the standard deviation.

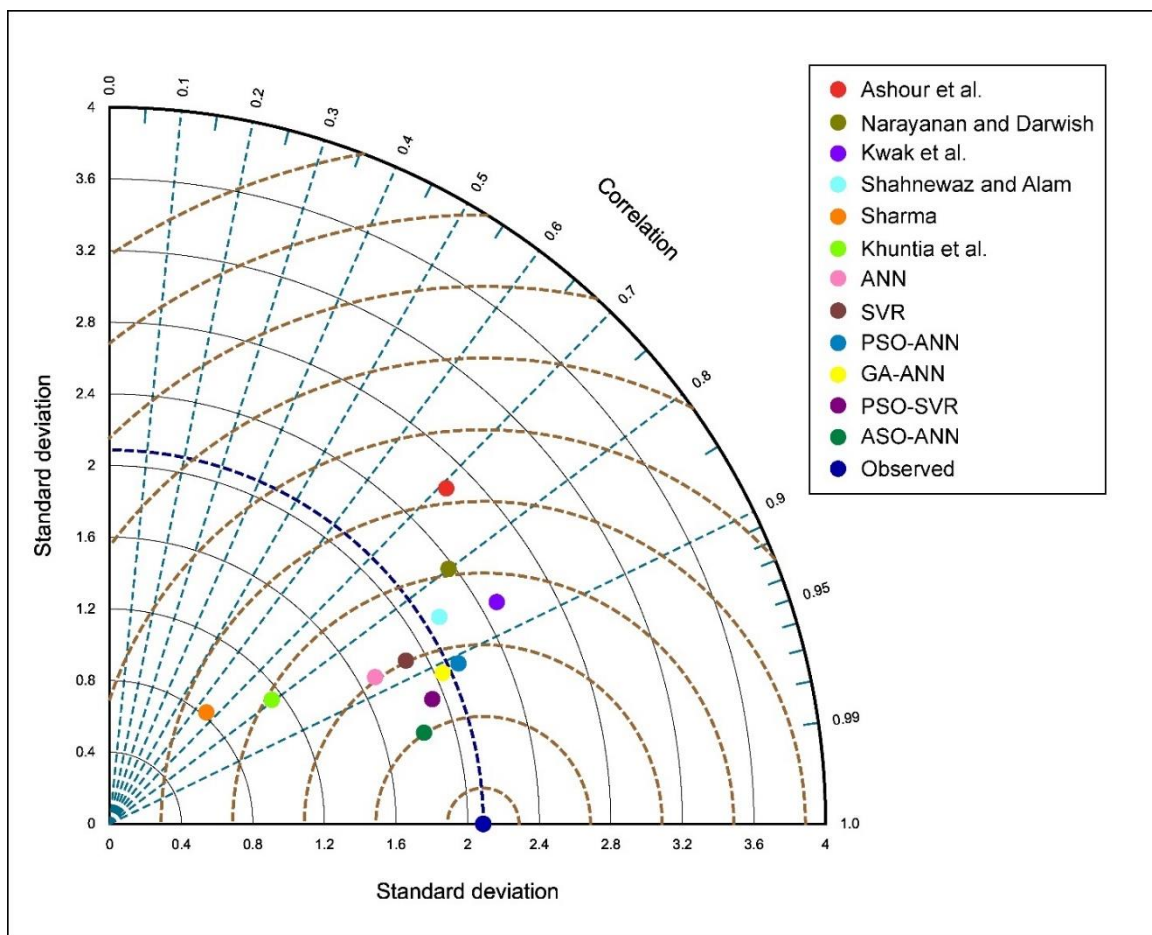


Figure 3.8: Taylor Diagram visualization of model performance in SFRC shear strength prediction.

It can be observed from **Figure 3.8** that the closest prediction to the point representing actual data has been recorded for the proposed ASO-ANN model, affirming earlier discussion above. In addition, the formulation proposed by Ashour et al., (1992) showed

higher values of standard deviation and root mean-square-centered difference, which means that the accuracy of the model over the testing data was rather very low compared to the other empirical equations. The diagram also confirms the superiority of ML models over empirical formulations.

When solving problems in a highly nonlinear environment involving composite materials, it is desirable to adopt ML techniques with superior exploration capability since they have been generated with extensive datasets comprising a wide variety of input features. Those features can significantly affect the shear strength of SFRC, but their level of impact might be different. For a black-box model like ASO-ANN, where there is no transparent equation describing the relationship between input parameters and output, it is crucial to reveal the significance of input variables to the response and to discover some of the model aspects. Therefore, sensitivity analysis was carried out to highlight the contribution of each feature to the shear capacity.

3.5.1.3 Sensitivity analysis of shear strength

Sensitivity analysis (SA) captures how significantly the output of the model is affected by changes within input variables (Kumar and Barai, 2010; Vu-Bac et al., 2015; Xu et al., 2019). There are two main categories of SA: local sensitivity analysis and the global sensitivity analysis (GSA). The former focuses on the local impact of input parameters on the final output (Sudret, 2008). The latter examines the influence of input factors over their entire spatial range and quantify the uncertainty of the output caused by input uncertainty taken individually or in interaction with other parameters. Therefore, using GSA for complex nonlinear problems, such as the case of SFRC shear capacity, is much more rational for examining the impact of input variables on the output.

Amongst GSA techniques, variance-based methods have been widely considered as an effective and versatile approach in sensitivity analysis (Saltelli et al., 2010). The technique presents a specific methodology for determining first-order and total order sensitivity indices for each input parameter of the ASO-ANN model. Given a model of the form $Y = f(X_1, X_2, \dots, X_k)$ where Y is scalar, the variance-based method employs a variance ratio to assess the significance of parameters through variance decomposition expressed as follows:

$$V = \sum_{i=1}^k V_i + \sum_{i=1}^k \sum_{j>i}^k V_{ij} + \cdots + V_{1,2,\dots,k} \quad (3.19)$$

where V represents the variance of the model output, V_i is the first-order variance for the input X_i , and V_{ij} to $V_{1,2,\dots,k}$ correspond to the variance of the interaction of the k parameters. V_i and V_{ij} , which reflect the importance of the input to the variance of the output, depend on the variance of the conditional expectation as follows:

$$V_i = V_{X_i} [E_{X_{\sim i}}(Y|X_i)] \quad (3.20)$$

$$V_{ij} = V_{X_i X_j} [E_{X_{\sim ij}}(Y|X_i, X_j)] - V_i - V_j \quad (3.21)$$

with $X_{\sim i}$ indicates the set of all variables excluding X_i . The first-order sensitivity index (S_i) describing the first-order effect of an input X_i on the final output is given by:

$$S_i = \frac{V_i}{V(Y)} \quad (3.22)$$

Conversely, the total effect of the input factor X_i which comprises the first-order effect along with effects coming from the interaction with other factors is given by the following formula (Saltelli et al., 2010) :

$$S_{Ti} = \frac{E_{X_{\sim i}}(V_{X_i}(Y|X_{\sim i}))}{V(Y)} = 1 - \frac{V_{X_{\sim i}}(E_{X_i}(Y|X_{\sim i}))}{V(Y)} \quad (3.23)$$

The methodology presented by Saltelli et al., (2008) for calculating first- and total-order sensitivity indices was adopted herein. Data sampling was performed via the Latin hypercube sample (LHS) generated from the mean vector and covariance matrix of the input matrix involving all data examples and all input features considered in the current study for the regression model. The model used for determining the final output is ASO-ANN with the same structure and parameters used in the previous section.

Results of the sensitivity analysis are presented in **Figure 3.9**. It can be observed that the shear span-to-depth ratio was the most influential amongst all input features. The first order and total order sensitivity of a/d are significantly higher than that of the other variables with $S_i = 0.4662$ and $S_{Ti} = 0.5997$. The compressive strength of concrete can be

classified as the second most important input feature with $S_i = 0.1520$ and $S_{Ti} = 0.2526$. Conversely, the beam width revealed poor first-order influence on the shear capacity of SFRC beams. The first-order effect is almost zero, while the total order effect is 0.0665. An interesting aspect of GSA can be revealed for instance through comparing indices of b_w and f_{tf} . In terms of first order impact, f_{tf} outperformed b_w . However, the interaction with the other input parameters made the beam width a more influencing parameter. Such discovery cannot be revealed through single-variate sensitivity analysis, which makes GSA a strong contender for studying the impact of input parameters in complex nonlinear environments.

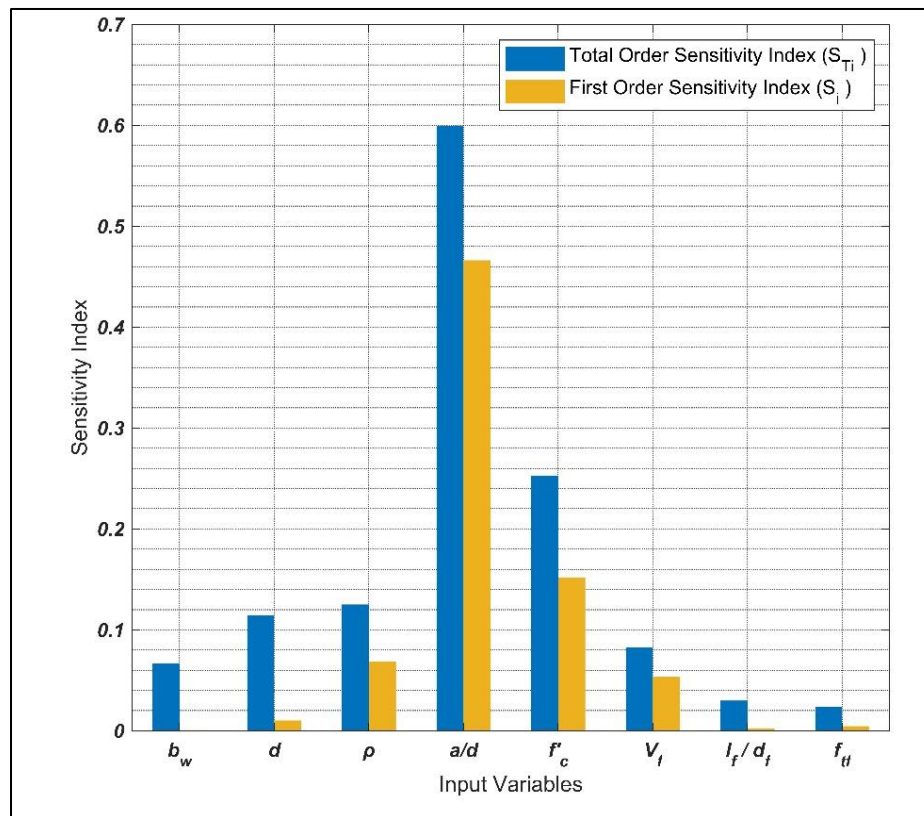


Figure 3.9: Sensitivity indices of input variables.

3.5.2 Prediction of failure mode

Earlier regression models are unable to predict SFRC failure mode. In the present study, the classification models were trained through 75% of data examples and tested with the

remaining data. Each model is trained with 10-fold cross-validation method applied to the training set. Training data is therefore clustered into 10 subsamples. One subsample is used to test the model, while the rest is used for model training. The process is repeated 10 times, and average results are retained to construct each model. Each model is then applied to assess its predictive accuracy over the testing set. The parameters of the various classification models are entailed in **Table 3.8**.

Table 3.8: Parameters of the classification models

Model	Parameters
KNN	Number of neighbors: 10 Distance Metric: Euclidean Distance weight: Squared inverse
SVM	Kernel function: Quadratic Kernel scale: automatic Multiclass method: One vs One
Decision Tree	Maximum number of splits: 100 Split criterion: Gini's diversity index
Naïve Bayes	Distribution name for numeric predictors: Kernel Distribution name for categorical predictors: Multivariate multinomial distribution Kernel type: Gaussian

Results of the classification process are depicted in **Figure 3.10**, which illustrates scatter plots of the classification process of SFRC beams into S , FS , and F failure modes. Results are plotted as a function of f'_c and a/d , the most influential input parameters according to sensitivity analysis. Since the number of specimens that failed in S mode was higher than that of FS and F modes, a new performance metric that considers this gap between numbers was needed.

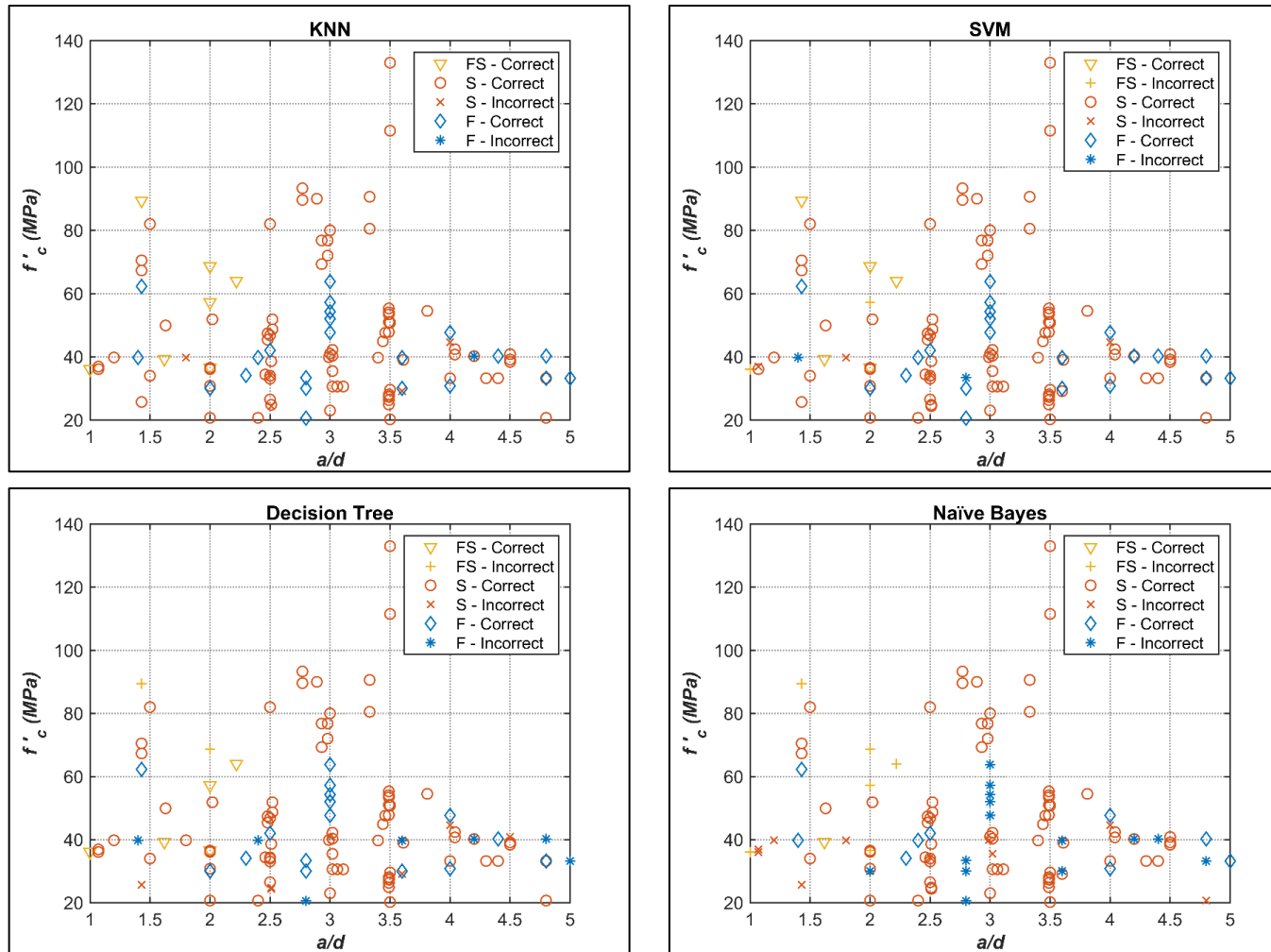


Figure 3.10: Scatter plots of failure mode classification.

Thus, the model performance can be expressed as follows:

$$\gamma = \left(\frac{1}{3}\right) \left[\frac{c_{FS}}{N_{FS}} + \frac{c_S}{N_S} + \frac{c_F}{N_F} \right] \times 100 \quad (3.24)$$

with c_{FS} , c_S and c_F are the numbers of correctly predicted FS , S , and F modes, respectively, while N_{FS} , N_S and N_F are the total number of specimens that failed in FS , S , and F modes, respectively. **Table 3.9** entails the performance evaluation of each classification algorithm. It can be observed that the worst classification accuracy was recorded for the naïve Bayes model, with a precision of 47.02%. This low accuracy can be explained by the assumption of features independence, which is not in compliance with the present study as two features comprised one variable in common (the effective depth of the beam), and sensitivity analysis revealed possible interaction between variables. The k -nearest neighbor achieved the best classification accuracy on the testing phase with $\gamma = 96.68\%$, while SVM provided lower accuracy with $\gamma = 86.08\%$.

Table 3.9: Performance evaluation of classification algorithms

Model	c_{FS}	c_S	c_F	N_{FS}	N_S	N_F	γ (%)
Naïve Bayes	1	78	9	7	89	23	47.02
k -nearest neighbor	7	84	22	7	89	23	96.68
SVM	5	85	21	7	89	23	86.08
Decision tree	5	82	16	7	89	23	77.71

Another graphical tool that can further describe the performance of each classification model is the confusion matrix. As shown in **Figure 3.11**, each row of the matrix corresponds to the actual data and each column is associated with predicted data. The best percentages have been recorded for the k -nearest neighbor and SVM.

It can be observed that amongst all actual data, beams that failed in FS mode were correctly classified by KNN. Also, all specimens that failed in S mode in the predicted data have the same classification as their counterparts in actual data. Regarding SVM, classification accuracy was slightly better compared to KNN for the S mode with 95.5%, but lower for F and FS modes.

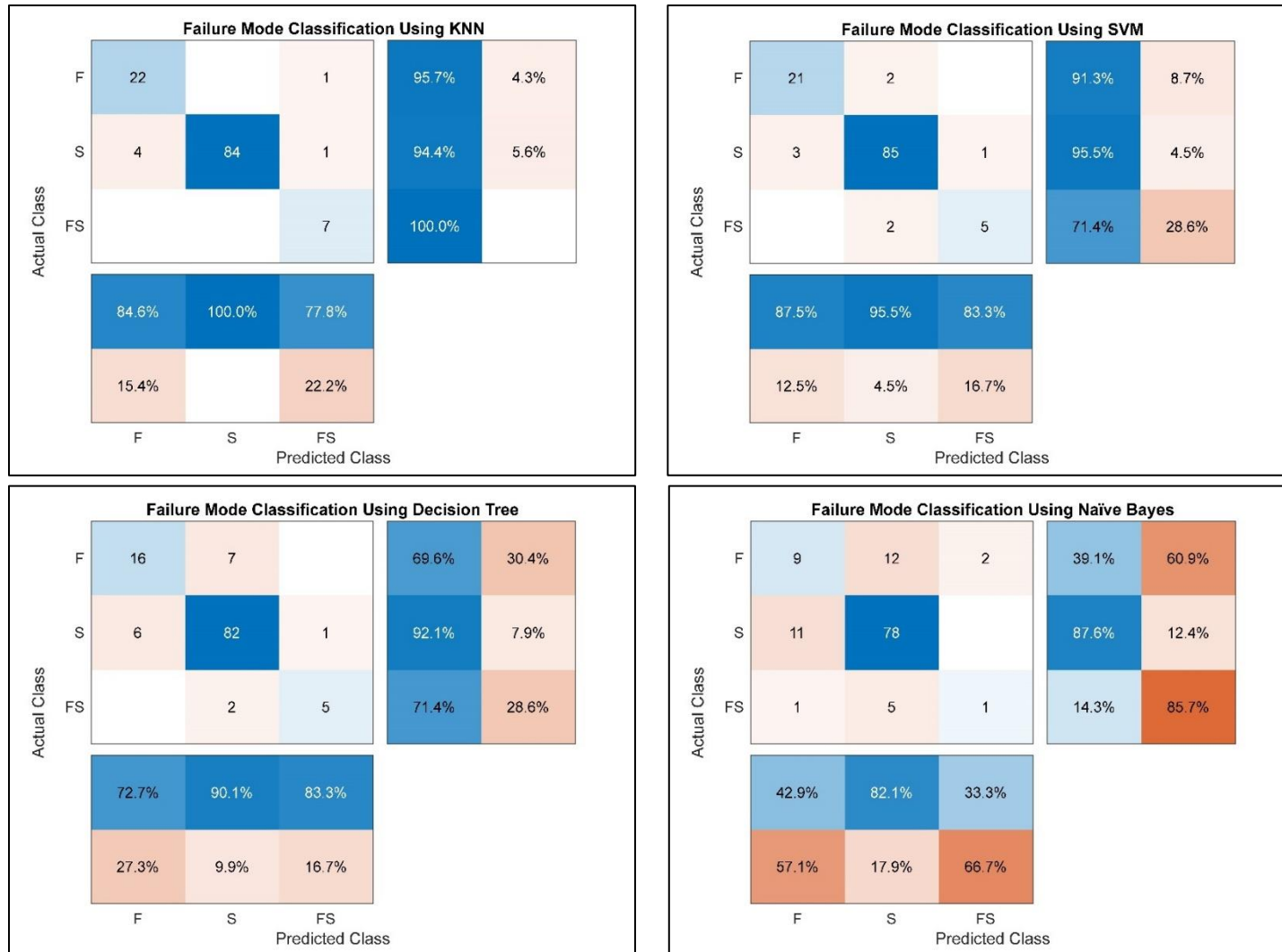


Figure 3.11: Confusion matrix of each classification model.

The confusion matrix of naïve Bayes demonstrates the lowest classification accuracy with 39.1% and 14.3% for F and FS modes, respectively, which is in good agreement with previous results. According to the obtained results, KNN achieved the best performance amongst all models. The advantage of k -nearest neighbor is its ability to perform well with problems having a lot of data examples. Appropriate selection of the parameter k is also key to getting better accuracy. Hence, k -nearest neighbor can be adopted by engineers to forecast the likelihood of shear failure and to estimate the ductile behavior of SFRC beams without transverse reinforcement. This can help in avoiding sudden failures that can occur in some structures due to lack of ductility. In addition, forecasting the failure mode of beams allows selecting the most suitable structural retrofitting approaches at early stages of the construction process, making such operations less costly and more effective.

3.5.3 Improvement of developed models

Even though the suggested ASO-ANN model yielded superior accuracy, there is one drawback associated with its implementation. The repulsive forces governing the motion of the atomic population help the algorithm seek more promising regions in the search space and consequently more accurate solutions. However, they can delay the model convergence, which leads to relatively higher computation time. An effective method to overcome this issue is by using suitable ML models to reduce the number of inputs through feature selection techniques. Recently, sequential feature selection (SFS) and neural interpretation diagram (NID) have gained great momentum in such applications owing to their ability to identify the most influential parameters and reduce data dimensionality (Abuodeh et al., 2020b). SFS appends features sequentially to the model until more addition does not generate an effective change in the selected objective function. Regarding NID, the importance of each variable to the output is illustrated by the magnitudes and signs of the network weights (Abuodeh et al., 2020a, 2020b). Analysis of such weights can prompt insights into the most influential parameters affecting the response variable. Therefore, linking the abovementioned techniques, i.e. SFS and NID, to the suggested ASO-ANN model can effectively decrease computation time and simplify the model architecture, while possibly maintaining adequate predictive accuracy. The same algorithms can also be applied to simplify the suggested classification model by identifying

the most important parameters affecting the failure mode of SFRC beams. Training k -nearest neighbor with the reduced number of features can engender faster training process without affecting its accuracy. This model improvement approach is worth exploring in future studies.

3.6 Conclusions

Shear failure of SFRC beams is a brittle and sudden failure mode. Developing reliable models that can accurately forecast the shear capacity of SFRC beams has long been a concern. Several recent studies have been conducted to achieve this goal, exploring the benefits of various approaches. In the present study, a novel metaheuristic algorithm named atom search optimization was used to optimize the weights and biases of an artificial neural network for predicting the shear strength of SFRC beams without stirrups. ASO is based on molecular dynamics, where velocities and positions of atoms are updated to achieve the best position in the search space, thus helping the ANN to avoid local minima and converge to the near global solution.

Performance assessment of the hybrid ASO-ANN model was carried out in this study via several statistical metrics. The performance of the model was also benchmarked against six hybrid and standalone machine learning models, along with six existing empirical formulations. It was found that the ASO-ANN achieved the best accuracy, outperforming the other models in terms of R , MAE , $RMSE$, and d' . Sensitivity analysis using the ASO-ANN revealed that the shear span-to-depth ratio and the compressive strength of concrete had significant influence on the shear capacity, while the tensile strength of fibers had the lowest total effect.

Moreover, four classification machine learning algorithms were trained and tested for predicting the failure mode of SFRC beams. Results indicated that the k -nearest neighbor demonstrated the most reliable accuracy. This is very encouraging since engineers could adopt it for estimating the likelihood of shear failure, which would allow taking precautions to avert unwanted brittle structural shear failures and choosing the most suitable retrofitting techniques.

However, it is suggested that the developed regression and classification models be improved via feature selection techniques, such as SFS and NID, to ensure higher model transparency. Moreover, the inability of the suggested “black-box” ASO-ANN model and k-nearest neighbor to generate transparent mathematical equations for SFRC shear strength and illustrate real-time crack propagation in the structure, respectively, should trigger further research to explore the effectiveness of alternative ML models, such as genetic programming and recurrent neural networks in mitigating such shortcomings.

3.7 References

- Abuodeh, O. R., Abdalla, J. A., and Hawileh, R. A. (2020a). Prediction of shear strength and behavior of RC beams strengthened with externally bonded FRP sheets using machine learning techniques. *Composite Structures*, 234, 111698.
- Abuodeh, O. R., Abdalla, J. A., and Hawileh, R. A. (2020b). Assessment of compressive strength of Ultra-high Performance Concrete using deep machine learning techniques. *Applied Soft Computing Journal*, 95, 106552.
- Ahmadi-Nedushan, B. (2012). An optimized instance based learning algorithm for estimation of compressive strength of concrete. *Engineering Applications of Artificial Intelligence*, 25(5), 1073–1081.
- Amin, A., and Foster, S. J. (2016). Shear strength of steel fibre reinforced concrete beams with stirrups. *Engineering Structures*, 111, 323–332.
- Ashour, S. A., Hasanain, G. S., and Wafa, F. F. (1992). Shear behavior of high-strength fiber reinforced concrete beams. *ACI Structural Journal*, 89(2), 176–184.
- Batson, G., Jenkins, E., and Spatney, R. (1972). Steel Fibers as Shear Reinforcement in Beams. *ACI Journal Proceedings*, 69(10), 640–644.
- Chai, T., and Draxler, R. R. (2014). Root mean square error (RMSE) or mean absolute error (MAE)? -Arguments against avoiding RMSE in the literature. *Geoscientific Model Development*, 7(3), 1247–1250.
- Cho, S. H., and Kim, Y. Il. (2003). Effects of Steel Fibers on Short Beams Loaded in Shear. *ACI Structural Journal*, 100(6), 765–774.
- Cracknell, M. J., and Reading, A. M. (2014). Geological mapping using remote sensing data: A comparison of five machine learning algorithms, their response to variations in the spatial distribution of training data and the use of explicit spatial information. *Computers and Geosciences*, 63, 22–33.
- DeRousseau, M. A., Kasprzyk, J. R., and Srubar, W. V. (2018). Computational design optimization of concrete mixtures: A review. In *Cement and Concrete Research* (Vol. 109, Issue December 2017, pp. 42–53). Elsevier.
- Huang, L., Xu, L., Chi, Y., and Xu, H. (2015). Experimental investigation on the seismic

- performance of steel-polypropylene hybrid fiber reinforced concrete columns. *Construction and Building Materials*, 87, 16–27.
- Kang, T. H. K., Kim, W., Kwak, Y. K., and Hong, S. G. (2011). Shear testing of steel fiber-reinforced lightweight concrete beams without web reinforcement. *ACI Structural Journal*, 108(5), 553–561.
- Karbassi, A., Mohebi, B., Rezaee, S., and Lestuzzi, P. (2014). Damage prediction for regular reinforced concrete buildings using the decision tree algorithm. *Computers and Structures*, 130, 46–56.
- Khuntia, M., Stojadinovic, B., and Goel, S. C. (1999). Shear strength of normal and high-strength fiber reinforced concrete beams without stirrups. *ACI Structural Journal*, 96(2), 282–289.
- Kumar, S., and Barai, S. V. (2010). Neural networks modeling of shear strength of SFRC corbels without stirrups. *Applied Soft Computing Journal*, 10(1), 135–148.
- Kwak, Y.-K. K., Eberhard, M. O., Kim, W.-S. S., and Kim, J. (2002). Shear Strength of Steel Fiber-Reinforced Concrete Beams without Stirrups. *ACI Structural Journal*, 99(4), 530–538.
- Lantsoght, E. O. L. (2019). Database of shear experiments on steel fiber reinforced concrete beams without stirrups. *Materials*, 16(6), 1–36.
- Lim, T. Y., Paramasivam, P., and Lee, S. L. (1987). Shear and moment capacity of reinforced steel-fibre-concrete beams. *Magazine of Concrete Research*, 39(140), 148–160.
- Mangalathu, S., and Jeon, J. S. (2018). Classification of failure mode and prediction of shear strength for reinforced concrete beam-column joints using machine learning techniques. *Engineering Structures*, 160(September 2017), 85–94.
- Mansur, M. A., Ong, K. C. G., and Paramasivam, P. (1986). Shear Strength of Fibrous Concrete Beams Without Stirrups. *Journal of Structural Engineering*, 112(9), 2066–2079.
- Marugán, A. P., Márquez, F. P. G., Perez, J. M. P., and Ruiz-Hernández, D. (2018). A survey of artificial neural network in wind energy systems. In *Applied Energy* (Vol. 228, Issue April, pp. 1822–1836). Elsevier.
- Moayedi, H., Mehrabi, M., Mosallanezhad, M., Rashid, A. S. A., and Pradhan, B. (2019). Modification of landslide susceptibility mapping using optimized PSO-ANN technique. *Engineering with Computers*, 35(3), 967–984.
- Mohandes, S. R., Zhang, X., and Mahdiyar, A. (2019). A comprehensive review on the application of artificial neural networks in building energy analysis. *Neurocomputing*, 340, 55–75.
- Narayanan, R., and Darwish, I. Y. S. (1987). Use of steel fibers as shear reinforcement. *ACI Structural Journal*, 84(3), 216–227.

- Nazemi, E., Dinca, M., Movafeghi, A., Rokrok, B., and Choopan Dastjerdi, M. H. (2019). Estimation of volumetric water content during imbibition in porous building material using real time neutron radiography and artificial neural network. *Nuclear Instruments and Methods in Physics Research, Section A: Accelerators, Spectrometers, Detectors and Associated Equipment*, 940, 344–350.
- Nehdi, M., El Chabib, H., and Aly Saïd, A. (2007). Proposed shear design equations for FRP-reinforced concrete beams based on genetic algorithms approach. *Journal of Materials in Civil Engineering*, 19(12), 1033–1042.
- Nehdi, Moncef, and Nikopour, H. (2011). Genetic algorithm model for shear capacity of RC beams reinforced with externally bonded FRP. *Materials and Structures/Materiaux et Constructions*, 44(7), 1249–1258.
- Omran, B. A., Chen, Q., and Jin, R. (2016). Comparison of Data Mining Techniques for Predicting Compressive Strength of Environmentally Friendly Concrete. *Journal of Computing in Civil Engineering*, 30(6), 1–13.
- Raghavendra, S., and Deka, P. C. (2014). Support vector machine applications in the field of hydrology: A review. In *Applied Soft Computing Journal* (Vol. 19, pp. 372–386).
- Ryckaert, J. P., Ciccotti, G., and Berendsen, H. J. C. (1977). Numerical integration of the cartesian equations of motion of a system with constraints: molecular dynamics of n-alkanes. *Journal of Computational Physics*, 23(3), 327–341.
- Safarzadegan Gilan, S., Bahrami Jovein, H., and Ramezani-pour, A. A. (2012). Hybrid support vector regression - Particle swarm optimization for prediction of compressive strength and RCPT of concretes containing metakaolin. *Construction and Building Materials*, 34, 321–329.
- Sahoo, D. R., Bhagat, S., and Reddy, T. C. V. (2016). Experimental study on shear-span to effective-depth ratio of steel fiber reinforced concrete T-beams. *Materials and Structures/Materiaux et Constructions*, 49(9), 3815–3830.
- Sahoo, D. R., and Sharma, A. (2014). Effect of steel fiber content on behavior of concrete beams with and without stirrups. *ACI Structural Journal*, 111(5), 1157–1166.
- Saltelli, A., Annoni, P., Azzini, I., Campolongo, F., Ratto, M., and Tarantola, S. (2010). Variance based sensitivity analysis of model output. Design and estimator for the total sensitivity index. *Computer Physics Communications*, 181(2), 259–270.
- Saltelli, A., Ratto, M., Andres, T., Campolongo, F., Cariboni, J., Gatelli, D., Saisana, M., and Tarantola, S. (2008). Global Sensitivity Analysis. The Primer. In *Global Sensitivity Analysis. The Primer*. John Wiley and Sons.
- Shahnewaz, M., and Alam, M. S. (2014). Improved shear equations for steel fiber-reinforced concrete deep and slender beams. *ACI Structural Journal*, 111(4), 851–860.
- Sharifzadeh, M., Sikinioti-Lock, A., and Shah, N. (2019). Machine-learning methods for integrated renewable power generation: A comparative study of artificial neural networks, support vector regression, and Gaussian Process Regression. *Renewable*

- and Sustainable Energy Reviews*, 513–538.
- Sharma, A. K. (1986). Shear strength of steel fiber reinforced concrete beams. *Journal of the American Concrete Institute*, 83(4), 624–628.
- Shoaib, A., Lubell, A. S., and Bindiganavile, V. S. (2015). Shear response of lightweight steel fiber reinforced concrete members without stirrups. *Materials and Structures/Materiaux et Constructions*, 48(10), 3141–3157.
- Stone, A. (2013). The Theory of Intermolecular Forces. In *The Theory of Intermolecular Forces*.
- Sudret, B. (2008). Global sensitivity analysis using polynomial chaos expansions. In *Reliability Engineering and System Safety* (Vol. 93, Issue 7, pp. 964–979). Elsevier.
- Tahenni, T., Chemrouk, M., and Lecompte, T. (2016). Effect of steel fibers on the shear behavior of high strength concrete beams. *Construction and Building Materials*, 105, 14–28.
- Taylor, K. E. (2001). Summarizing multiple aspects of model performance in a single diagram. *Journal of Geophysical Research Atmospheres*, 106(D7), 7183–7192.
- Vu-Bac, N., Silani, M., Lahmer, T., Zhuang, X., and Rabczuk, T. (2015). A unified framework for stochastic predictions of mechanical properties of polymeric nanocomposites. *Computational Materials Science*, 96(PB), 520–535.
- Xu, J., Zhao, X., Yu, Y., Xie, T., Yang, G., and Xue, J. (2019). Parametric sensitivity analysis and modelling of mechanical properties of normal- and high-strength recycled aggregate concrete using grey theory, multiple nonlinear regression and artificial neural networks. *Construction and Building Materials*, 211, 479–491.
- Yuan, Z., Wang, L. N., and Ji, X. (2014). Prediction of concrete compressive strength: Research on hybrid models genetic based algorithms and ANFIS. *Advances in Engineering Software*, 67, 156–163.
- Zhao, W., Wang, L., and Zhang, Z. (2019). Atom search optimization and its application to solve a hydrogeologic parameter estimation problem. *Knowledge-Based Systems*, 163, 283–304.
- Zheng, B., Myint, S. W., Thenkabail, P. S., and Aggarwal, R. M. (2015). A support vector machine to identify irrigated crop types using time-series Landsat NDVI data. *International Journal of Applied Earth Observation and Geoinformation*, 34(1), 103–112.

Chapter 4

Genetic Programming Based Symbolic Regression for Shear Capacity Prediction of SFRC Beams

4.1 Introduction

Complex shear transfer mechanisms in steel fiber-reinforced concrete beams (SFRC) have motivated researchers to develop diverse methods for predicting the shear capacity of SFRC beams, including empirical and soft-computing models. However, existing models were developed with relatively limited databases, making their generalization capability uncertain. To account for the limited experimental data, a novel approach based on tabular generative adversarial network (TGAN) has been employed in the present study to generate synthetic data comprising 2000 data examples. A “train on synthetic - test on real” philosophy was adopted. Accordingly, the synthetic data was used for training a genetic programming-based symbolic regression (GP-SR) model to develop a shear strength equation for SFRC beams without stirrups. Feature selection techniques were used to train the model effectively and avoid irrelevant data that can negatively impact the model accuracy. Unlike the “black-box” models developed in the previous chapter, the analysis of the evolved GP-SR based equation can generally prompt human insights into underlying mechanical and physical phenomena characterizing the problem, which helps instill trust in the developed equation. The evolved equation was tested on 309 real experimental data examples thus far unknown to the model. The accuracy of the model was also benchmarked against eleven existing equations for SFRC shear strength. In addition, multiple validation criteria were employed to validate the predictive capacity of the proposed equation. Global sensitivity analysis was finally carried out to determine the most influential parameters to the model. Deploying TGAN for training a GP-SR and using real experimental test data has never been done for modeling the shear capacity of SFRC beams in the open literature. The new predictive equation established with this novel approach should expand the accuracy of pertinent design codes while mitigating the “black box” limitations of existing soft computing models.

4.2 Database Description

The experimental database used in the present study comprises results obtained via three-point and four-point shear testing methods applied on 309 SFRC beams without stirrups. Only specimens that exhibited pure shear failure mode were included in the database. The dataset englobes eight features including the beam width (b_w), effective depth of the beam (d), shear span-to-depth ratio (a/d), longitudinal steel ratio (ρ), compressive strength of concrete (f'_c), steel fiber volume fraction (V_f), fiber aspect ratio (l_f/d_f), and fiber type. **Table 4.1** entails the range of features along with the references from which test results have been retrieved. It was reported that the fiber volume fraction had a noteworthy effect on the shear strength of SFRC beams. However, its combination with the fiber aspect ratio led to a more significant effect (Slater et al., 2012). This combination is commonly known as the fiber factor (F), which also involves the bond factor (d_f) determined by the type of steel fibers. The fiber factor is expressed as follows:

$$F = V_f \times \frac{l_f}{d_f} \times d_f \quad (4.1)$$

The bond factor is equal to 0.5, 0.75, and 1 for straight, crimped, and hooked fibers, respectively. Owing to its important influence, the fiber factor was used herein as an input parameter that accounts for the fiber type. The descriptive statistics of the various input variables and the corresponding output of the final database used in subsequent sections are provided in **Table 4.2**.

Data pre-processing was also conducted to ensure that data can effectively train the models without impacting accuracy. For this purpose, data visualization was performed to check the distribution of values for the different input parameters and ensure that outliers that deviate significantly from the entire dataset were discounted. It is also worth mentioning that only reliable data was collected and examples with assumed feature values in the open literature were not included in the dataset to ensure the most accurate results. Feature selection is another data pre-processing technique that can help remove irrelevant data and ensure better model accuracy. The process of this technique is discussed in detail in the subsequent section.

Table 4.1: Database of SFRC beams without stirrups

No. of data	Geometric properties of the beam						Steel properties		Concrete properties		Fiber properties				Shear capacity		Ref.	
	b_w (mm)		d (mm)		a/d		ρ (%)		f'_c (MPa)		V_f (%)		l_f/d_f		Fiber type	v_u (MPa)		
	min	max	min	max	min	max	min	max	min	max	min	max	min	max		min		max
32	150	150	251	251	3.49	3.49	2.67	2.67	24.90	64.60	0.50	1.50	50	85	hooked, crimped	1.726	5.179	(Singh and Jain, 2014)
3	150	150	261	261	3.45	3.45	1.95	1.95	23.80	32.90	0.75	1.25	80	80	hooked	2.376	2.912	(Sahoo and Sharma, 2014)
6	140	140	175	175	1.50	2.50	1.28	1.28	82.00	83.80	0.50	1.50	80	80	hooked	2.531	7.592	(Manju et al., 2017)
8	150	150	200	200	2.50	4.50	1.34	1.34	9.77	33.68	1.00	3.00	55	55	hooked	1.067	2.133	(Arslan et al., 2017)
3	150	150	217	217	1.59	2.95	1.85	1.85	35.00	35.00	0.75	0.75	80	80	hooked	2.581	4.547	(Sahoo et al., 2016)
2	300	300	622	622	2.81	2.81	1.98	1.98	34.00	36.00	0.32	0.69	65	65	hooked	1.527	1.903	(Amin and Foster, 2016)
3	100	100	135	135	2.22	2.22	1.16	1.16	64.20	64.20	0.50	0.50	65	65	hooked	3.037	3.185	(Tahenni et al., 2016)
28	85	85	126	130	2.02	3.52	2.05	5.72	30.60	53.55	0.25	2.00	100	133	crimped	1.901	7.096	(Narayanan and Darwish, 1987)
4	150	150	219	219	2.00	2.80	1.91	1.91	40.85	43.23	1.00	2.00	60	60	hooked	2.922	3.531	(Cucchiara et al., 2004)
2	125	125	212	212	2.00	3.00	1.52	1.52	30.80	30.80	0.50	0.50	63	63	hooked	2.528	4.038	(Y.-K. K. Kwak et al., 2002)
2	100	100	130	130	3.08	3.08	3.09	3.09	38.69	42.40	1.00	2.00	60	60	straight	4.462	5.692	(D. H. Lim and Oh, 1999)
21	152	205	381	610	3.44	3.50	1.52	2.63	28.70	50.80	0.75	1.50	55	80	hooked	1.815	3.782	(Dinh et al., 2010)
1	125	125	225	225	2.89	2.89	3.49	3.49	90.00	90.00	1.25	1.25	60	60	hooked	5.582	5.582	(Pascal Casanova et al., 1997)
4	150	300	202	437	2.97	3.09	1.17	1.50	19.60	21.30	0.50	1.00	55	55	hooked	1.220	1.848	(Hassan Aoude et al., 2012)
6	200	200	435	910	2.50	2.51	0.99	1.04	24.40	55.00	0.25	0.38	50	50	hooked	1.368	1.857	(Minelli and Plizzari, 2013)
1	125	125	210	210	4.00	4.00	1.53	1.53	44.60	44.60	0.50	0.50	63	63	hooked	1.333	1.333	(Kang et al., 2011)
1	125	125	225	225	2.89	2.89	3.49	3.49	90.00	90.00	1.25	1.25	60	60	hooked	4.907	4.907	(P. Casanova and Rossi, 1999)
6	152	152	221	221	1.50	3.50	1.20	2.39	34.00	34.00	0.50	1.00	60	60	hooked	1.459	4.376	(T. Y. Lim et al., 1987)
9	150	150	197	197	2.00	3.60	1.36	2.04	20.60	33.40	0.50	0.75	60	60	hooked	1.523	2.910	(Mansur et al., 1986)
8	152	610	254	813	3.45	3.61	2.47	2.86	29.00	50.00	0.75	0.75	67	67	hooked	2.477	3.506	(Zarrinpour and Chao, 2017)
13	200	300	180	570	2.77	3.33	2.87	4.47	60.20	93.30	0.50	1.00	40	86	hooked, straight	2.673	8.306	(Noghabai, 2000)
6	200	200	314	314	3.50	3.50	3.50	3.50	132.00	154.00	1.00	2.00	75	75	straight	3.201	5.717	(Randl et al., 2018)

Table 4.1 (Continued)

No. of data	Geometric properties of the beam						Steel properties		Concrete properties		Fiber properties				Shear capacity		Ref.	
	b_w (mm)		d (mm)		a/d		ρ (%)		f'_c (MPa)		V_f (%)		l_f/d_f		Fiber type	v_u (MPa)		
	min	max	min	max	min	max	min	max	min	max	min	max	min	max		min		max
5	55	55	265	265	2.00	4.91	2.76	4.31	33.95	41.90	1.00	1.00	100	100	crimped	2.882	5.489	(R. Narayan Swamy et al., 1993)
6	150	150	560	560	1.63	1.63	2.14	2.14	40.80	56.50	0.40	1.50	60	60	hooked	2.441	3.869	(Adebar et al., 1997)
6	120	120	168	168	1.43	1.43	1.32	2.82	25.70	86.10	0.50	1.50	60	60	hooked	2.985	9.254	(Cho and Kim, 2003)
3	200	200	265	265	3.02	3.02	1.78	1.78	38.00	47.90	0.50	1.00	50	50	hooked	1.717	2.811	(Greenough and Nehdi, 2008)
2	200	200	285	310	2.55	2.77	1.13	3.33	39.80	39.80	0.38	0.38	80	80	hooked	2.145	3.895	(Kang et al., 2012)
19	200	200	260	305	1.54	4.04	1.03	3.55	26.50	47.60	0.25	0.75	45	80	hooked	1.584	5.789	(Dupont and Vandewalle, 2003)
5	175	175	210	210	4.50	4.50	3.10	4.01	36.41	40.84	0.40	1.20	100	100	crimped	1.905	3.238	(R. N. Swamy and Bahia, 1985)
34	101	101	127	127	1.20	5.00	3.09	3.09	33.22	40.21	0.22	1.76	62	102	straight, crimped	1.715	11.226	(Batson et al., 1972)
6	100	100	175	175	2.00	4.50	3.59	3.59	80.00	80.00	0.50	1.00	100	100	straight	2.743	7.371	(Shin et al., 1994)
3	200	200	300	300	2.50	4.50	3.08	3.08	110.00	111.50	0.75	0.75	75	75	hooked	3.517	4.767	(Vandewalle and Mortelmans, 1994)
4	152	152	283	283	2.50	2.50	1.99	1.99	33.03	34.38	1.00	2.00	100	100	hooked	3.088	3.367	(K.-H. Kwak et al., 1993)
7	100	100	159	166	3.02	3.14	3.43	4.78	35.50	88.00	0.50	2.00	60	60	hooked	1.813	5.094	(Hwang et al., 2013)
2	150	150	219	219	2.00	2.80	1.91	1.91	80.04	80.04	1.00	1.00	55	55	hooked	3.470	4.292	(Spinella et al., 2012)
1	100	100	275	275	2.00	2.00	0.55	0.55	28.40	28.40	0.50	0.50	75	75	hooked	1.527	1.527	(Chalioris and Sfiri, 2011)
5	125	125	210	212	3.77	3.81	1.52	2.28	49.60	59.40	0.50	1.00	55	80	hooked	1.623	2.248	(H Aoude and Cohen, 2014)
8	100	100	140	245	0.90	2.50	0.64	1.12	36.08	36.90	0.50	0.75	63	63	hooked	1.235	6.143	(Qissab and Salman, 2018)
6	100	100	85	85	3.52	3.52	1.66	1.66	49.30	54.80	0.50	2.00	127	191	crimped	1.994	2.581	(Furlan and De Hanai, 1997)

Table 4.1 (Continued)

No. of data	Geometric properties of the beam						Steel properties		Concrete properties		Fiber properties				Shear capacity		Ref.	
	b_w (mm)		d (mm)		a/d		ρ (%)		f'_c (MPa)		V_f (%)		l_f/d_f		Fiber type	v_u (MPa)		
	min	max	min	max	min	max	min	max	min	max	min	max	min	max		min		max
2	200	200	273	273	2.75	2.75	3.48	3.48	109.20	110.90	0.75	0.75	64	67	hooked	3.681	3.846	(Dancygier and Savir, 2011)
2	80	80	165	165	2.99	2.99	1.71	1.71	39.87	41.23	1.00	1.50	50	50	hooked	2.424	3.030	(Krassowska and Kosior-Kazberuk, 2018)
1	300	300	420	420	3.21	3.21	3.22	3.22	62.30	62.30	0.75	0.75	65	65	hooked	3.302	3.302	(Yoo and Yang, 2018)
2	125	125	222	222	1.80	1.80	1.45	1.45	30.00	30.00	0.50	0.50	80	80	hooked	2.811	3.063	(Gali and Subramaniam, 2017)
2	310	310	240	258	3.00	3.00	2.50	4.03	23.00	41.00	1.00	1.00	55	55	hooked	2.638	3.777	(Shoaib et al., 2014)
7	300	300	523	923	3.00	3.00	1.44	2.55	23.00	80.00	1.00	1.00	55	55	hooked	1.555	2.843	(Shoaib, 2012)
2	200	200	300	300	2.00	3.50	3.60	3.60	199.00	215.00	2.00	2.00	55	55	hooked	6.217	9.767	(Bae et al., 2013)

Table 4.2: Descriptive statistics of the database

	b_w (mm)	d (mm)	a/d	ρ (%)	f'_c (MPa)	V_f (%)	l_f/d_f	F	v_u (MPa)
μ	150.889	263.582	3.043	2.505	47.922	0.833	74.803	0.538	3.252
σ	60.332	161.975	0.812	1.034	26.365	0.470	25.700	0.346	1.642
Minimum	55.000	85.250	0.900	0.550	9.770	0.220	40.000	0.102	1.067
25%	101.000	150.000	2.500	1.810	33.220	0.500	60.000	0.315	2.183
50%	150.000	221.000	3.080	2.540	40.210	0.750	65.000	0.499	2.882
75%	200.000	275.000	3.500	3.090	53.200	1.000	80.000	0.645	3.598
Maximum	610.000	923.000	5.000	5.720	215.000	3.000	191.000	2.865	11.226
Skewness	2.066	2.008	-0.229	0.857	2.704	1.356	1.995	2.043	1.927
Kurtosis	13.450	7.469	2.883	4.008	13.296	5.722	8.404	11.040	7.605

4.3 Feature Selection

Irrelevant features with relatively low consequence on the target variable may adversely affect the model performance and increase computation time. Thus, identifying informative features with feature selection methods is key to decreasing the dimensionality of data, removing irrelevant data, simplifying the generated model, and speeding up the learning mechanism (Xue et al., 2016). One way to select the most relevant features is through their importance scores. Importance scores reflect the significance of the input parameter to the target variable. Decision tree models included in the scikit-learn library of Python offer a simple way to extract such importance scores using the “.feature_importances_” attribute.

Hence, three models, namely classification and regression trees (CART), random forest (RF), and stochastic gradient boosting (XGBoost) have been deployed to assess feature relevance. For each algorithm, five different values of “random state” were specified to randomly select 70% of the experimental database used for training the model. Results are depicted in **Figure 4.1**.

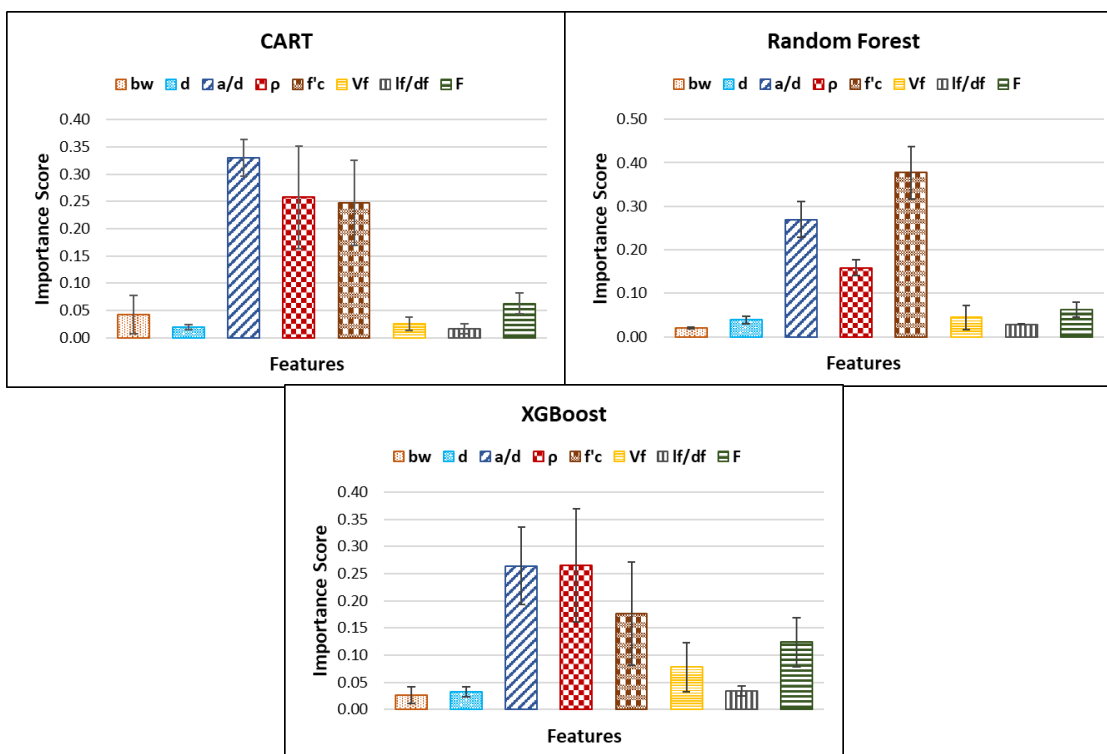


Figure 4.1: Feature importance scores.

The results correspond to the mean values obtained from the five simulations, and the error bars represent the standard deviation. It can be observed that a/d , ρ , and f'_c had the most significant effect on the shear capacity. The beam width presented the lowest importance score except for CART, where its standard deviation was significant. The effective depth of the beam had lower effect compared to that of the fiber volume fraction. The fiber factor had superior influence over V_f and l_f/d_f , affirming the aforementioned assumptions. Furthermore, the correlation matrix illustrated in **Figure 4.2** reflects a strong linear dependency between F and V_f . All of these factors can help disregard b_w , d , V_f , and l_f/d_f due to their little impact and/or linear dependency with other more influential parameters. Therefore, only a/d , ρ , f'_c , and F have been selected for training TGAN in the next sections.

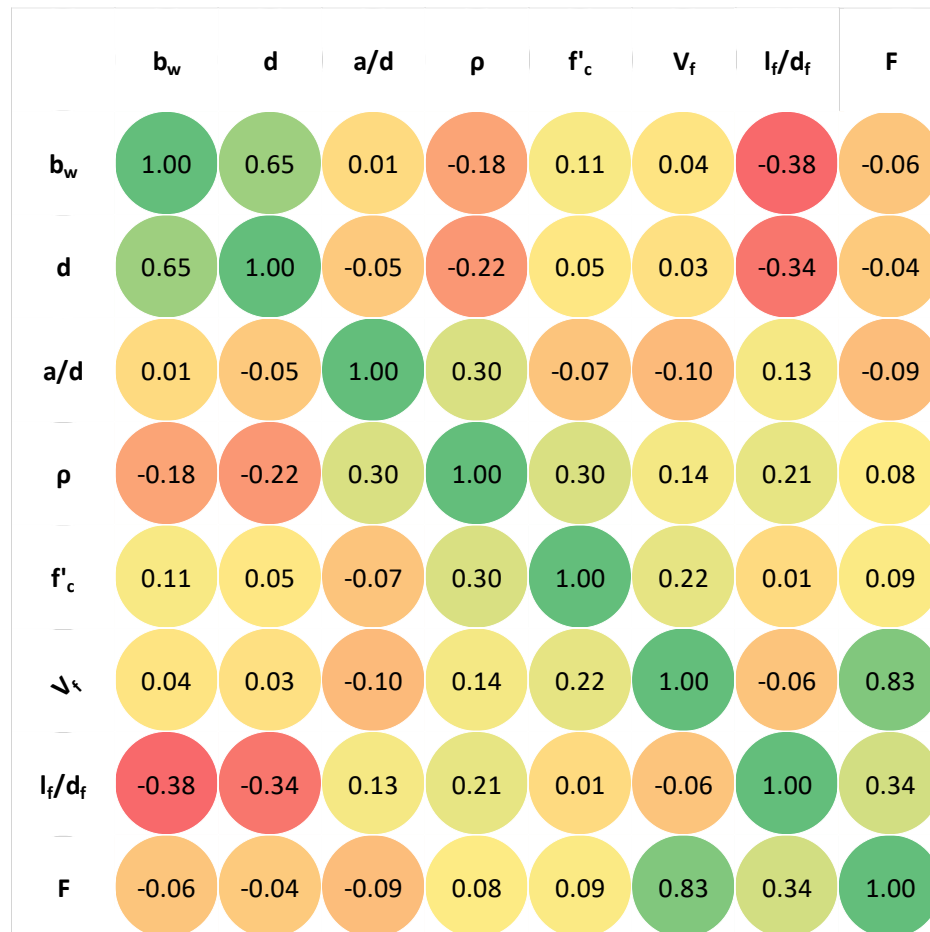


Figure 4.2: Correlation matrix of input features.

4.4 Genetic Programming Based Symbolic Regression

Genetic programming (GP) is an evolutionary algorithm that develops a population of computer programs for solving specific problems (Koza, 1994). GP is based on Darwinian principles of natural selection and genetic spread of features adopted by biologically developing species (Deshpande et al., 2013; Ghugare and Tambe, 2017). Symbolic regression (SR) is a particular application of GP in which GP evolves populations of symbolic tree expressions to generate the mathematical formula that provides the best fitness value. Accordingly, GP based symbolic regression (GP-SR) aims to optimize the expression and the corresponding parameters of a linear or nonlinear function expressed as follows:

$$y = f(x, p) \quad (4.2)$$

where $x = (x_1, \dots, x_n)^T$ is an n -dimensional vector of model inputs, y represents the model output, and $p = (p_1, \dots, p_m)^T$ denotes the m -dimensional vector of the model parameters.

Before the start of the analysis, the tree depth and size are initialized. Then, the algorithm generates a random population of tree-structured symbolic expressions by combining several functions such as addition, multiplication, and subtraction, with input parameters and random constants. Each developed expression is evaluated via the mean squared error (MSE), which represents the selected fitness function. Expressions with the best fitness value are prone to a probabilistic selection and recombination via two genetic operations named crossover and mutation (Nembhard and Sun, 2019). As illustrated in **Figure 4.3**, crossover corresponds to an exchange of sub-trees between a pair of expressions that recorded high fitness values. This exchange leads to new offspring formulations. Regarding mutation, a randomly selected node of the previously formed tree is modified as shown in **Figure 4.4**, to stimulate diversity within the tree-structured populations and expand the exploration of better data fitting models. The newly generated expressions replace those with lower fitness values in the tree population. The iterative process of evaluation, selection, crossover, and mutation defines one generation of the analysis. The process is repeated until the maximum number of generations is achieved.

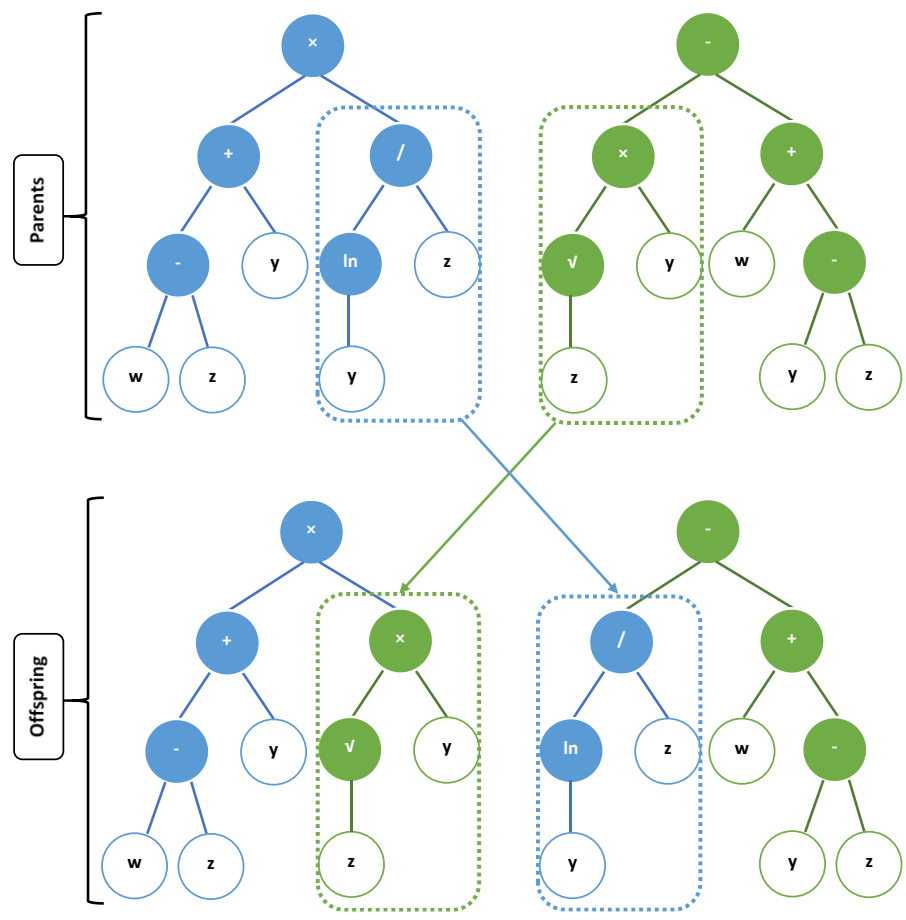


Figure 4.3: Crossover in GP-SR model.

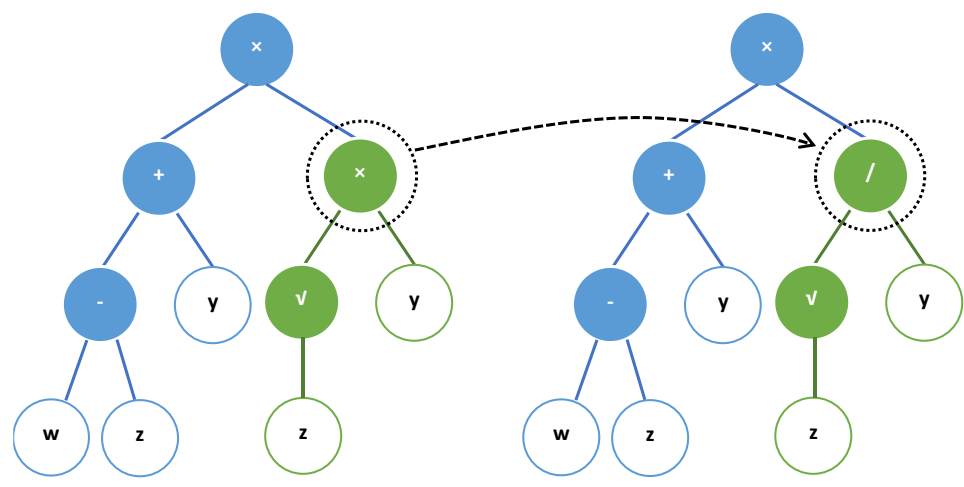


Figure 4.4: Mutation in GP-SR model.

As entailed in **Table 4.3**, different parameters have been selected for model deployment in python. Ramped half-and-half is an initialization approach that combines the “full” and “grow” methods, leading to a population of trees with different shapes and depths that range from the selected initial tree depth to the maximum tree depth. Tournament size refers to the number of individuals that will vie to produce the next generation. Parsimony coefficient is applied to penalize large programs by making their fitness less favorable and ensure that trees have reasonable length and enough transparency.

Table 4.3: Set of parameters used to develop GP-SR

Parameter	Values
Population size	1000, 2000, 3000, 4000, 5000
Crossover rate (%)	70, 80, 90
Mutation rate (%)	30, 20, 10
Tournament size	5, 10, 15, 20, 25, 30
Parsimony coefficient	0.1, 0.01, 0.001, 0.0001
Function set	+, -, ×, /, √, ln, exp
Methods used	Initialization: Ramped half-and-half Selection: Tournament selection Crossover: Subtree exchange Mutation: Subtree replacement
Initial tree depth	2
Maximum tree depth	12

4.5 Model Training through TGAN

Training machine learning models with limited databases can create overfitting issues. Models trained with further clean data acquire greater generalization capability compared to those developed with few data examples. Nevertheless, gathering large datasets might be challenging for certain problems due to the restricted number of experimental tests. Recently, tabular generative adversarial networks (TGAN) has been introduced as a new approach to expand existing databases with synthetic data. TGAN consists of building a generative model that can produce synthetic data with similar characteristics to the actual data (Xu and Veeramachaneni, 2018). The approach comprises two key components called the generator and the discriminator. As shown in **Figure 4.5**, the generator receives a random noise as input and generates synthetic data. Conversely, the discriminator learns to

distinguish between real examples and “fake” examples and assigns a specific score to indicate whether data is actual or synthetic. The key objective of the generator is to fool the discriminator by enhancing the quality of synthetic data and make the distinction process harder.

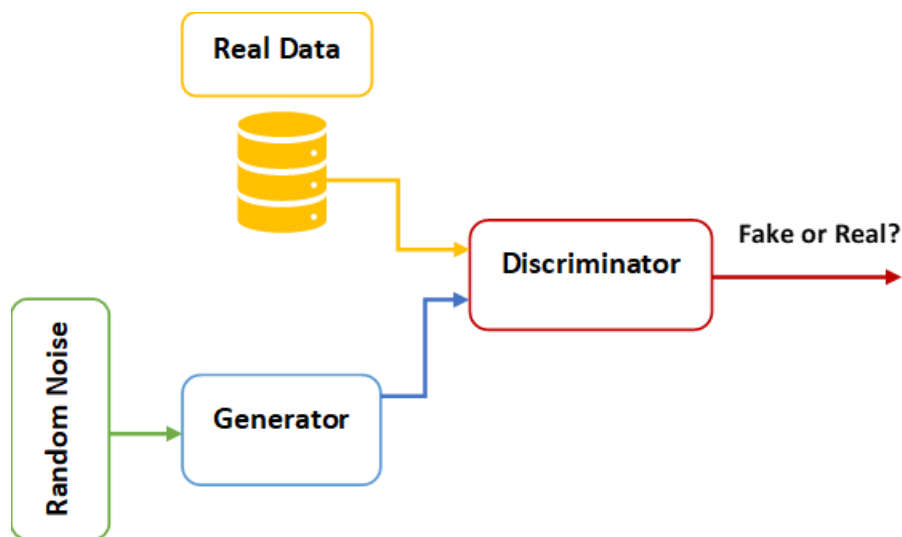


Figure 4.5: Simplified process of TGAN.

Generally, long short-term memory (LSTM) network and multi-layer perceptron are used as generator and discriminator, respectively. For the present study, the collected experimental database of 309 samples was used to train TGAN. The generative model produced 2000 synthetic samples that will be involved in the training GP-SR model. The trained GP-SR model is tested afterwards over real experimental data to verify the generalization capability of the model as well as the reliability of synthetic data. The entire process of developing GP-SR model is schematically represented in **Figure 4.6**. It is to be understood that the “fake” synthetic data is only used for training the model. The robustness and predictive accuracy of the GP-SR model is exclusively validated on real experimental data that is unknown to the model, and thus far never presented to it.

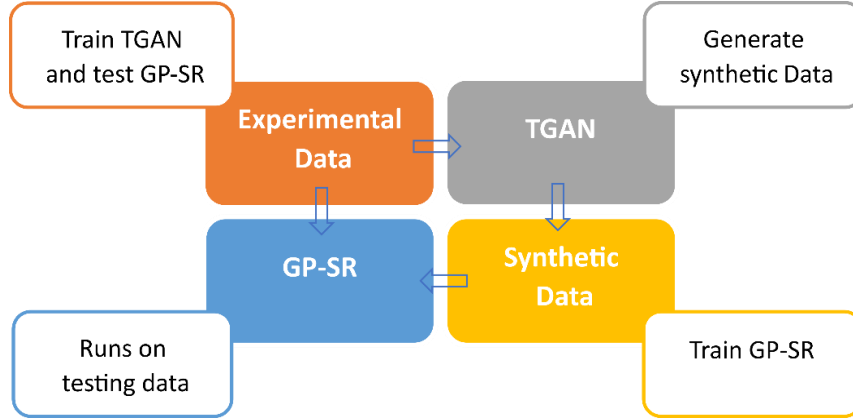


Figure 4.6: Process of training and testing GP-SR.

4.6 Results and Discussion

4.6.1 Statistical metrics

Statistical metrics are commonly used for assessing the predictive accuracy of ML models as well as comparing the performance of various algorithms. The metrics used in this study are the correlation coefficient (R), root mean squared error ($RMSE$), mean absolute error (MAE), and three other parameters characterizing the ratio of the predicted value (v_p) and tested value (v_t) including the mean (μ), standard deviation (σ), and coefficient of variation (COV). The expression of each metric is indicated below.

$$R = \frac{n \sum_{i=1}^n v_{p_i} v_{t_i} - (\sum_{i=1}^n v_{p_i})(\sum_{i=1}^n v_{t_i})}{\sqrt{n(\sum_{i=1}^n v_{p_i}^2) - (\sum_{i=1}^n v_{p_i})^2} \sqrt{n(\sum_{i=1}^n v_{t_i}^2) - (\sum_{i=1}^n v_{t_i})^2}} \quad (4.3)$$

$$RMSE = \sqrt{\frac{\sum_{i=1}^n (v_{p_i} - v_{t_i})^2}{n}} \quad (4.4)$$

$$MAE = \frac{1}{n} \sum_{i=1}^n |v_{p_i} - v_{t_i}| \quad (4.5)$$

$$\mu = \frac{1}{n} \sum_{i=1}^n \left(\frac{v_{p_i}}{v_{t_i}} \right) \quad (4.6)$$

$$\sigma = \sqrt{\frac{\sum_{i=1}^n \left(\left(\frac{v_{p_i}}{v_{t_i}} \right) - \mu \right)^2}{n}} \quad (4.7)$$

$$COV (\%) = \frac{\sigma}{\mu} \times 100 \quad (4.8)$$

Higher values of *RMSE* and *MAE* reflect greater error between values, while lower *COV* indicates a lower level of dispersion of the different data points around the mean.

4.6.2 Proposed new shear equation

As indicated earlier, the proposed equation for predicting the shear capacity of SFRC beams without stirrups is a function of four parameters that have the highest influence on its value. It is worth mentioning that the suggested equation has been selected based on two criteria. The first criterion is the program length, which represents the total number of nodes. Extremely complex equations were discounted and only those with a length of less than 30 were considered to ensure enough model transparency. The second criterion is the fitness value described above. The equation that provides the best fitness value will be considered as the best solution. The final equation obtained from the GP-SR model is expressed as follows:

$$v_u(MPa) = 0.921 + \frac{0.694 \times \ln(1.786 F + 1.091 \rho) \times \sqrt{0.787 f'_c + \frac{4.863 \rho \sqrt{0.798 f'_c}}{\left(\frac{a}{d}\right)^3}}}{\left(\frac{a}{d}\right)} \quad (4.9)$$

where f'_c is expressed in (MPa), while ρ , F , and $\frac{a}{d}$ are dimensionless numbers. Several observations can be extracted from the proposed formula by altering one variable and keeping the others constant at their mean values. **Figure 4.7** shows that an increase in the shear span-to-depth ratio leads to lower shear capacity. This can be explained by the arch action effect, which represents the compressive force generated along the loading points and beam supports. In the region of short shear spans, loads are carried in part via the arch action. The arch action tends to resist the applied shear, leading to higher capacity (Jeong and Kim, 2014). Moreover, an increase in the value of the fiber factor engenders higher

shear strength. The increase of shear capacity is attributed to the improvement of both the arch action and dowel action caused by fiber inclusion (Narayanan and Darwish, 1987). The shear capacity is also improved by the increase of the compressive strength of concrete. The rate of increase diminishes with higher compressive strength, contrarily to some studies that reported exponential relationships (Khuntia et al., 1999). Similarly, the rate of increase in the shear capacity is reduced when a higher reinforcement ratio is included. This is reflected by the logarithmic function and the square root function applied to the reinforcement ratio. This was previously confirmed by Swamy and Bahia (1985). The decrease of the shear capacity improvement rate for the longitudinal reinforcement ratio was linked to the influence of the steel area and net concrete width at the steel level (Li et al., 1992; R. N. Swamy and Bahia, 1978). These two factors exhibited an important influence on the dowel resistance and consequently on the shear capacity.

The other important aspect that needs further investigation is the size effect. Several recent studies reported a significant influence of this factor on shear strength (Chao, 2020; Minelli et al., 2014; Shoaib et al., 2014). The abovementioned equation determines the shear stress, which represents the shear force per unit area. When the original database was collected, the shear stress representing the shear force divided by the product of beam width and effective depth of beam has been considered as the output variable. This dependency explains the low importance scores attributed to these two input features. The resultant shear force is therefore expressed as follows:

$$v_u(MN) = \left[0.921 + \frac{0.694 \times \ln(1.786 F + 1.091 \rho) \times \sqrt{0.787 f'_c + \frac{4.863 \rho \sqrt{0.798 f'_c}}{\left(\frac{a}{d}\right)^3}}}{\left(\frac{a}{d}\right)} \right] b_w d \quad (4.10)$$

It was reported that larger beams would generally fail at lower stress because of the size effect. In the resultant shear force equation, the shear span and effective depth of the beam are both related to the size effect. Chao (2020) reported that the shear span is a significant parameter that influences the size effect. When the depth of the beam is increased, the shear

span also increases to maintain specific ratios and ensure realistic specimen configuration. Thus, the compression zone for larger beams typically has lower contribution to shear resistance, which leads to lower shear capacity (Chao, 2020). The fiber factor in the equation also influences the size effect. Minelli et al., (2014) posited that incorporating steel fibers can mitigate the size effect in shear, which makes the results for plain concrete not applicable to SFRC beams.

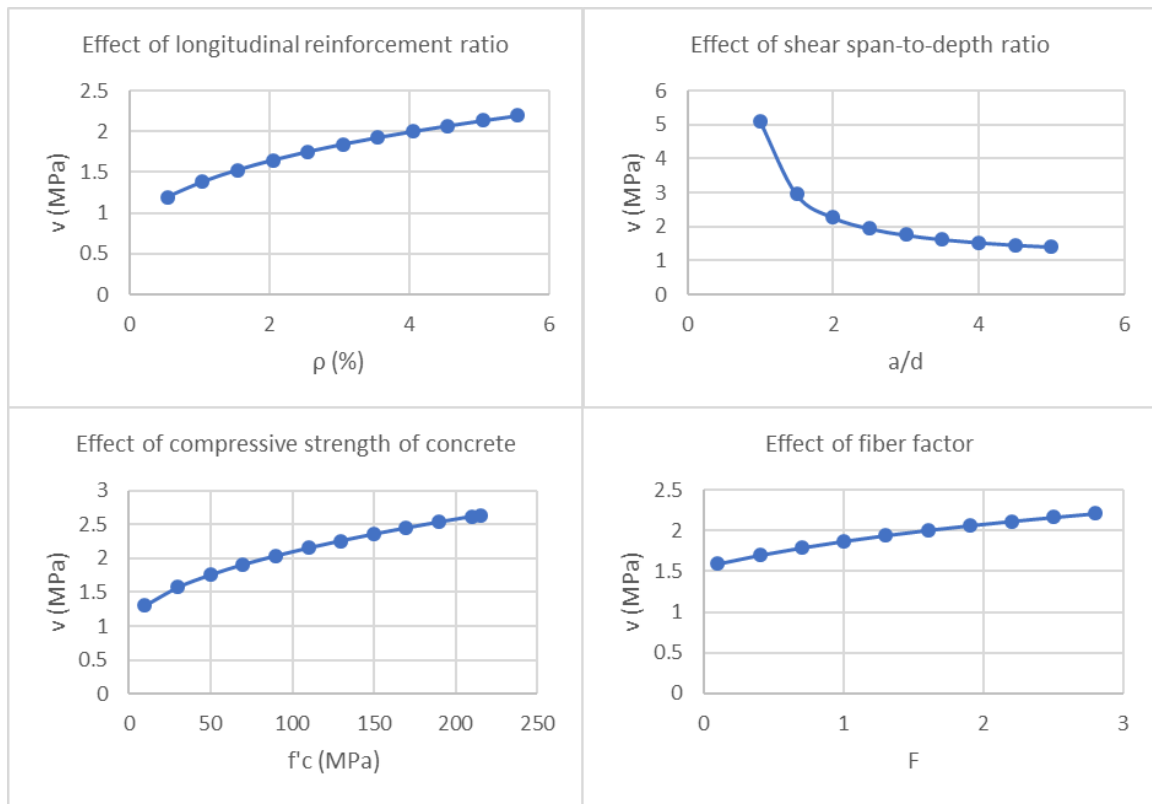


Figure 4.7: Effect of input features on the shear capacity.

4.6.3 Performance assessment of proposed equation

Evaluation of the proposed model has been performed through the statistical metrics described earlier. Also, the model was benchmarked against several existing equations outlined in **Table 4.4**. Some of the equations are based on an empirical approach, while others were developed using soft computing techniques (Sarveghadi et al., 2019;

Shahnewaz and Alam, 2014, 2020). The performance of each model over the experimental database is captured in **Table 4.5**. It can be observed that the proposed equation outperformed all the other models with $R = 0.8878$, $RMSE = 0.8421$, and $MAE = 0.6099$. This indicates that the model generates lower error as well as stronger uphill linear pattern between predicted and experimental values. Smith (1986) argued that if a positive correlation coefficient is higher than 0.8 then there is a strong correlation between actual and predicted values. To better investigate the model validity, Golbraikh and Tropsha (2002) introduced several validation criteria. As outlined in **Table 4.6**, k and k' that denote the slope of regression lines through the origin should be close to 1, and the correlation coefficients through the origin (R_0^2 and $R_0'^2$) should be close to R . Moreover, Roy and Roy (2008) suggested another validation criterion (R_m) that evaluates the external predictability of a model, and stated that for a good model, R_m should be greater than 0.5. It was found that the proposed equation satisfied all the validation criteria, indicating a strong predictive ability for new unseen data.

In addition, the model exhibited the lowest COV amongst the presented equations, which means that the obtained values had lower level of dispersion around the mean. The main reason behind the superior accuracy of the proposed model is the extensive database used in its training. Even though the data used for training was synthetic and generated from TGAN, the model exhibited strong generalization capability, which indicates that TGAN can produce reliable data examples for training. It is worth mentioning that this is the biggest database that has ever been used for training a soft computing model to predict the shear strength of SFRC beams. Moreover, the model has shown compliance with previous research findings as described in the previous section, which also explains its reliability. The ranking system presented in **Table 4.7** can further confirm the superior performance of the developed model. The system uses the average scores based on the values of statistical metrics. Higher scores are assigned with higher R values, and lower scores are attributed to higher $RMSE$, MAE and COV . The other existing equations demonstrated lower accuracy compared to the proposed model. For example, The formula suggested by Shahnewaz and Alam (2020) achieved the second best predictive accuracy in terms of R , $RMSE$, and MAE , which is also reflected in the ranking system.

Table 4.4: Existing equations for SFRC shear strength

Reference	Suggested model
(Sharma, 1986)	$v_u = k f_t (d/a)^{\frac{1}{4}}$ $k = \begin{cases} 1 & \text{if } f_t \text{ is obtained by direct tension test} \\ 2/3 & \text{if } f_t \text{ is obtained by indirect tension test} \\ 4/9 & \text{if } f_t \text{ is obtained via modulus of rupture} \end{cases}$
(Narayanan and Darwish, 1987)	$v_u = e(0.24 f_{spfc} + 80\rho(d/a)) + v_b$ $v_b = 0.41\tau F; F = (l_f/d_f)V_f\rho_f; \tau = 4.15 \text{ MPa}$ $e = \begin{cases} 1 & \text{if } (a/d) \geq 2.8 \\ 2.8 (d/a) & \text{if } (a/d) < 2.8 \end{cases}$ $f_{spfc} = \frac{f_{cuf}}{(20 - \sqrt{F})} + 0.7 + \sqrt{F}$
(Ashour et al., 1992)	$v_u = \begin{cases} (2.11^3 \sqrt{f'_c} + 7F)(\rho(d/a))^{\frac{1}{3}} & \text{if } (a/d) \geq 2.5 \\ (2.11^3 \sqrt{f'_c} + 7F)(\rho(d/a))^{\frac{1}{3}}(5d/2a) + v_b(2.5 - a/d) & \text{if } (a/d) < 2.5 \end{cases}$ $v_u = (0.7\sqrt{f'_c} + 7F)(d/a) + 17.2 \rho(d/a)$
(Khuntia et al., 1999)	$v_u = (0.167\alpha + 0.25F)\sqrt{f'_c}$ $\alpha = \begin{cases} 1 & \text{if } (a/d) \geq 2.5 \\ 2.5 (d/a) & \text{if } (a/d) < 2.5 \end{cases}$
(Y.-K. K. Kwak et al., 2002)	$v_u = 3.7 e f_{spfc}^{\frac{2}{3}} (\rho(d/a))^{\frac{1}{3}} + 0.8 v_b$ $e = \begin{cases} 1 & \text{if } (a/d) > 3.4 \\ 3.4 (d/a) & \text{if } (a/d) \leq 3.4 \end{cases}$
(Shahnewaz and Alam, 2014)	$v_u = 0.2 + 0.034 f'_c + 19\rho^{0.087} - 5.8(a/d)^{\frac{1}{2}} + 3.4V_f^{0.4} - 800(l_f/d_f)^{-1.6}$ $- 12((a/d)V_f)^{0.05} - 197((a/d)(l_f/d_f))^{-1.4}$ $+ 105(V_f(l_f/d_f))^{-2.12} \text{ if } (a/d) \leq 2.5$ $v_u = 0.2 + 0.072(f'_c)^{0.85} + 12.5\rho^{0.084} - 24(a/d)^{0.07} + 13.5V_f^{0.07} + 450(l_f/d_f)^{-2}$ $- 0.0002((a/d)V_f)^{3.9} - 27.69((a/d)(l_f/d_f))^{-0.84}$ $+ 1181(V_f(l_f/d_f))^{-2.69} - 21.89((a/d)V_f)(l_f/d_f)^{-0.9} \text{ if } (a/d) > 2.5$
(Gandomi et al., 2011)	$v_u = \frac{2d}{a}(\rho f'_c + v_b) + \frac{d}{2a} \frac{\rho}{(288\rho - 11)^4} + 2$
(Shahnewaz and Alam, 2020)	$v_u = 3.2 + 0.072 f'_c + \rho V_f(1.26 - 0.25(a/d)) - (a/d)(1.92 + 0.017f'_c - 0.38(a/d))$
(Arslan, 2014)	$v_u = \left(0.2 f'_c^{\frac{2}{3}} \left(\frac{c}{d}\right) + \sqrt{\rho(1 + 4F)f'_c}\right) \left(\frac{3}{\frac{c}{d}}\right)^{\frac{1}{3}}$ $\frac{c}{d} \text{ is a solution of } \left(\frac{c}{d}\right)^2 + \frac{600\rho c}{f'_c d} - \frac{600\rho}{f'_c} = 0$

Table 4.4 (Continued)

Reference	Suggested model
(Sarveghadi et al., 2019)	$v_u = \begin{cases} \frac{f'_t + v_b}{\frac{a}{d} - \rho + \frac{3\rho}{v_b} \left(v_b + 2 + \frac{a}{d} - f'_t + 4\rho f'_t \right)} + v_b & \text{if } f'_c < 41.4 \text{ MPa} \\ \frac{d}{a} \left(2f'_t + \frac{\frac{a}{d}}{\rho + \rho(4 + v_b) \left(\frac{a}{d} + \rho \right) \left(-1 - \frac{a}{d} \right)} - 2 \right) + v_b & \text{if } f'_c > 41.4 \text{ MPa} \end{cases}$ $f'_t = 0.79\sqrt{f'_c}$
RILEM (RILEM TC, 2003)	$v_{Rd} = v_{cd} + v_{fd}$ $v_{cd} = 0.12k(100\rho f'_c)^{1/3}; k = 1 + \sqrt{\frac{200}{d}} \leq 2; \rho \leq 2\%$ $v_{fd} = k_f k_l \tau_{fd}; k_l = 1 + \sqrt{\frac{200}{d}} \leq 2; k_f = 1 \text{ (rectangular section)}; \tau_{fd} = 0.12f_{Rk,A}; f_{Rk,A} = 1 \text{ MPa (assuming sufficient fiber dosage)}$

However, this equation is not consistent with real-world findings. The longitudinal steel reinforcement ratio has a linear relationship with the output, which means that the rate of increase of the shear capacity remains constant for higher reinforcement ratios. Similarly, Narayanan and Darwish's equation (Narayanan and Darwish, 1987) assumes a linear relationship between both variables. The low accuracy of existing formulas can also be attributed to the lack of important parameters involved in it. For instance, Khuntia et al., (1999) disregarded the influence of ρ . Sharma's formula (Sharma, 1986) did neither consider the effect of fibers nor that of ρ . For these reasons, both equations achieved relatively low accuracy with a correlation coefficient less than 0.7.

The RILEM equation revealed the worst precision amongst the different equations with $R = 0.6072$, $RMSE = 2.0013$, and $MAE = 1.8154$. The low accuracy presented by RILEM formula is mainly linked to safety factors included in the equation for design precautions, which leads to inaccurate results when predicting the shear capacity measured by laboratory tests. The Taylor diagram illustrated in **Figure 4.8** is a visual metric that can further depict the performance of the various equations. Taylor diagram considers the correlation coefficient, the standard deviation, and the root mean-square-centered difference to illustrate the predictive accuracy of each model.

Table 4.5: Performance evaluation of existing models

Reference	R	RMSE	MAE	v_p/v_t		
				μ	σ	COV (%)
(Sharma, 1986)	0.6622	1.3933	0.8792	0.9438	0.2987	31.6513
(Narayanan and Darwish, 1987)	0.8038	1.2902	0.9926	0.7571	0.2842	36.1127
(Ashour et al., 1992)	0.7989	1.1665	0.8646	0.8486	0.3009	35.4641
(Khuntia et al., 1999)	0.6489	1.6794	1.2247	0.716	0.2657	37.1101
(Y.-K. K. Kwak et al., 2002)	0.8086	0.9811	0.6761	1.0142	0.3557	35.0734
(Shahnewaz and Alam, 2014)	0.7464	1.9003	1.5764	0.4975	0.4591	92.2946
(Gandomi et al., 2011)	0.8133	1.0438	0.7749	1.2177	0.3581	29.4112
(Shahnewaz and Alam, 2020)	0.8172	0.9668	0.6712	1.0376	0.3035	29.2529
(Sarveghadi et al., 2019)	0.6156	1.9592	1.5749	0.7881	0.6065	76.9602
(Arslan, 2014)	0.765	1.1011	0.6716	0.9767	0.2374	24.3084
(RILEM TC 162-TDF, 2003)	0.6072	2.0013	1.8154	1.6841	0.5455	32.3902
Suggested Model	0.8878	0.8421	0.6099	0.9489	0.2242	23.6299

Table 4.6: Validation of proposed new equation

Condition number	Formula	Calculated values
1	$0.85 \leq k = \frac{\sum_{i=1}^n v_{t_i} v_{p_i}}{\sum_{i=1}^n v_{p_i}^2} \leq 1.15$	$k = 0.9998$
2	$0.85 \leq k' = \frac{\sum_{i=1}^n v_{t_i} v_{p_i}}{\sum_{i=1}^n v_{t_i}^2} \leq 1.15$	$k' = 0.9573$
3	$\left \frac{R^2 - R_0^2}{R^2} \right < 0.1$	$\frac{R^2 - R_0^2}{R^2} = -0.0612$
4	$\left \frac{R^2 - R_0'^2}{R^2} \right < 0.1$	$\frac{R^2 - R_0'^2}{R^2} = -0.0254$
	with	
	$R_0^2 = 1 - \frac{\sum_{i=1}^n (v_{p_i} - k v_{p_i})^2}{\sum_{i=1}^n (v_{p_i} - \bar{v}_p)^2}$	
	$R_0'^2 = 1 - \frac{\sum_{i=1}^n (v_{t_i} - k' v_{t_i})^2}{\sum_{i=1}^n (v_{t_i} - \bar{v}_t)^2}$	
5	$R_m = R^2 \times (1 - \sqrt{ R^2 - R_0^2 }) > 0.5$	$R_m = 0.5080$

Table 4.7: Ranking of the different shear equations

Reference	Ranking				
	<i>R</i>	<i>RMSE</i>	<i>MAE</i>	<i>COV</i>	Average
Suggested Model	12	12	12	12	12
(Shahnewaz and Alam, 2020)	11	11	11	10	11
(Arslan, 2014)	6	8	10	11	9
(Gandomi et al., 2011)	10	9	8	9	9
(Y.-K. K. Kwak et al., 2002)	9	10	9	6	9
(Ashour et al., 1992)	7	7	7	5	7
(Sharma, 1986)	4	5	6	8	5.5
(Narayanan and Darwish, 1987)	8	6	5	4	5.5
(Khuntia et al., 1999)	3	4	4	3	3.5
(Shahnewaz and Alam, 2014)	5	3	2	2	2.5
(Sarveghadi et al., 2019)	2	2	3	1	2
(RILEM TC 162-TDF, 2003)	1	1	1	7	1

Based on the diagram, the closest point to the point representing observed data is that of the proposed equation. This means that the suggested formula has the highest accuracy, confirming the abovementioned results. Conversely, The equation proposed by Sarveghadi et al., (2019) showed the lowest accuracy, which was indicated by the relatively high root mean-square-centered difference. Thereupon, this model has a rather low accuracy compared to its counterparts.

The model proposed in the present study proved to have superior predictive accuracy. Yet, it is crucial to understand the degree to which each parameter of the equation affects the shear capacity. Thus, sensitivity analysis can provide a better understanding of the equation by revealing the most influential parameters. The process adopted for sensitivity analysis is discussed below.

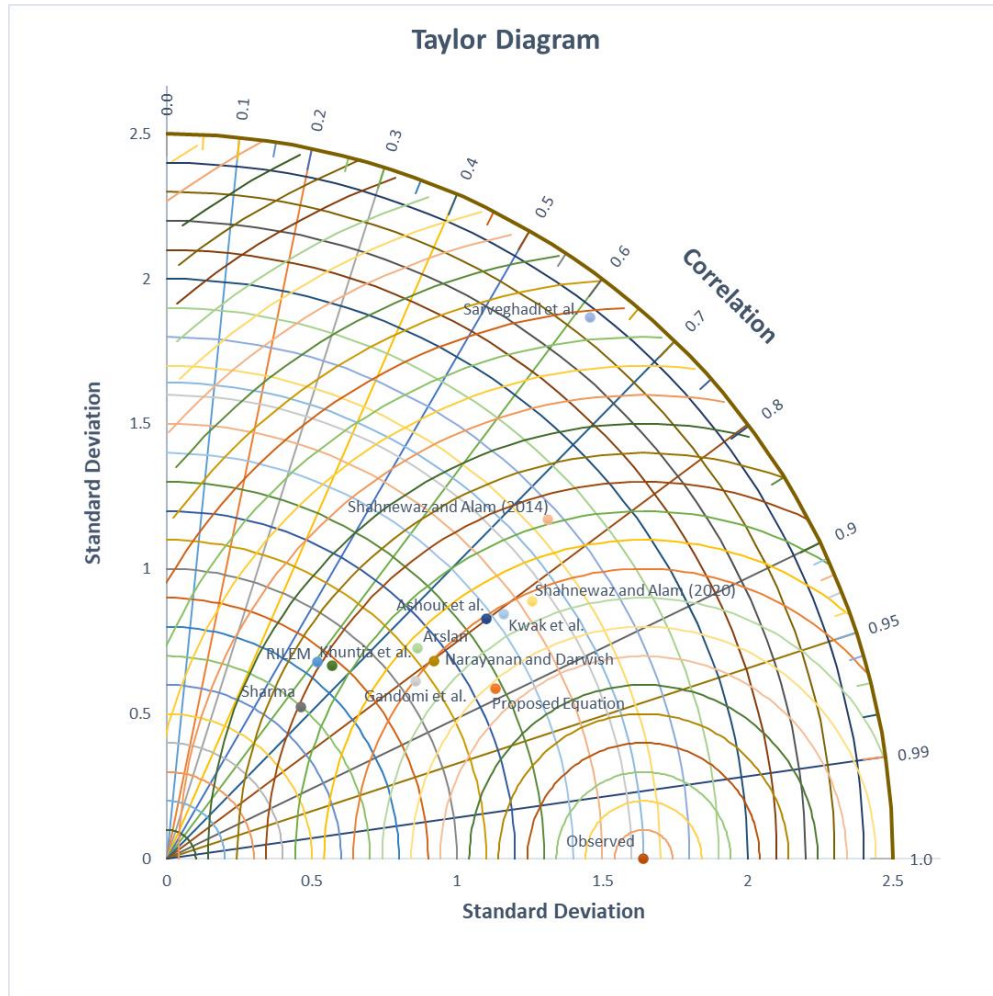


Figure 4.8: Taylor Diagram for SFRC shear strength prediction.

4.6.4 Sensitivity analysis

Sensitivity analysis (SA) aims to quantify the uncertainty of a model output linked to various sources of uncertainty in the different inputs (M. Nehdi and Al Martini, 2009; Moncef Nehdi and Nikopour, 2011). For complex nonlinear problems, global sensitivity analysis models such as variance-based sensitivity analysis are widely adopted owing to their ability in considering the interactions of the input with the other variables when quantifying the output uncertainty (Saltelli et al., 2010). Variance-based methods present a specific methodology to determine first-order and total-order sensitivity indices for each input variable of the developed equation. For a model having the form $Y =$

$f(X_1, X_2, \dots, X_k)$, the variance-based approach employs a variance ratio to assess the relevance of parameters through variance decomposition that can be expressed as follows:

$$V = \sum_{i=1}^k V_i + \sum_{i=1}^k \sum_{j>i}^k V_{ij} + \dots + V_{1,2,\dots,k} \quad (4.11)$$

where V denotes the variance of the model output, V_i is the first-order variance for the input X_i , and V_{ij} to $V_{1,2,\dots,k}$ represent the variance of the interaction of the k parameters. V_i and V_{ij} , which indicate the significance of the input to the variance of the output, depends on the variance of the conditional expectation as shown in **Eq. (4.12)** and **Eq. (4.13)**.

$$V_i = V_{X_i} [E_{X_{\sim i}}(Y|X_i)] \quad (4.12)$$

$$V_{ij} = V_{X_i X_j} [E_{X_{\sim ij}}(Y|X_i, X_j)] - V_i - V_j \quad (4.13)$$

with $X_{\sim i}$ notation corresponds to the set of all variables excluding X_i . The first-order sensitivity index (S_i) for an input X_i is therefore given by:

$$S_i = \frac{V_i}{V(Y)} \quad (4.14)$$

Conversely, the total effect of the input factor X_i , which comprises the first-order effect along with effects coming from the interaction with other features, is given by the following formula (Saltelli et al., 2010) :

$$S_{Ti} = \frac{E_{X_{\sim i}}(V_{X_i}(Y|X_{\sim i}))}{V(Y)} = 1 - \frac{V_{X_{\sim i}}(E_{X_i}(Y|X_{\sim i}))}{V(Y)} \quad (4.15)$$

The approach suggested by Saltelli et al., (2008) for calculating first- and total-order sensitivity indices has been used in the current study. The number, names, and bounds of the variables were first specified. Data sampling was then conducted via Saltelli's extension of the Sobol sequence to generate 10000 samples. The analysis was repeated 5 times, each time a random subset that consists of 70% of the entire database was generated by using a different random state. Consequently, different variable bounds are specified in each analysis. Results are illustrated in **Figure 4.9**. It can be observed that shear span-to-depth ratio demonstrated the greatest effect on the model output. The second most

influential parameter was the longitudinal steel reinforcement ratio, followed by the compressive strength of concrete. The lowest influence was recorded for the fiber factor. Moreover, total-order sensitivity index was greater than the first-order index for each parameter due to the interaction of the feature with the other variables. The presented results of sensitivity analysis are also consistent with previous studies in the open literature (Shahnewaz and Alam, 2020). However, the results are not in compliance with studies which reported that the fiber factor had the most significant effect. It is worth mentioning that those studies were based on a limited number of data examples, as well as a specific types of fibers. The type of fiber has a significant effect on the experimental results. Thus, equations developed from data using certain types of fibers are more sensitive to the fiber factor than others developed with a different type of fiber. For example, some studies mentioned that hooked fibers have higher efficiency in resisting pull out forces compared to straight fibers (Qi et al., 2018), which also affects the shear capacity. This contrast engenders different results when the model is developed with extensive databases because the model will search for a solution that can be applied to different fiber types.

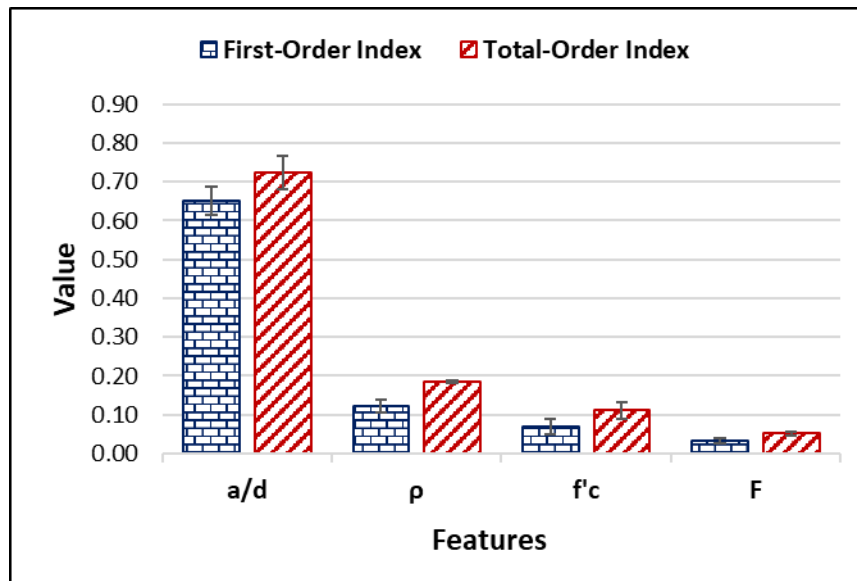


Figure 4.9: Sobol indices of different variables.

4.7 Verification of model applicability for reinforced concrete beams

Verification of model applicability for reinforced concrete (RC) beams without steel fibers consists of evaluating the predictive accuracy of the equation when the fiber factor approaches zero. Therefore, the equation for RC without fiber reinforcement will have the following expression:

$$v_u(\text{MPa}) = 0.921 + \frac{0.694 \times \ln(1.091 \rho) \times \sqrt{0.787 f'_c + \frac{4.863 \rho \sqrt{0.798 f'_c}}{\left(\frac{a}{d}\right)^3}}}{\left(\frac{a}{d}\right)} \quad (4.16)$$

Such verification is of paramount importance since it can extend the range of validity of the proposed equation to RC beams without steel fibers. In order to investigate that, 20 different RC samples were used for assessing the model accuracy. The specimens were gathered from different references in the open literature to ensure sufficient data diversity and adequate model generalization capability (Ahmad et al., 1986; Bhal, 1968; Bresler and Scordelis, 1963; Chana, 1981; Cossio and Siess, 1960; Elzanaty et al., 1986; Feldman and Siess, 1955; Grimm, 1997; Hallgren, 1994; Hamadi and Regan, 1980). The results are shown in **Figure 4.10**.

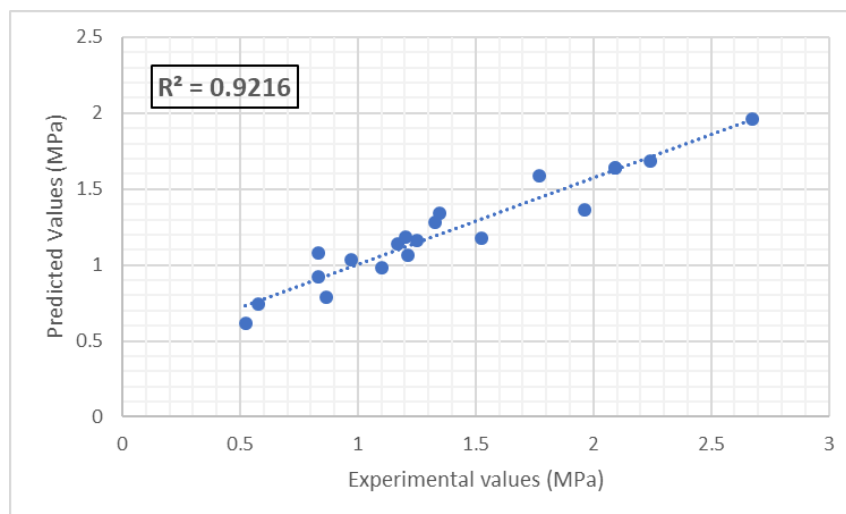


Figure 4.10: Correlation between predicted and experimental RC Shear strength.

The obtained coefficient of determination is $R^2 = 0.9216$, which indicates that there is a strong linear relationship between the predicted and experimental values of RC beam shear strength. Therefore, the model validity can be extended to RC beam specimens without steel fiber reinforcement.

4.8 Conclusions

The current study proposes a new equation for assessing the shear capacity of SFRC beams without stirrups. The data preprocessing stage involved a feature selection approach using CART, RF, and XGBoost. The equation was evolved using a GP-SR model trained with 2000 examples of a synthetic database generated from TGAN. The accuracy of the proposed new model was assessed on 309 experimental data examples retrieved from the open literature. The model was also benchmarked against 11 existing equations developed either with empirical approaches or soft-computing models. The following conclusions can be drawn:

- The feature importance analysis indicated that the shear span-to-depth ratio, longitudinal reinforcement ratio, compressive strength of concrete, and fiber factor had the most significant effect on SFRC beam shear capacity. Further analysis with a correlation matrix revealed a strong linear dependency between V_f and F .
- Validation of the proposed equation reflected its superior predictive accuracy on new data unknown to the model, which was indicated by the values of k , k' , and R_m .
- The proposed new model exhibited the highest predictive accuracy with an R value of 0.8878 and $RMSE$ and MAE of 0.8421 and 0.6099, respectively. This reflects the reliability of the model in providing accurate estimations as well as the effectiveness of synthetic data generated by TGAN in properly training the GP-SR mode.
- Analysis of the proposed equation showed consistency with experimental findings. Higher a/d values led to decreased shear capacity, while greater values of ρ , F , and f'_c led to enhanced shear capacity. This is attributed to the effect of the arch action,

which increases with lower a/d , and the influence of the dowel action which is enhanced with greater ρ and F .

- Sensitivity analysis showed that a/d had the greatest influence on the shear capacity, while the lowest effect was linked to F .

4.9 References

- Adebar, P., Mindess, S., St.-Pierre, D., and Olund, B. (1997). Shear tests of fiber concrete beams without stirrups. *ACI Structural Journal*, 94(1), 68–76.
- Ahmad, S. H., Khaloo, A. R., and Poveda, A. (1986). Shear Capacity of Reinforced High-Strength Concrete Beams. *Journal of the American Concrete Institute*, 83(2), 297–305.
- Amin, A., and Foster, S. J. (2016). Shear strength of steel fibre reinforced concrete beams with stirrups. *Engineering Structures*, 111, 323–332.
- Aoude, H, and Cohen, M. (2014). Shear response of SFRC beams constructed with SCC and steel fibers. *Electronic Journal of Structural Engineering*, 14, 71–83.
- Aoude, Hassan, Belghiti, M., Cook, W. D., and Mitchell, D. (2012). Response of steel fiber-reinforced concrete beams with and without stirrups. *ACI Structural Journal*, 109(3), 359–367.
- Arslan, G. (2014). Shear strength of Steel Fiber Reinforced Concrete (SFRC) slender beams. *KSCE Journal of Civil Engineering*, 18(2), 587–594.
- Arslan, G., Keskin, R. S. O., and Ulusoy, S. (2017). An experimental study on the shear strength of SFRC beams without stirrups. *Journal of Theoretical and Applied Mechanics (Poland)*, 55(4), 1205–1217.
- Ashour, S. A., Hasanain, G. S., and Wafa, F. F. (1992). Shear behavior of high-strength fiber reinforced concrete beams. *ACI Structural Journal*, 89(2), 176–184.
- Bae, B., Choi, H., and Choi, C. (2013). Flexural and Shear Capacity Evaluation of Reinforced Ultra-High Strength Concrete Members with Steel Rebars. *Key Engineering Materials*, 577–578, 17–20.
- Batson, G., Jenkins, E., and Spatney, R. (1972). Steel Fibers as Shear Reinforcement in Beams. *ACI Journal Proceedings*, 69(10), 640–644.
- Bhal, N. S. (1968). *On the Influence of Beam Depth on Shear Capacity of Single-Span RC Beams with and without Shear Reinforcement*. Universität Stuttgart, Germany.
- Bresler, B., and Scordelis, A. C. (1963). Shear Strength of Reinforced Concrete Beams. *ACI Journal Proceedings*, 60(1), 51–74.

- Casanova, P., and Rossi, P. (1999). High-Strength Concrete Beams Submitted to Shear: Steel Fibers Versus Stirrups. *Special Publication*, 182, 53–68.
- Casanova, Pascal, Rossi, P., and Schaller, I. (1997). Can steel fibers replace transverse reinforcements in reinforced concrete beams? *ACI Materials Journal*, 94(5), 341–354.
- Chalioris, C. E., and Sfiri, E. F. (2011). Shear performance of steel fibrous concrete beams. *Procedia Engineering*, 14, 2064–2068.
- Chana, P. S. (1981). Some Aspects of Modelling the Behaviour of Reinforced Concrete under Shear Loading. *Cement and Concrete Association*.
- Chao, S. H. (2020). Size effect on ultimate shear strength of steel fiber-reinforced concrete slender beams. *ACI Structural Journal*, 117(1), 145–158.
- Cho, S. H., and Kim, Y. Il. (2003). Effects of Steel Fibers on Short Beams Loaded in Shear. *ACI Structural Journal*, 100(6), 765–774.
- Cossio, R. D. De, and Siess, C. P. (1960). Behavior and Strength in Shear of Beams and Frames Without Web Reinforcement. *ACI Journal Proceedings*, 56(2), 695–736.
- Cucchiara, C., La Mendola, L., and Papia, M. (2004). Effectiveness of stirrups and steel fibres as shear reinforcement. *Cement and Concrete Composites*, 26(7), 777–786.
- Dancygier, A. N., and Savir, Z. (2011). Effects of Steel Fibers on Shear Behavior of High-Strength Reinforced Concrete Beams. *Advances in Structural Engineering*, 14(5), 745–761.
- Deshpande, N., Londhe, S., and Kulkarni, S. S. (2013). Modelling Compressive Strength of Recycled Aggregate Concrete Using Neural Networks and Regression. *Concrete Research Letters*.
- Dinh, H. H., Parra-Montesinos, G. J., and Wight, J. K. (2010). Shear behavior of steel fiber-reinforced concrete beams without stirrup reinforcement. *ACI Structural Journal*, 107(5), 597–606.
- Dupont, D., and Vandewalle, L. (2003). Shear Capacity of Concrete Beams Containing Longitudinal Reinforcement and Steel Fibers. *Special Publication*, 216, 79–94.
- Elzanaty, A. H., Nilson, A. H., and Slate, F. O. (1986). Shear Capacity of Reinforced Concrete Beams Using High-Strength Concrete. *Journal of the American Concrete Institute*, 83(2), 290–296.
- Feldman, A., and Siess, C. P. (1955). Effect of moment-shear ratio on diagonal tension cracking and strength in shear of reinforced concrete beams. In *University of Illinois Urbana* (Issue 107).
- Furlan, S., and De Hanai, J. B. (1997). Shear behaviour of fiber reinforced concrete beams. *Cement and Concrete Composites*, 19(4), 359–366.
- Gali, S., and Subramaniam, K. V. L. (2017). Shear behavior of steel fiber reinforced concrete using full-field displacements from digital image correlation. In *MATEC*

Web of Conferences (Vol. 120). EDP Sciences.

- Gandomi, A. H., Alavi, A. H., and Yun, G. J. (2011). Nonlinear modeling of shear strength of SFRC beams using linear genetic programming. *Structural Engineering and Mechanics*, 38(1), 1–25.
- Ghugare, S. B., and Tambe, S. S. (2017). Genetic programming based high performing correlations for prediction of higher heating value of coals of different ranks and from diverse geographies. *Journal of the Energy Institute*, 90(3), 476–484.
- Golbraikh, A., and Tropsha, A. (2002). Beware of q^2 ! *Journal of Molecular Graphics and Modelling*, 20(4), 269–276.
- Greenough, T., and Nehdi, M. (2008). Shear behavior of fiber-reinforced self-consolidating concrete slender beams. *ACI Materials Journal*, 105(5), 468–477.
- Grimm, R. (1997). Einfluß bruchmechanischer kenngrößen auf das biege- und schubtragverhalten hochfester betone. In *Deutscher Ausschuss für Stahlbeton* (Issue 477).
- Hallgren, M. (1994). *Flexural and Shear capacity of Reinforced High Strength Concrete Beams without Stirrups*. Royal Institute of Technology, Stockholm.
- Hamadi, Y. D., and Regan, P. E. (1980). Behaviour of normal and lightweight aggregate beams with shear cracks. *Struct Eng Part B*, 58 B(4), 71–79.
- Hwang, J.-H., Lee, D. H., Kim, K. S., Ju, H., and Seo, S.-Y. (2013). Evaluation of shear performance of steel fibre reinforced concrete beams using a modified smeared-truss model. *Magazine of Concrete Research*, 65(5), 283–296.
- Jeong, J. P., and Kim, W. (2014). Shear Resistant Mechanism into Base Components: Beam Action and Arch Action in Shear-Critical RC Members. *International Journal of Concrete Structures and Materials*, 8(1), 1–14.
- Kang, T. H. K., Kim, W., Kwak, Y. K., and Hong, S. G. (2011). Shear testing of steel fiber-reinforced lightweight concrete beams without web reinforcement. *ACI Structural Journal*, 108(5), 553–561.
- Kang, T. H. K., Kim, W., Massone, L. M., and Galleguillos, T. A. (2012). Shear-flexure coupling behavior of steel fiber-reinforced concrete beams. *ACI Structural Journal*, 109(4), 435–444.
- Khuntia, M., Stojadinovic, B., and Goel, S. C. (1999). Shear strength of normal and high-strength fiber reinforced concrete beams without stirrups. *ACI Structural Journal*, 96(2), 282–289.
- Koza, J. R. (1994). Genetic programming as a means for programming computers by natural selection. *Statistics and Computing*, 4(2), 87–112.
- Krassowska, J., and Kosior-Kazberuk, M. (2018). Failure mode in shear of steel fiber reinforced concrete beams. *MATEC Web of Conferences*, 163, 02003.
- Kwak, K.-H., Suh, J., and Hsu, C.-T. T. (1993). Shear behavior of steel fiber reinforced

- concrete beams. *ACI Structural Journal*, 90(1), 3–11.
- Kwak, Y.-K. K., Eberhard, M. O., Kim, W.-S. S., and Kim, J. (2002). Shear Strength of Steel Fiber-Reinforced Concrete Beams without Stirrups. *ACI Structural Journal*, 99(4), 530–538.
- Li, V. C., Ward, R., and Hamza, A. M. (1992). Steel and synthetic fibers as shear reinforcement. *ACI Materials Journal*, 89(5), 499–508.
- Lim, D. H., and Oh, B. H. (1999). Experimental and theoretical investigation on the shear of steel fibre reinforced concrete beams. *Engineering Structures*, 21(10), 937–944.
- Lim, T. Y., Paramasivam, P., and Lee, S. L. (1987). Shear and moment capacity of reinforced steel-fibre-concrete beams. *Magazine of Concrete Research*, 39(140), 148–160.
- Manju, R., Sathya, S., and Sylviya, B. (2017). Shear strength of high – Strength steel fibre reinforced concrete rectangular beams. *International Journal of Civil Engineering and Technology*, 8(8), 1716–1729.
- Mansur, M. A., Ong, K. C. G., and Paramasivam, P. (1986). Shear Strength of Fibrous Concrete Beams Without Stirrups. *Journal of Structural Engineering*, 112(9), 2066–2079.
- Minelli, F., and Plizzari, G. A. (2013). On the effectiveness of steel fibers as shear reinforcement. *ACI Structural Journal*, 110(3), 379–389.
- Minelli, F., Conforti, A., Cuenca, E., and Plizzari, G. (2014). Are steel fibres able to mitigate or eliminate size effect in shear? *Materials and Structures/Materiaux et Constructions*, 47(3), 459–473.
- Narayanan, R., and Darwish, I. Y. S. (1987). Use of steel fibers as shear reinforcement. *ACI Structural Journal*, 84(3), 216–227.
- Nehdi, M., and Al Martini, S. (2009). Estimating time and temperature dependent yield stress of cement paste using oscillatory rheology and genetic algorithms. *Cement and Concrete Research*, 39(11), 1007–1016.
- Nehdi, Moncef, and Nikopour, H. (2011). Genetic algorithm model for shear capacity of RC beams reinforced with externally bonded FRP. *Materials and Structures/Materiaux et Constructions*, 44(7), 1249–1258.
- Nembhard, D. A., and Sun, Y. (2019). A symbolic genetic programming approach for identifying models of learning-by-doing. *Computers and Industrial Engineering*, 131, 524–533.
- Noghabai, K. (2000). Beams of Fibrous Concrete in Shear and Bending: Experiment and Model. *Journal of Structural Engineering*, 126(2), 243–251.
- Qi, J., Wu, Z., Ma, Z. J., and Wang, J. (2018). Pullout behavior of straight and hooked-end steel fibers in UHPC matrix with various embedded angles. *Construction and Building Materials*, 191, 764–774.

- Qissab, M., and Salman, M. (2018). Shear strength of non-prismatic steel fiber reinforced concrete beams without stirrups. *Structural Engineering & Mechanics*, 67, 347–358.
- Randl, N., Mészöly, T., and Harsányi, P. (2018). *Shear Behaviour of UHPC Beams with Varying Degrees of Fibre and Shear Reinforcement* (pp. 500–507).
- RILEM TC 162-TDF. (2003). Test and design methods for steel fibre reinforced concrete σ - ε -design method. *Materials and Structures/Materiaux et Constructions*, 36(262), 560–567.
- Roy, P. P., and Roy, K. (2008). On some aspects of variable selection for partial least squares regression models. *QSAR and Combinatorial Science*, 27(3), 302–313.
- Sahoo, D. R., Bhagat, S., and Reddy, T. C. V. (2016). Experimental study on shear-span to effective-depth ratio of steel fiber reinforced concrete T-beams. *Materials and Structures/Materiaux et Constructions*, 49(9), 3815–3830.
- Sahoo, D. R., and Sharma, A. (2014). Effect of steel fiber content on behavior of concrete beams with and without stirrups. *ACI Structural Journal*, 111(5), 1157–1166.
- Saltelli, A., Annoni, P., Azzini, I., Campolongo, F., Ratto, M., and Tarantola, S. (2010). Variance based sensitivity analysis of model output. Design and estimator for the total sensitivity index. *Computer Physics Communications*, 181(2), 259–270.
- Saltelli, A., Ratto, M., Andres, T., Campolongo, F., Cariboni, J., Gatelli, D., Saisana, M., and Tarantola, S. (2008). Global Sensitivity Analysis. The Primer. In *Global Sensitivity Analysis. The Primer*. John Wiley and Sons.
- Sarveghadi, M., Gandomi, A. H., Bolandi, H., and Alavi, A. H. (2019). Development of prediction models for shear strength of SFRCB using a machine learning approach. *Neural Computing and Applications*, 31(7), 2085–2094.
- Shahnewaz, M., and Alam, M. S. (2014). Improved shear equations for steel fiber-reinforced concrete deep and slender beams. *ACI Structural Journal*, 111(4), 851–860.
- Shahnewaz, M., and Alam, M. S. (2020). Genetic algorithm for predicting shear strength of steel fiber reinforced concrete beam with parameter identification and sensitivity analysis. *Journal of Building Engineering*, 29(April 2019), 101205.
- Sharma, A. K. (1986). Shear strength of steel fiber reinforced concrete beams. *Journal of the American Concrete Institute*, 83(4), 624–628.
- Shin, S.-W., Oh, J.-G., and Ghosh, S. K. (1994). Shear Behavior of Laboratory-Sized High-Strength Concrete Beams Reinforced With Bars and Steel Fibers. *Special Publication*, 142, 181–200.
- Shoaib, A. (2012). *Shear in Steel Fiber Reinforced Concrete Members without Stirrups*.
- Shoaib, A., Lubell, A. S., and Bindiganavile, V. S. (2014). Size effect in shear for steel fiber-reinforced concrete members without stirrups. *ACI Structural Journal*, 111(5), 1081–1090.

- Singh, B., and Jain, K. (2014). Appraisal of steel fibers as minimum shear reinforcement in concrete beams. *ACI Structural Journal*, 111(5), 1191–1202.
- Slater, E., Moni, M., and Alam, M. S. (2012). Predicting the shear strength of steel fiber reinforced concrete beams. *Construction and Building Materials*, 26(1), 423–436.
- Smith, G. N. (1986). Probability and statistics in civil engineering. *Collins Professional and Technical Books*, 244.
- Spinella, N., Colajanni, P., and La Mendola, L. (2012). Nonlinear analysis of beams reinforced in shear with stirrups and steel fibers. *ACI Structural Journal*, 109(1), 53–64.
- Swamy, R. N., and Bahia, H. M. (1985). The Effectiveness of Steel Fibers as Shear Reinforcement. *Concrete International*, 7(3), 35–40.
- Swamy, R. N., and Bahia, H. M. (1978). Influence of Fiber Reinforcement on the Dowel Resistance to Shear. *J Am Concr Inst*, 76(2), 327–356.
- Swamy, R. Narayan, Jones, R., and Chiam, A. T. P. (1993). Influence of steel fibers on the shear resistance of lightweight concrete I- beams. *ACI Structural Journal*, 90(1), 103–114.
- Tahenni, T., Chemrouk, M., and Lecompte, T. (2016). Effect of steel fibers on the shear behavior of high strength concrete beams. *Construction and Building Materials*, 105, 14–28.
- Vandewalle, M. I., and Mortelmans, F. (1994). Shear Capacity of Steel Fiber High-Strength Concrete Beams. *Special Publication*, 149, 227–242.
- Xu, L., and Veeramachaneni, K. (2018). *Synthesizing Tabular Data using Generative Adversarial Networks*.
- Xue, B., Zhang, M., Browne, W. N., and Yao, X. (2016). A Survey on Evolutionary Computation Approaches to Feature Selection. *IEEE Transactions on Evolutionary Computation*, 20(4), 606–626.
- Yoo, D. Y., and Yang, J. M. (2018). Effects of stirrup, steel fiber, and beam size on shear behavior of high-strength concrete beams. *Cement and Concrete Composites*, 87, 137–148.
- Zarrinpour, M. R., and Chao, S. H. (2017). Shear strength enhancement mechanisms of steel fiber-reinforced concrete slender beams. *ACI Structural Journal*, 114(3), 729–742.

Chapter 5

Conclusions and Recommendations

5.1 Summary and Conclusions

This thesis presents a compilation of three studies conducted to better estimate the complex shear behavior and capacity of SFRC beams subjected to three- and four-point testing.

In Chapter 2, a critical review of the various machine learning models employed to predict the mechanical properties of concrete was conducted. The review aimed to identify the most accurate and reliable ML models for predicting the mechanical strength of concrete with high accuracy. Four major techniques were employed in the open literature including ANN, SVM, decision trees, and EA. The applications of each model in hybrid or standalone form along with its performance were critically reviewed and discussed. Moreover, a comparison between the performance of each approach over the same testing data was carried out. The study revealed the superiority of hybrid ANN- and SVM-based models in accurately predicting the mechanical properties of concrete.

Based on the conclusions of Chapter 2, a hybrid ANN-based model was developed in Chapter 3 to predict the shear strength of SFRC beams with superior accuracy. An ASO algorithm was combined with ANN to form a hybrid model in which weights and biases of ANN were optimized with the searching capabilities of ASO. Results revealed that the ASO-ANN model achieved superior predictive accuracy, outperforming existing widely used standalone and hybrid soft-computing models, as well as other empirical formulations in terms of R , MAE , $RMSE$, and d' . It was found that the superior accuracy achieved by ASO-ANN was mainly linked to the searching strategy of ASO. Repulsive forces affecting the atomic motion help the algorithm explore more promising regions of the search space and consequently ensuring the discovery of better solutions. The search strategy also helped overcome the drawbacks of standalone ANN trained with gradient descent, which can be easily trapped in local minima. In addition, a global sensitivity analysis involving a variance-based method was conducted to reveal the important parameters affecting the

shear strength. It was found that the shear span-to-depth ratio was the most influential parameter for the suggested model. Furthermore, four classification models were deployed to forecast the failure mode of SFRC, which cannot be achieved by regression models. Scatter plots, confusion matrices, and an accuracy metric, γ were used to compare the performance of the models. It was concluded that k -nearest neighbor was the most accurate model, providing the best predictions of the likelihood of shear failure. Even though the suggested models could accurately predict the shear capacity and failure mode of SFRC beams, they fall inside the “black-box” category of soft-computing models. This makes the generation of transparent mathematical formulas using such models unfeasible.

In Chapter 4, a genetic programming-based symbolic regression model was developed to generate a shear strength equation for SFRC beams without stirrups and overcome the shortcomings of “black-box” models. Synthetic data generated from TGAN was used to train the proposed model and overcome the problem associated with the relatively small experimental database existing in the open literature. Results of the “train on synthetic - test on real” philosophy adopted in this chapter reflected the satisfactory accuracy of the new formula, which outperformed existing empirical and ML-based equations. The suggested equation also showed consistency with real-world findings that describe the relationship between the input parameters and the shear strength. Sensitivity analysis was finally performed to identify the most influential parameters. It was found that the shear span-to-depth ratio had the greatest impact on the output, which is in good agreement with the findings of the previous Chapter.

The two models suggested in the present study exhibited good predictive accuracy. The ASO-ANN model has better accuracy than the GP-SR model. However, a non-programming expert who is not familiar with machine learning models might find the use of ASO-ANN challenging. The GP-SR based equation presents an alternative approach to estimate the shear strength by providing an explicit formula that can be used by engineers regardless of their programming skills. Therefore, the selection of the suitable approach depends mainly on the designer’s programming background along with the extent to which the user can trust a “black-box” model that doesn’t explicitly reveal the relationship between the input parameters and the shear strength.

5.2 Model Limitations

The presented models exhibited robust accuracy. Yet, there are some limitations associated with their application. The validity of each model is limited to predicting the shear capacity of simply supported beams made in laboratory conditions and subjected to three- and four-point shear testing methods. This will make their accuracy for on-site developed beams as well as beams embedded in complex structural buildings questionable because of the different load combinations and conditions to which these specimens are exposed. Moreover, training and testing the ASO-ANN was performed via 75% and 25% of the dataset, respectively. These proportions need to be also tuned to verify what percentages of training and testing data provide an optimal accuracy because assuming such values does not guarantee the best results. Moreover, the models do not account for an important parameter, which is the effect of concrete aggregate type and proportions. Aggregate interlock influences the shear capacity and future ML-based models need to be developed with a database that comprises aggregate properties.

5.3 Recommendations for Future Work

The present study presented novel approaches to predict the shear capacity of SFRC. Conversely, the study induces the need for future research as follows:

1. Even though the suggested models can predict the shear capacity of SFRC beams, they cannot reflect the behavior of the entire structure. Designers need to understand the load distribution in the structure, which can be achieved by alternative techniques such as finite element methods.
2. Identifying real-time crack growth using recurrent neural network is of paramount importance especially that it can provide better visualization of the cracked SFRC structures and avert sudden failures.
3. TGAN proved to generate reliable synthetic data that can effectively train evolutionary algorithms and overcome the small database issues. Therefore, the potential of TGAN can be explored when there is a lack of data in certain types of

concretes such as shrinkage-compensating concrete, concrete containing phase change materials, etc.

4. Shear design provisions for concrete structures in some building codes are based on the modified compression field theory. The consistency between this theory and ML-based equations is worth investigation in future studies.

Appendix

Table 5.1: Database used to develop ASO-ANN and the classification algorithms

Beam Geometry			Longitudinal Steel	Concrete Properties	Fiber Properties			Shear Strength	Failure Mode
$b_w(mm)$	$d(mm)$	a/d	ρ	$f'_c(Mpa)$	V_f	l_f/d_f	$f_{if}(MPa)$	$v_u(MPa)$	
150	251	3.49	0.0267	28.1	0.75	65	1100	3.0013	S
150	251	3.49	0.0267	25.3	0.75	65	1100	2.0983	S
150	251	3.49	0.0267	27.9	1	65	1100	2.8951	S
150	251	3.49	0.0267	26.2	1	65	1100	3.2669	S
150	251	3.49	0.0267	28.1	1.5	65	1100	2.9482	S
150	251	3.49	0.0267	27.3	1.5	65	1100	3.4794	S
150	251	3.49	0.0267	27.5	0.5	80	1050	1.7264	S
150	251	3.49	0.0267	24.9	0.5	80	1050	2.0452	S
150	251	3.49	0.0267	27.8	0.75	80	1050	2.4170	S
150	251	3.49	0.0267	27.3	0.75	80	1050	2.6826	S
150	251	3.49	0.0267	26.3	1	80	1050	3.0810	S
150	251	3.49	0.0267	27.1	1	80	1050	2.7623	S
150	251	3.49	0.0267	53.4	0.75	65	1100	3.0013	S
150	251	3.49	0.0267	54.1	0.75	65	1100	3.3466	S
150	251	3.49	0.0267	53.2	1	65	1100	3.8247	S
150	251	3.49	0.0267	55.3	1	65	1100	4.3825	S
150	251	3.49	0.0267	64.6	1.5	65	1100	5.1793	S
150	251	3.49	0.0267	59.9	1.5	65	1100	4.2497	S
150	251	3.49	0.0267	47.8	0.5	80	1050	3.3732	S
150	251	3.49	0.0267	49.5	0.5	80	1050	4.0372	S
150	251	3.49	0.0267	55.3	0.75	80	1050	3.8778	S
150	251	3.49	0.0267	56.4	0.75	80	1050	4.7278	S
150	251	3.49	0.0267	53.4	1	80	1050	3.3997	S
150	251	3.49	0.0267	51	1	80	1050	4.1700	S
150	251	3.49	0.0267	27.8	1	50	1025	2.0983	S
150	251	3.49	0.0267	27.2	1	50	1025	2.0717	S
150	251	3.49	0.0267	27.6	1	85	1050	2.6029	S
150	251	3.49	0.0267	27.9	1	85	1050	2.1514	S
150	251	3.49	0.0267	34.7	1	50	1025	2.6295	S
150	251	3.49	0.0267	36.2	1	50	1025	2.6560	S
150	251	3.49	0.0267	37	1	85	1050	2.9216	S
150	251	3.49	0.0267	38.3	1	85	1050	2.7623	S
150	261	2.3	0.0116	28.7	0.5	80	1100	3.6526	FS
150	261	3.45	0.0195	32.9	0.75	80	1100	2.7586	S
150	261	3.45	0.0195	23.8	1	80	1100	2.3755	S

Table A.1 (continued)

Beam Geometry			Longitudinal Steel	Concrete Properties	Fiber Properties			Shear Strength	Failure Mode
$b_w(mm)$	$d(mm)$	a/d	ρ	$f'_c(Mpa)$	V_f	l_f/d_f	$f_{ff}(MPa)$	$v_u(MPa)$	
150	261	3.45	0.0195	24.1	1.25	80	1100	2.9119	S
310	258	3	0.0184	22	1	55	1100	2.5381	FS
310	258	3	0.0245	31	1	55	1100	3.7259	FS
300	550	3	0.0119	30	1	55	1100	1.8848	FS
140	175	1.5	0.0128	82	0.5	80	1100	4.8163	S
140	175	1.5	0.0128	83.2	1	80	1100	6.3265	S
140	175	1.5	0.0128	83.8	1.5	80	1100	7.5918	S
140	175	2.5	0.0128	82	0.5	80	1100	2.5306	S
140	175	2.5	0.0128	83.2	1	80	1100	3.2245	S
140	175	2.5	0.0128	83.8	1.5	80	1100	5.5102	S
150	200	2.5	0.0134	33.68	1	55	1100	2.1333	S
150	200	2.5	0.0134	24.53	1	55	1100	1.4333	S
150	200	2.5	0.0134	21.43	2	55	1100	1.6333	S
150	200	2.5	0.0134	9.77	3	55	1100	1.2667	S
150	200	3.5	0.0134	20.21	1	55	1100	1.0667	S
150	200	3.5	0.0134	21.43	2	55	1100	1.4000	S
150	200	3.5	0.0134	27.91	3	55	1100	1.9333	S
150	200	4.5	0.0134	24.53	1	55	1100	1.4000	S
150	200	4.5	0.0134	21.43	2	55	1100	1.1667	FS
152	381	3.4	0.0271	49.2	1	80	1100	2.9873	NA
152	381	3.4	0.0271	31	1.5	60	1100	2.5901	NA
152	381	3.4	0.0271	44.9	1.5	60	1100	3.2808	NA
152	381	3.4	0.0271	44.9	1.5	60	1100	3.2981	NA
152	381	3.4	0.0271	49.2	1	80	1100	3.7816	NA
152	381	3.4	0.0271	31	1.5	60	1100	3.4017	NA
152	381	3.5	0.0271	38.1	1	60	1100	2.5556	NA
152	381	3.5	0.0271	38.1	1	60	1100	3.4881	NA
152	381	3.5	0.0197	38.1	1	60	1100	3.0564	NA
152	381	3.5	0.0197	38.1	1	60	1100	3.1082	NA
200	260	1.5	0.0181	41.2	0.25	67	1100	5.3654	NA
200	260	1.5	0.0181	40.3	0.76	67	1100	5.7500	NA
200	260	2.5	0.0181	40	0.25	67	1100	2.0577	NA
200	260	2.5	0.0181	38.7	0.76	67	1100	2.7500	NA
200	260	2.5	0.0115	40	0.25	67	1100	1.5577	NA
200	260	2.5	0.0115	38.7	0.76	67	1100	2.0385	NA
200	460	3.4	0.028	37.7	0.5	67	1100	2.6413	NA
200	460	3.4	0.028	38.8	0.5	67	1100	2.7283	NA
200	460	3.4	0.028	37.7	0.5	67	1100	2.8043	NA
200	460	3.4	0.028	37.7	0.5	67	1100	2.8478	NA
200	260	3.5	0.0356	46.9	0.25	67	1100	2.0962	NA
200	260	3.5	0.0356	43.7	0.51	67	1100	2.2885	NA

Table A.1 (continued)

Beam Geometry			Longitudinal Steel	Concrete Properties	Fiber Properties			Shear Strength	Failure Mode
$b_w(mm)$	$d(mm)$	a/d	ρ	$f'_c(Mpa)$	V_f	l_f/d_f	$f_{ff}(MPa)$	$v_u(MPa)$	
200	260	3.5	0.0356	48.3	0.76	67	1100	2.9615	NA
200	260	3.5	0.0283	37.7	0.5	67	1100	2.1154	NA
200	260	3.5	0.0283	38.8	0.5	67	1100	2.5192	NA
200	540	3.5	0.0273	37.7	0.25	67	1100	1.4074	NA
200	560	3.5	0.0273	38.8	0.5	67	1100	2.0446	NA
200	260	4	0.0181	41.2	0.25	67	1100	1.5577	NA
200	260	4	0.0181	40.3	0.76	67	1100	2.2308	NA
150	217	1.59	0.0185	35	0.75	80	1100	4.5469	S
150	217	2.47	0.0185	35	0.75	80	1100	3.0108	S
150	217	2.95	0.0185	35	0.75	80	1100	2.5806	S
300	622	2.81	0.0198	34	0.321	65	2300	1.5273	S
300	622	2.81	0.0198	36	0.687	65	2300	1.9025	S
100	135	2.22	0.0116	64.2	0.5	65	1100	3.0370	S
100	135	2.22	0.0116	64.2	0.5	65	1100	3.1852	S
100	135	2.22	0.0116	64.2	0.5	65	1100	3.1111	S
100	135	2.22	0.0116	64	1	65	1100	3.2593	FS
100	135	2.22	0.0116	64	1	65	1100	3.4815	FS
100	135	2.22	0.0116	64	1	65	1100	3.1111	FS
100	135	2.22	0.0116	60	1	80	1100	3.6296	FS
100	135	2.22	0.0116	60	1	80	1100	3.7778	FS
100	135	2.22	0.0116	60	1	80	1100	3.2593	FS
85	130	2.02	0.0205	51.85	0.25	100	2000	2.8959	S
85	130	2.52	0.0205	51.85	0.25	100	2000	2.6244	S
85	130	3.02	0.0205	51.85	0.25	100	2000	2.7149	S
85	130	2.02	0.0205	33.32	0.25	100	2000	2.6244	S
85	130	2.52	0.0205	33.32	0.25	100	2000	1.9910	S
85	130	3.02	0.0205	33.32	0.25	100	2000	1.9005	S
85	130	3.02	0.0205	51.68	0.5	133	2000	3.1674	S
85	130	3.02	0.0205	30.6	0.5	133	2000	1.9005	S
85	130	3.02	0.0205	31.025	1	100	2000	2.8959	S
85	130	2.02	0.0205	51.68	0.5	133	2000	4.5249	S
85	130	2.52	0.0205	51.68	0.5	133	2000	3.6199	S
85	130	3.52	0.0205	41.65	0.5	133	2000	2.5339	S
85	130	2.02	0.0205	48.705	1	133	2000	5.5204	S
85	130	2.52	0.0205	48.705	1	133	2000	4.3439	S
85	130	3.52	0.0205	48.79	1	133	2000	2.8959	S
85	128	3.06	0.037	41.65	0.5	133	2000	2.8493	S
85	126	3.11	0.0572	41.65	0.5	133	2000	3.4547	S
85	128	3.06	0.037	30.6	0.5	133	2000	2.2059	S
85	126	3.11	0.0572	30.6	0.5	133	2000	2.2409	S
85	128	3.06	0.037	48.79	1	133	2000	4.3199	S

Table A.1 (continued)

Beam Geometry			Longitudinal Steel	Concrete Properties	Fiber Properties			Shear Strength	Failure Mode
$b_w(mm)$	$d(mm)$	a/d	ρ	$f'_c(Mpa)$	V_f	l_f/d_f	$f_{ff}(MPa)$	$v_u(MPa)$	
85	126	3.11	0.0572	48.79	1	133	2000	4.9486	S
85	126	3.11	0.0572	53.55	1.5	100	2000	4.7619	S
85	126	3.11	0.0572	43.18	2	100	2000	4.8553	S
85	128	3.06	0.037	53.55	1.5	100	2000	4.4118	S
85	126	2.08	0.0572	50.15	0.5	100	2000	5.4155	S
85	126	2.08	0.0572	45.9	1	100	2000	6.7227	S
85	126	2.08	0.0572	53.55	1.5	100	2000	7.0962	S
85	126	2.08	0.0572	43.18	2	100	2000	6.2558	S
150	219	2.8	0.0191	40.85	1	60	1115	2.9224	S
150	219	2.8	0.0191	40.85	2	60	1115	3.1355	S
150	219	2	0.0191	43.23	1	60	1115	3.5008	S
150	219	2	0.0191	43.23	2	60	1115	3.5312	S
125	212	2	0.0152	63.8	0.5	63	1079	5.0566	FS
125	212	2	0.0152	68.6	0.75	63	1079	5.4340	FS
125	212	2	0.0152	30.8	0.5	63	1079	4.0377	S
125	212	3	0.0152	30.8	0.5	63	1079	2.5283	S
100	130	3.08	0.0309	38.69	1	60	1303	4.4615	S
100	130	3.08	0.0309	42.4	2	60	1303	5.6923	S
152	381	3.44	0.0196	44.8	0.75	55	1100	2.9528	S
152	381	3.44	0.0196	44.8	0.75	55	1100	2.7801	S
152	381	3.44	0.0196	38.1	1	55	1100	2.9355	S
152	381	3.44	0.0196	38.1	1	55	1100	2.9873	S
152	381	3.44	0.0263	31	1.5	55	1100	2.5729	S
152	381	3.44	0.0263	31	1.5	55	1100	3.4017	S
152	381	3.44	0.0263	44.9	1.5	55	1100	3.3154	S
152	381	3.44	0.0263	44.9	1.5	55	1100	3.2808	S
152	381	3.44	0.0263	49.2	1	80	1100	2.9873	S
152	381	3.44	0.0263	49.2	1	80	1100	3.7816	S
152	381	3.44	0.0196	43.3	0.75	80	2300	3.3326	S
152	381	3.44	0.0196	43.3	0.75	80	2300	3.2808	S
205	610	3.5	0.0196	50.8	0.75	55	1100	2.9428	S
205	610	3.5	0.0196	50.8	0.75	55	1100	2.7189	S
205	610	3.5	0.0196	28.7	0.75	80	1100	2.8309	S
205	610	3.5	0.0196	28.7	0.75	80	1100	2.7749	S
205	610	3.5	0.0152	42.3	0.75	55	1100	2.7989	S
205	610	3.5	0.0152	29.6	0.75	80	1100	2.1591	S
205	610	3.5	0.0152	29.6	0.75	80	1100	1.8153	S
205	610	3.5	0.0196	44.4	1.5	55	1100	3.4946	S
205	610	3.5	0.0196	42.8	1.5	80	1100	3.3826	S
150	340	2.5	0.0308	58.87	1	65	1150	5.1176	NA
150	340	2.5	0.0308	51.67	2	65	1150	5.7059	NA

Table A.1 (continued)

Beam Geometry			Longitudinal Steel	Concrete Properties	Fiber Properties			Shear Strength	Failure Mode
$b_w(mm)$	$d(mm)$	a/d	ρ	$f'_c(Mpa)$	V_f	l_f/d_f	$f_{ff}(MPa)$	$v_u(MPa)$	
150	735	3.81	0.0106	42	1.25	75	1200	3.2562	NA
150	735	3.81	0.0106	38	1.25	60	1200	3.2562	NA
125	225	2.89	0.0349	90	1.25	60	1200	5.5822	S
150	202	2.97	0.0117	21.3	0.5	55	1100	1.5512	S
150	202	2.97	0.0117	19.6	1	55	1100	1.8482	S
300	437	3.09	0.015	21.3	0.5	55	1100	1.2204	S
300	437	3.09	0.015	19.6	1	55	1100	1.5561	S
200	435	2.51	0.0104	24.8	0.38	50	1100	1.5287	S
200	435	2.51	0.0104	33.5	0.38	50	1100	1.3678	S
200	435	2.51	0.0104	33.5	0.57	78	1333	1.6207	S
200	435	2.51	0.0104	38.6	0.38	50	1100	1.6092	S
200	435	2.51	0.0104	61.1	0.64	48	1250	2.1839	FS
200	455	2.51	0.0099	24.4	0.25	50	1100	2.1538	FS
200	455	2.51	0.0099	24.4	0.25	50	1100	1.7143	S
200	910	2.5	0.0104	24.4	0.25	50	1100	1.4121	S
200	910	2.5	0.0104	55	0.25	50	1100	1.8571	S
125	210	2	0.0153	44.6	0.5	63	1100	3.0857	FS
125	210	4	0.0153	44.6	0.5	63	1100	1.3333	S
125	210	2	0.0153	57.2	0.5	63	1100	2.9333	FS
125	225	2.89	0.0349	90	1.25	60	1200	4.9067	S
125	225	2.89	0.0349	90	1.25	60	1200	4.9067	S
152	221	2.5	0.012	34	0.5	60	1130	1.7266	S
152	221	1.5	0.0239	34	1	60	1130	4.3760	S
152	221	2.5	0.0239	34	1	60	1130	2.4708	S
152	221	3.5	0.0239	34	1	60	1130	1.9945	FS
152	221	1.5	0.0239	34	0.5	60	1130	4.0188	S
152	221	2.5	0.0239	34	0.5	60	1130	1.9052	S
152	221	3.5	0.0239	34	0.5	60	1130	1.4587	S
150	197	2	0.0136	29.1	0.5	60	1260	2.5381	S
150	197	2.8	0.0136	29.1	0.5	60	1260	1.7597	S
150	197	3.6	0.0136	29.1	0.5	60	1260	1.5228	S
150	197	2	0.0136	29.9	0.75	60	1260	2.8765	S
150	197	2.8	0.0136	29.9	0.75	60	1260	2.0305	S
150	197	2.8	0.0204	29.9	0.75	60	1260	2.1997	S
150	197	2.8	0.0136	20.6	0.75	60	1260	1.5228	S
150	197	2.8	0.0204	20.6	0.75	60	1260	2.0305	S
150	197	2.8	0.0204	33.4	0.75	60	1260	2.9103	S
152	254	3.5	0.0248	29	0.75	67	1096	3.1082	S
610	254	3.5	0.0247	29	0.75	67	1096	3.1044	S
152	394	3.61	0.0286	39	0.75	67	1096	2.7050	S
152	394	3.61	0.0286	39	0.75	67	1096	3.2561	S

Table A.1 (continued)

Beam Geometry			Longitudinal Steel	Concrete Properties	Fiber Properties			Shear Strength	Failure Mode
$b_w(mm)$	$d(mm)$	a/d	ρ	$f'_c(Mpa)$	V_f	l_f/d_f	$f_{ff}(MPa)$	$v_u(MPa)$	
203	541	3.45	0.0254	50	0.75	67	1096	2.4767	S
203	541	3.45	0.0254	50	0.75	67	1096	3.5056	S
254	813	3.5	0.027	50	0.75	67	1096	3.3850	S
254	813	3.5	0.027	50	0.75	67	1096	3.4866	S
200	180	3.33	0.0447	90.6	1	40	2600	8.3056	S
200	180	3.33	0.0447	83.2	1	48	1850	8.1944	S
200	180	3.33	0.0447	80.5	0.5	86	2200	7.0000	S
200	180	3.33	0.0447	80.5	0.75	86	2200	7.2778	S
200	195	3.08	0.0309	39.4	1	48	1850	4.8462	S
200	235	2.77	0.0428	91.4	1	50	1100	6.5957	S
200	235	2.77	0.0428	93.3	1	40	2600	7.7234	S
200	235	2.77	0.0428	89.6	1	48	1850	8.6596	S
200	410	2.93	0.0306	76.8	1	40	2600	3.5610	S
200	410	2.93	0.0306	76.8	1	40	2600	4.1341	S
200	410	2.93	0.0306	72	1	48	1850	4.5122	S
200	410	2.93	0.0306	72	1	48	1850	4.0244	S
200	410	2.93	0.0306	69.3	0.5	86	2200	3.2561	S
200	410	2.93	0.0306	69.3	0.5	86	2200	3.8415	S
200	410	2.93	0.0306	60.2	0.75	86	2200	4.1707	S
200	410	2.93	0.0306	75.7	0.75	86	2200	3.5976	S
300	570	2.98	0.0287	76.8	1	40	2600	2.6725	S
300	570	2.98	0.0287	72	1	48	1850	3.5556	S
300	570	2.98	0.0287	60.2	0.75	86	2200	3.0468	S
200	314	3.5	0.035	132	2	75	2000	4.0287	S
200	314	3.5	0.035	154	2	75	2000	5.0955	S
200	314	3.5	0.035	146	2	75	2000	5.7166	S
200	314	3.5	0.035	133	1	75	2000	4.2675	S
200	314	3.5	0.035	143	1	75	2000	3.2006	S
200	314	3.5	0.035	153	1	75	2000	4.9363	S
125	215	2	0.0037	92	1	75	260	1.6744	NA
125	215	4	0.0037	92.6	1	75	260	0.8930	NA
125	215	6	0.0037	93.7	1	75	260	0.5581	NA
125	215	1	0.0283	99	0.5	75	260	9.0791	NA
125	215	2	0.0283	99.1	0.5	75	260	4.8000	NA
125	215	4	0.0283	95.4	0.5	75	260	2.2698	NA
125	215	6	0.0283	95.83	0.5	75	260	1.9721	NA
125	215	1	0.0283	95.3	1	75	260	12.7256	NA
125	215	2	0.0283	95.3	1	75	260	6.0279	NA
125	215	4	0.0283	97.53	1	75	260	3.1628	NA
125	215	6	0.0283	100.5	1	75	260	1.9721	NA
125	215	1	0.0283	96.4	1.5	75	260	13.9163	NA

Table A.1 (continued)

Beam Geometry			Longitudinal Steel	Concrete Properties	Fiber Properties			Shear Strength	Failure Mode
$b_w(mm)$	$d(mm)$	a/d	ρ	$f'_c(Mpa)$	V_f	l_f/d_f	$f_{ff}(MPa)$	$v_u(MPa)$	
125	215	2	0.0283	96.6	1.5	75	260	7.1814	NA
125	215	4	0.0283	97.1	1.5	75	260	3.4977	NA
125	215	6	0.0283	101.32	1.5	75	260	1.9721	NA
125	215	2	0.0458	94.5	1	75	260	6.6977	NA
125	215	4	0.0458	93.8	1	75	260	3.8698	NA
125	215	6	0.0458	95	1	75	260	2.9395	NA
140	340	2	0.0167	35	0.5	60	1100	4.5798	NA
140	340	2	0.0167	33	0.75	60	1100	3.8025	NA
140	340	2	0.0167	36	1	60	1100	4.4328	NA
140	340	2.5	0.0167	36	1	60	1100	3.2353	NA
140	340	1.5	0.0167	36	1	60	1100	6.4496	NA
150	350	2.86	0.0561	121.1058	0.8	65	2000	6.4952	NA
150	350	2.86	0.0561	120.3022	1.6	65	2000	10.1333	NA
260	340	4	0.0172	21	0.75	60	1336	1.3235	NA
260	340	4	0.0172	56	0.75	60	1336	2.3416	NA
150	276	1.81	0.0146	48.6	0.96	85	1100	2.9710	NA
100	345	0.7	0.0355	52.89	0.25	100	2000	10.1449	NA
100	345	0.7	0.0355	51.004	0.5	100	2000	9.4203	NA
100	345	0.7	0.0355	47.56	0.75	100	2000	10.4638	NA
100	345	0.7	0.0355	55.924	1	100	2000	11.4783	NA
100	345	0.7	0.0355	54.94	1.25	100	2000	11.3913	NA
100	345	0.46	0.0355	50.512	1	100	2000	13.1594	NA
100	345	0.58	0.0355	47.806	1	100	2000	11.7101	NA
100	345	0.81	0.0355	45.592	1	100	2000	9.9130	NA
100	345	0.93	0.0355	49.118	1	100	2000	9.9710	NA
100	345	0.7	0.0355	30.996	1	100	2000	8.5217	NA
100	345	0.7	0.0355	34.686	1	100	2000	9.6522	NA
63.5	102	3	0.022	53	1	29	1000	2.4703	NA
127	204	3	0.0221	53	1	29	1000	1.9299	NA
63.5	102	3	0.022	50.2	2	29	1000	3.0878	NA
127	204	3	0.0221	50.2	2	29	1000	2.5475	NA
63.5	102	3	0.022	62.6	1	29	1000	2.6247	NA
127	204	3	0.0221	62.6	1	29	1000	2.3545	NA
63.5	102	1	0.022	62.6	1	29	1000	7.7196	NA
63.5	102	1.5	0.022	62.6	1	29	1000	4.9406	NA
63.5	102	1.75	0.022	62.6	1	29	1000	4.4774	NA
63.5	102	2	0.022	62.6	1	29	1000	3.8598	NA
63.5	102	2.25	0.022	62.6	1	29	1000	3.3966	NA
63.5	102	2.5	0.022	62.6	1	29	1000	3.0878	NA
63.5	102	2.75	0.022	62.6	1	29	1000	2.6247	NA
63.5	102	3	0.011	62.6	1	29	1000	1.8527	NA

Table A.1 (continued)

Beam Geometry			Longitudinal Steel	Concrete Properties	Fiber Properties			Shear Strength	Failure Mode
$b_w(mm)$	$d(mm)$	a/d	ρ	$f'_c(Mpa)$	V_f	l_f/d_f	$f_{if}(MPa)$	$v_u(MPa)$	
63.5	102	3	0.033	62.6	1	29	1000	2.6247	NA
63.5	102	3	0.033	54.1	1	57	1000	3.7054	NA
127	204	3	0.0221	22.7	1	60	1172	3.0107	NA
63.5	102	3	0.022	22.7	1	60	1172	3.0878	NA
63.5	102	3	0.011	22.7	1	60	1172	2.3159	NA
63.5	102	1.5	0.011	22.7	1	60	1172	5.5581	NA
127	204	3	0.0221	26	1	100	1172	3.0107	NA
63.5	102	3	0.022	26	1	100	1172	3.3966	NA
55	265	2	0.0431	36.49	1	100	1570	5.4889	S
55	265	3.43	0.0431	41.902	1	100	1570	3.9794	S
55	265	4.91	0.0431	36.9	1	100	1570	2.8816	S
55	265	2	0.0276	38.704	1	100	1570	4.8714	S
55	265	3.43	0.0276	33.948	1	100	1570	3.0875	S
55	265	4.91	0.0276	36.818	1	100	1570	2.8816	FS
55	265	2	0.0155	36.572	1	100	1570	4.5969	FS
150	560	1.63	0.0214	54.1	0.75	60	1200	3.2976	S
150	560	1.63	0.0214	49.9	1.5	60	1200	3.8690	S
150	560	1.63	0.0214	54.8	0.4	60	1200	2.4405	S
150	560	1.63	0.0214	56.5	0.6	60	1200	2.7738	S
150	560	1.63	0.0214	46.9	0.4	60	1200	2.9524	S
150	560	1.63	0.0214	40.8	0.6	60	1200	2.8333	S
120	167.5	1.43	0.0132	25.7	0.5	60	1100	2.9851	S
120	167.5	1.43	0.0132	25.3	1	60	1100	3.9303	FS
120	167.5	1.43	0.0132	23.9	1.5	60	1100	4.1791	FS
120	167.5	1.43	0.0132	57.8	0.5	60	1100	4.6766	FS
120	167.5	1.43	0.0132	61.5	1	60	1100	5.0746	FS
120	167.5	1.43	0.0282	70.5	0.5	60	1100	8.8557	S
120	167.5	1.43	0.0282	67.3	1	60	1100	8.4080	S
120	167.5	1.43	0.0282	67.3	1.5	60	1100	9.2537	S
120	167.5	1.43	0.02	82.4	0.5	60	1100	7.8109	S
120	167.5	1.43	0.02	81.1	1	60	1100	8.0597	FS
120	167.5	1.43	0.0282	86.1	0.5	60	1100	7.6119	S
120	167.5	1.43	0.0282	89.4	1	60	1100	8.4577	FS
200	265	3.02	0.0178	47.9	0.5	50	1100	1.7170	S
200	265	3.02	0.0178	38	0.75	50	1100	2.0000	S
200	265	3.02	0.0178	42.2	1	50	1100	2.8113	S
200	265	3.02	0.0178	45.4	0.5	50	1100	2.1887	S
200	265	3.02	0.0178	44.4	0.75	50	1100	2.7358	S
200	265	3.02	0.0178	40.3	1	50	1100	2.7736	S
200	265	3.02	0.0178	53.7	0.5	43	1100	2.0189	S
200	265	3.02	0.0178	46	0.75	43	1100	2.3208	S

Table A.1 (continued)

Beam Geometry			Longitudinal Steel	Concrete Properties	Fiber Properties			Shear Strength	Failure Mode
$b_w(mm)$	$d(mm)$	a/d	ρ	$f'_c(Mpa)$	V_f	l_f/d_f	$f_{ff}(MPa)$	$v_u(MPa)$	
200	265	3.02	0.0178	42.2	1	43	1100	2.8679	S
200	310	2.55	0.0113	39.8	0.375	80	1100	2.1452	S
200	285	2.77	0.0333	39.8	0.375	80	1100	3.8947	S
200	260	3.46	0.0355	46.4	0.25	65	1100	2.1154	S
200	260	3.46	0.0355	43.2	0.5	65	1100	2.3077	S
200	260	3.46	0.0355	47.6	0.75	65	1100	2.9808	S
200	260	1.54	0.0181	40.7	0.25	65	1100	5.4038	S
200	260	1.54	0.0181	42.4	0.75	65	1100	5.7885	S
200	262	2.48	0.0115	39.1	0.25	65	1100	1.5840	S
200	262	2.48	0.0115	38.6	0.75	65	1100	2.0802	S
200	260	2.5	0.0181	39.1	0.25	65	1100	2.0962	S
200	260	2.5	0.0181	38.6	0.75	65	1100	2.7885	S
200	260	4.04	0.0181	40.7	0.25	65	1100	1.5962	S
200	260	4.04	0.0181	42.4	0.75	65	1100	2.2692	S
200	262	2.48	0.0115	26.5	0.25	45	1100	1.9275	S
200	262	2.48	0.0115	27.2	0.75	45	1100	2.3092	S
200	260	2.5	0.0181	26.5	0.25	45	1100	1.9423	S
200	260	2.5	0.0181	27.2	0.75	45	1100	2.3269	S
200	262	2.48	0.0115	47.4	0.5	65	1100	2.5000	S
200	260	2.5	0.0181	46.8	0.5	65	1100	3.0385	S
200	262	2.48	0.0115	45.4	0.5	80	1100	2.8244	S
200	305	2.46	0.0103	34.4	0.57	80	1100	2.6885	S
200	305	2.46	0.0103	30.2	0.38	80	1100	2.6885	FS
175	210	4.5	0.0401	36.408	0.4	100	1050	2.1769	S
175	210	4.5	0.0401	38.376	0.8	100	1050	3.1293	S
175	210	4.5	0.0401	40.836	1.2	100	1050	3.1565	S
175	210	4.5	0.031	39.114	0.8	100	1050	3.2381	S
175	210	4.5	0.0401	38.54	0.8	100	1050	1.9048	S
101	127	4.8	0.0309	33.22	0.22	102	1100	2.1049	FS
101	127	4.8	0.0309	33.22	0.22	102	1100	2.1049	FS
101	127	4.8	0.0309	33.22	0.22	102	1100	2.0270	FS
101	127	4.8	0.0309	33.22	0.22	46	1100	2.1049	FS
101	127	4.8	0.0309	33.22	0.22	46	1100	2.1049	FS
101	127	4.8	0.0309	33.22	0.22	46	1100	2.0270	FS
101	127	4.8	0.0309	33.22	0.22	102	1100	2.0270	FS
101	127	4.4	0.0309	33.22	0.22	102	1100	2.4168	S
101	127	4.2	0.0309	33.22	0.22	102	1100	2.4168	S
101	127	4.2	0.0309	33.22	0.22	102	1100	2.1049	S
101	127	4.2	0.0309	33.22	0.22	102	1100	1.8711	S
101	127	4.3	0.0309	33.22	0.22	102	1100	2.2609	S
101	127	4.3	0.0309	33.22	0.22	102	1100	2.1049	S

Table A.1 (continued)

Beam Geometry			Longitudinal Steel	Concrete Properties	Fiber Properties			Shear Strength	Failure Mode
$b_w(mm)$	$d(mm)$	a/d	ρ	$f'_c(Mpa)$	V_f	l_f/d_f	$f_{ff}(MPa)$	$v_u(MPa)$	
101	127	4.2	0.0309	40.21	0.44	102	1100	2.4947	FS
101	127	4	0.0309	40.21	0.44	102	1100	2.4947	S
101	127	4	0.0309	40.21	0.44	102	1100	2.3388	S
101	127	4	0.0309	40.21	0.44	102	1100	2.4947	S
101	127	4.4	0.0309	33.22	0.22	102	1100	2.1829	S
101	127	4.4	0.0309	33.22	0.22	102	1100	2.0270	S
101	127	4	0.0309	33.22	0.22	62	1100	2.2609	S
101	127	4	0.0309	33.22	0.22	62	1100	2.3388	S
101	127	4	0.0309	33.22	0.22	62	1100	2.4947	S
101	127	4.6	0.0309	33.22	0.22	62	1100	1.9490	S
101	127	4.4	0.0309	33.22	0.22	62	1100	2.0270	S
101	127	4.4	0.0309	33.22	0.22	62	1100	1.9490	S
101	127	5	0.0309	33.22	0.22	62	1100	1.8711	S
101	127	4.8	0.0309	33.22	0.22	62	1100	1.7151	S
101	127	4	0.0309	40.21	0.44	62	1100	2.4168	S
101	127	4.2	0.0309	40.21	0.44	62	1100	2.5727	S
101	127	4.2	0.0309	40.21	0.44	62	1100	2.2609	S
101	127	4.2	0.0309	40.21	0.44	62	1100	2.4947	S
101	127	3.2	0.0309	39.72	0.88	62	1100	2.8066	S
101	127	3.4	0.0309	39.72	0.88	62	1100	2.6507	S
101	127	3.4	0.0309	39.72	0.88	62	1100	2.4947	S
101	127	3.4	0.0309	39.72	0.88	62	1100	3.1964	S
101	127	3.4	0.0309	39.72	0.88	62	1100	3.0405	S
101	127	2.8	0.0309	39.79	1.76	62	1100	4.3658	FS
101	127	1.8	0.0309	39.79	1.76	62	1100	5.9250	S
101	127	1.2	0.0309	39.79	1.76	62	1100	11.2263	S
101	127	1.2	0.0309	39.79	1.76	62	1100	10.8365	S
101	127	4.8	0.0309	33.22	0.22	62	1100	1.8711	S
101	127	4.8	0.0309	33.22	0.22	62	1100	1.7931	S
101	127	4.8	0.0309	33.22	0.22	62	1100	1.9490	S
150	259.5	2	0.0252	34.45	0.5	35	700	2.9030	S
150	259.5	2	0.0252	36.08	1	35	700	3.5453	S
150	259.5	2	0.0252	37.13	1.5	35	700	4.0077	S
150	259.5	2	0.0252	35.26	2	35	700	3.8279	S
100	127	3.6	0.0199	20.68966	1	25	4913	1.5748	S
100	127	2	0.0199	20.68966	1	100	2350	2.2835	S
100	127	2.4	0.0199	20.68966	1	100	2350	2.2835	S
100	127	2	0.0199	20.68966	1	83	2350	3.0709	S
100	127	3.6	0.0199	20.68966	1	83	2350	2.2047	S
100	127	4.8	0.0199	20.68966	1	83	2350	1.8898	S
100	127	2	0.0199	20.68966	1	63	2350	2.5197	S

Table A.1 (continued)

Beam Geometry			Longitudinal Steel	Concrete Properties	Fiber Properties			Shear Strength	Failure Mode
$b_w(mm)$	$d(mm)$	a/d	ρ	$f'_c(Mpa)$	V_f	l_f/d_f	$f_{if}(MPa)$	$v_u(MPa)$	
100	175	2	0.0359	80	0.5	100	1856	6.8000	S
100	175	2	0.0359	80	1	100	1856	7.3714	S
100	175	3	0.0359	80	0.5	100	1856	3.1429	S
100	175	3	0.0359	80	1	100	1856	4.0571	S
100	175	4.5	0.0359	80	0.5	100	1856	2.7429	S
100	175	4.5	0.0359	80	1	100	1856	3.4286	S
200	300	1.75	0.0308	109.5	0.75	75	2000	8.8333	FS
200	300	2.5	0.0308	110	0.75	75	2000	4.7667	S
200	300	3.5	0.0308	111.5	0.75	75	2000	3.5167	S
200	300	4.5	0.0308	110.8	0.75	75	2000	3.5667	S
150	255	1.96	0.0493	55.842	1	47	700	6.6144	S
152.4	282.575	2.5	0.0199	33.06897	1	100	1100	3.1581	S
152.4	282.575	2.5	0.0199	33.24138	1	100	1100	3.3670	S
152.4	282.575	2.5	0.0199	33.03448	2	100	1100	3.0884	S
152.4	282.575	2.5	0.0199	34.37931	2	100	1100	3.2045	S
50	170	2.41	0.0237	32.062	3	100	1100	3.7647	FS
50	170	2.41	0.0237	39.278	4.5	100	1100	4.1176	FS
50	170	1.62	0.0237	32.062	3	100	1100	5.8824	FS
50	170	1.62	0.0237	39.278	4.5	100	1100	6.2353	FS
50	170	0.81	0.0237	32.062	3	100	1100	9.4118	S
50	170	0.81	0.0237	39.278	4.5	100	1100	12.5882	FS
100	165.5	3.02	0.0343	39.4	0.5	60	1200	1.8127	S
100	165.5	3.02	0.0343	39.2	1	60	1200	3.0816	S
100	165.5	3.02	0.0343	40	1.5	60	1200	3.2024	S
100	165.5	3.02	0.0343	35.5	2	60	1200	2.8399	S
100	159	3.14	0.0478	58	1	60	1200	4.5912	S
100	159	3.14	0.0478	80.1	0.5	60	1200	4.5283	S
100	159	3.14	0.0478	88	1	60	1200	5.0943	S
150	219	2.8	0.0191	80.04	1	55	1100	3.4703	S
150	219	2	0.0191	80.04	1	55	1100	4.2922	S
100	275	2	0.0055	28.4	0.5	75	1100	1.5273	S
125	212	3.77	0.0152	59.4	0.5	55	1100	1.6226	S
125	212	3.77	0.0152	49.6	0.5	80	1100	1.6981	S
125	210	3.81	0.0228	49.7	0.75	55	1100	1.6762	S
125	210	3.81	0.0228	51.5	1	55	1100	2.2095	S
125	210	3.81	0.0228	54.5	1	55	1100	2.2476	S
100	140	1.07	0.0112	36.08	0.5	63	1100	5.1429	S
100	140	1.07	0.0112	36.9	0.75	63	1100	6.1429	S
100	140	2.5	0.0112	36.08	0.5	63	1100	2.8571	S
100	140	2.5	0.0112	36.9	0.75	63	1100	3.5714	FS
100	150	1	0.0105	36.08	0.5	63	1100	7.0667	FS

Table A.1 (continued)

Beam Geometry			Longitudinal Steel	Concrete Properties	Fiber Properties			Shear Strength	Failure Mode
$b_w(mm)$	$d(mm)$	a/d	ρ	$f'_c(Mpa)$	V_f	l_f/d_f	$f_{ff}(MPa)$	$v_u(MPa)$	
100	150	1	0.0105	36.9	0.75	63	1100	8.3333	FS
100	150	2.33	0.0105	36.08	0.5	63	1100	2.9333	S
100	150	2.33	0.0105	36.9	0.75	63	1100	3.0667	S
100	170	2.41	0.0092	36.08	0.5	63	1100	2.4118	S
100	170	1.29	0.0092	36.08	0.5	63	1100	1.2353	S
100	245	0.9	0.0064	36.08	0.5	63	1100	2.0408	S
100	85.25	3.52	0.0166	54.8	1	127	1100	2.2287	S
100	85.25	3.52	0.0166	50	2	127	1100	2.4633	FS
100	85.25	3.52	0.0166	49.3	1	191	1100	2.4633	S
100	85.25	3.52	0.0166	49.3	1	191	1100	2.1114	S
100	85.25	3.52	0.0166	53.7	2	191	1100	2.2287	S
100	85.25	3.52	0.0166	53.5	0.5	191	1100	2.5806	S
100	85.25	3.52	0.0166	53.5	0.5	191	1100	1.9941	S
200	273	2.75	0.0348	110.9	0.75	64	1000	3.6813	S
200	273	2.75	0.0348	109.2	0.75	67	1000	3.8462	S
80	165	2.99	0.0171	41.23	1	50	800	2.4242	S
80	165	2.99	0.0171	39.87	1.5	50	800	3.0303	S
300	420	3.21	0.0322	62.3	0.75	65	1400	3.3016	S
125	222	1.8	0.0145	30	0.5	80	1225	2.8108	S
125	222	1.8	0.0145	30	0.5	80	1225	3.0631	S
70	270	2.56	0.0332	50	0.769	58	1100	4.2857	S
110	270	2.56	0.0212	50	0.769	58	1100	3.1987	S
150	270	2.56	0.0155	50	0.769	58	1100	2.6914	S
310	258	3	0.025	23	1	55	1100	2.6382	S
310	240	3	0.0403	41	1	55	1100	3.7769	S
310	258	3	0.025	41	1	55	1100	3.4759	FS
310	240	3	0.0403	80	1	55	1100	6.1559	FS
300	531	3	0.0188	23	1	55	1100	1.5945	S
300	523	3	0.0255	23	1	55	1100	1.5551	S
300	523	3	0.0255	41	1	55	1100	2.8426	S
300	923	3	0.0144	41	1	55	1100	1.8021	S
300	920	3	0.0203	41	1	55	1100	1.8261	S
300	923	3	0.0144	80	1	55	1100	2.3546	S
300	920	3	0.0203	80	1	55	1100	2.3551	S
200	300	3.5	0.036	215	2	55	1100	6.2167	S
200	300	2	0.036	199	2	55	1100	9.7667	S
120	266	1.13	0.0126	31.9	0.2	50	834	3.9474	S
120	266	1.13	0.0126	31.9	0.4	50	834	4.1353	S
120	266	1.13	0.0126	31.9	0.6	50	834	4.5426	S
150	261	2.3	0.0087	23.9	0.5	80	1100	NA	F
150	261	2.3	0.0087	27.4	1	80	1100	NA	F

Table A.1 (continued)

Beam Geometry			Longitudinal Steel	Concrete Properties	Fiber Properties			Shear Strength	Failure Mode
$b_w(mm)$	$d(mm)$	a/d	ρ	$f'_c(Mpa)$	V_f	l_f/d_f	$f_{ff}(MPa)$	$v_u(MPa)$	
150	261	2.3	0.0087	27.2	1.5	80	1100	NA	F
150	261	2.3	0.0115	34.9	1	80	1100	NA	F
150	261	2.3	0.0115	34.1	1.5	80	1100	NA	F
300	550	3	0.0091	30	1	55	1100	NA	F
300	950	3	0.0053	31	1	55	1100	NA	F
300	950	3	0.007	31	1	55	1100	NA	F
150	200	4.5	0.0134	27.91	3	55	1100	NA	F
150	217	1.6	0.0185	45.5	1	80	1100	NA	F
150	217	1.6	0.0185	42	1.5	80	1100	NA	F
150	217	2.5	0.0185	45.5	1	80	1100	NA	F
150	217	2.5	0.0185	42	1.5	80	1100	NA	F
150	217	3	0.0185	45.5	1	80	1100	NA	F
150	217	3	0.0185	42	1.5	80	1100	NA	F
100	135	2.2	0.0116	63.1	2	65	1100	NA	F
100	135	2.2	0.0116	65	2	80	1100	NA	F
100	135	2.2	0.0116	62.2	3	65	1100	NA	F
85	130	3	0.02	49.7	1.5	100	2000	NA	F
85	130	3	0.02	53.8	2	100	2000	NA	F
85	130	3	0.02	54.2	2.5	100	2000	NA	F
85	130	3	0.02	52.0	3	100	2000	NA	F
125	212	3	0.0152	63.8	0.5	62.5	1079	NA	F
125	212	3	0.0152	68.6	0.75	62.5	1079	NA	F
125	212	4	0.0152	63.8	0.5	62.5	1079	NA	F
125	212	4	0.0152	68.6	0.75	62.5	1079	NA	F
125	212	4	0.0152	30.8	0.5	62.5	1079	NA	F
205	610	3.5	0.016	42.3	0.75	55	1100	NA	F
200	435	2.5	0.0104	24.8	0.57	50	1100	NA	F
200	435	2.5	0.0104	58.3	0.64	79	1333	NA	F
125	210	2	0.015	47.7	0.75	63	1100	NA	F
125	210	3	0.015	44.6	0.5	63	1100	NA	F
125	210	3	0.015	47.7	0.75	63	1100	NA	F
125	210	4	0.015	47.7	0.75	63	1100	NA	F
125	210	3	0.015	57.2	0.5	63	1100	NA	F
125	210	4	0.015	57.2	0.5	63	1100	NA	F
152	221	1.5	0.011	34	1	60	1130	NA	F
152	221	2.5	0.011	34	1	60	1130	NA	F
152	221	3.5	0.011	34	1	60	1130	NA	F
152	221	1.5	0.011	34	0.5	60	1130	NA	F
152	221	3.5	0.011	34	0.5	60	1130	NA	F
150	197	4.4	0.0134	29.1	0.5	60	1260	NA	F
150	197	3.6	0.0134	29.9	0.75	60	1260	NA	F

Table A.1 (continued)

Beam Geometry			Longitudinal Steel	Concrete Properties	Fiber Properties			Shear Strength	Failure Mode
$b_w(mm)$	$d(mm)$	a/d	ρ	$f'_c(Mpa)$	V_f	l_f/d_f	$f_{ff}(MPa)$	$v_u(MPa)$	
150	197	4.4	0.0134	29.9	0.75	60	1260	NA	F
150	197	2.8	0.0079	29.9	0.75	60	1260	NA	F
150	197	2	0.0134	30	1	60	1260	NA	F
150	197	2.8	0.0134	30	1	60	1260	NA	F
150	197	3.6	0.0134	30	1	60	1260	NA	F
150	197	4.4	0.0134	30	1	60	1260	NA	F
150	197	2.8	0.0079	20.6	0.75	60	1260	NA	F
150	197	2.8	0.0079	33.4	0.75	60	1260	NA	F
150	197	2.8	0.0134	33.4	0.75	60	1260	NA	F
55	265	3.43	0.0155	35.342	1	100	1570	NA	F
55	265	4.91	0.0155	33.046	1	100	1570	NA	F
120	167.5	1.43	0.0132	28.8	2	60	1100	NA	F
120	167.5	1.43	0.0132	60.6	1.5	60	1100	NA	F
120	167.5	1.43	0.0132	62.3	2	60	1100	NA	F
120	167.5	1.43	0.0282	69.6	2	60	1100	NA	F
120	167.5	1.43	0.02	83	1.5	60	1100	NA	F
120	167.5	1.43	0.02	82.2	2	60	1100	NA	F
120	167.5	1.43	0.0282	82.7	1.5	60	1100	NA	F
120	167.5	1.43	0.0282	89.9	2	60	1100	NA	F
101	127	4.8	0.0309	33.22	0.22	102	1100	NA	F
101	127	4.8	0.0309	33.22	0.22	102	1100	NA	F
101	127	4.8	0.0309	33.22	0.22	102	1100	NA	F
101	127	4.8	0.0309	33.22	0.22	102	1100	NA	F
101	127	4.8	0.0309	33.22	0.22	102	1100	NA	F
101	127	4.8	0.0309	33.22	0.22	102	1100	NA	F
101	127	4.8	0.0309	33.22	0.22	102	1100	NA	F
101	127	4.8	0.0309	33.22	0.22	102	1100	NA	F
101	127	4.8	0.0309	33.22	0.22	102	1100	NA	F
101	127	4.8	0.0309	33.22	0.22	102	1100	NA	F
101	127	4.4	0.0309	33.22	0.22	102	1100	NA	F
101	127	4.4	0.0309	33.22	0.22	102	1100	NA	F
101	127	4.3	0.0309	33.22	0.22	102	1100	NA	F
101	127	4.2	0.0309	40.21	0.44	102	1100	NA	F
101	127	4.2	0.0309	40.21	0.44	102	1100	NA	F
101	127	2.2	0.0309	39.79	1.76	62	1100	NA	F
101	127	2.4	0.0309	39.79	1.76	62	1100	NA	F
101	127	2.6	0.0309	39.79	1.76	62	1100	NA	F
101	127	5	0.0309	33.22	0.22	62	1100	NA	F
101	127	4.4	0.0309	40.21	0.44	62	1100	NA	F
101	127	4.8	0.0309	40.21	0.44	62	1100	NA	F
101	127	4.4	0.0309	40.21	0.44	62	1100	NA	F
101	127	4.4	0.0309	40.21	0.44	62	1100	NA	F
101	127	4.4	0.0309	40.21	0.44	62	1100	NA	F
101	127	4.4	0.0309	40.21	0.44	62	1100	NA	F

Table A.1 (continued)

Beam Geometry			Longitudinal Steel	Concrete Properties	Fiber Properties			Shear Strength	Failure Mode
$b_w(mm)$	$d(mm)$	a/d	ρ	$f'_c (Mpa)$	V_f	l_f/d_f	$f_{if}(MPa)$	$v_u (MPa)$	
101	127	3.6	0.0309	39.72	0.88	62	1100	NA	F
100	85.25	3.52	0.017	54.8	1	127	1100	NA	F
100	85.25	3.52	0.017	50	2	127	1100	NA	F
100	85.25	3.52	0.017	53.7	2	161	1100	NA	F
205	610	3.5	1.6	42.3	0.75	55	1100	NA	F

Table 5.2: Database used to develop the GP-SR model

Beam Geometry		Longitudinal Steel		Concrete Properties	Fiber Properties			Shear Strength
$b_w(mm)$	$d(mm)$	a/d	$\rho(\%)$	$f'_c(Mpa)$	V_f	l_f/d_f	F	$v_u(MPa)$
150	251	3.49	2.67	28.1	0.75	65	0.488	3.001
150	251	3.49	2.67	25.3	0.75	65	0.488	2.098
150	251	3.49	2.67	27.9	1	65	0.650	2.895
150	251	3.49	2.67	26.2	1	65	0.650	3.267
150	251	3.49	2.67	28.1	1.5	65	0.975	2.948
150	251	3.49	2.67	27.3	1.5	65	0.975	3.479
150	251	3.49	2.67	27.5	0.5	80	0.400	1.726
150	251	3.49	2.67	24.9	0.5	80	0.400	2.045
150	251	3.49	2.67	27.8	0.75	80	0.600	2.417
150	251	3.49	2.67	27.3	0.75	80	0.600	2.683
150	251	3.49	2.67	26.3	1	80	0.800	3.081
150	251	3.49	2.67	27.1	1	80	0.800	2.762
150	251	3.49	2.67	53.4	0.75	65	0.488	3.001
150	251	3.49	2.67	54.1	0.75	65	0.488	3.347
150	251	3.49	2.67	53.2	1	65	0.650	3.825
150	251	3.49	2.67	55.3	1	65	0.650	4.383
150	251	3.49	2.67	64.6	1.5	65	0.975	5.179
150	251	3.49	2.67	59.9	1.5	65	0.975	4.250
150	251	3.49	2.67	47.8	0.5	80	0.400	3.373
150	251	3.49	2.67	49.5	0.5	80	0.400	4.037
150	251	3.49	2.67	55.3	0.75	80	0.600	3.878
150	251	3.49	2.67	56.4	0.75	80	0.600	4.728
150	251	3.49	2.67	53.4	1	80	0.800	3.400
150	251	3.49	2.67	51	1	80	0.800	4.170
150	251	3.49	2.67	27.8	1	50	0.375	2.098
150	251	3.49	2.67	27.2	1	50	0.375	2.072
150	251	3.49	2.67	27.6	1	85	0.638	2.603
150	251	3.49	2.67	27.9	1	85	0.638	2.151
150	251	3.49	2.67	34.7	1	50	0.375	2.630
150	251	3.49	2.67	36.2	1	50	0.375	2.656
150	251	3.49	2.67	37	1	85	0.638	2.922
150	251	3.49	2.67	38.3	1	85	0.638	2.762
150	261	3.45	1.95	32.9	0.75	80	0.600	2.759
150	261	3.45	1.95	23.8	1	80	0.800	2.376
150	261	3.45	1.95	24.1	1.25	80	1.000	2.912
140	175	1.5	1.28	82	0.5	80	0.400	4.816
140	175	1.5	1.28	83.2	1	80	0.800	6.327
140	175	1.5	1.28	83.8	1.5	80	1.200	7.592
140	175	2.5	1.28	82	0.5	80	0.400	2.531

Table A.2 (continued)

Beam Geometry			Longitudinal Steel	Concrete Properties	Fiber Properties			Shear Strength
$b_w(mm)$	$d(mm)$	a/d	ρ (%)	f'_c (Mpa)	V_f	l_f/d_f	F	v_u (MPa)
140	175	2.5	1.28	83.2	1	80	0.800	3.225
140	175	2.5	1.28	83.8	1.5	80	1.200	5.510
150	200	2.5	1.34	33.68	1	55	0.550	2.133
150	200	2.5	1.34	24.53	1	55	0.550	1.433
150	200	2.5	1.34	21.43	2	55	1.100	1.633
150	200	2.5	1.34	9.77	3	55	1.650	1.267
150	200	3.5	1.34	20.21	1	55	0.550	1.067
150	200	3.5	1.34	21.43	2	55	1.100	1.400
150	200	3.5	1.34	27.91	3	55	1.650	1.933
150	200	4.5	1.34	24.53	1	55	0.550	1.400
150	217	1.59	1.85	35	0.75	80	0.600	4.547
150	217	2.47	1.85	35	0.75	80	0.600	3.011
150	217	2.95	1.85	35	0.75	80	0.600	2.581
300	622	2.81	1.98	34	0.321	65	0.209	1.527
300	622	2.81	1.98	36	0.687	65	0.447	1.903
100	135	2.22	1.16	64.2	0.5	65	0.325	3.037
100	135	2.22	1.16	64.2	0.5	65	0.325	3.185
100	135	2.22	1.16	64.2	0.5	65	0.325	3.111
85	130	2.02	2.05	51.85	0.25	100	0.188	2.896
85	130	2.52	2.05	51.85	0.25	100	0.188	2.624
85	130	3.02	2.05	51.85	0.25	100	0.188	2.715
85	130	2.02	2.05	33.32	0.25	100	0.188	2.624
85	130	2.52	2.05	33.32	0.25	100	0.188	1.991
85	130	3.02	2.05	33.32	0.25	100	0.188	1.901
85	130	3.02	2.05	51.68	0.5	133	0.499	3.167
85	130	3.02	2.05	30.6	0.5	133	0.499	1.901
85	130	3.02	2.05	31.025	1	100	0.750	2.896
85	130	2.02	2.05	51.68	0.5	133	0.499	4.525
85	130	2.52	2.05	51.68	0.5	133	0.499	3.620
85	130	3.52	2.05	41.65	0.5	133	0.499	2.534
85	130	2.02	2.05	48.705	1	133	0.998	5.520
85	130	2.52	2.05	48.705	1	133	0.998	4.344
85	130	3.52	2.05	48.79	1	133	0.998	2.896
85	128	3.06	3.7	41.65	0.5	133	0.499	2.849
85	126	3.11	5.72	41.65	0.5	133	0.499	3.455
85	128	3.06	3.7	30.6	0.5	133	0.499	2.206
85	126	3.11	5.72	30.6	0.5	133	0.499	2.241
85	128	3.06	3.7	48.79	1	133	0.998	4.320
85	126	3.11	5.72	48.79	1	133	0.998	4.949
85	126	3.11	5.72	53.55	1.5	100	1.125	4.762

Table A.2 (continued)

Beam Geometry			Longitudinal Steel	Concrete Properties	Fiber Properties			Shear Strength
$b_w(mm)$	$d(mm)$	a/d	ρ (%)	f'_c (Mpa)	V_f	l_f/d_f	F	v_u (MPa)
85	126	3.11	5.72	43.18	2	100	1.500	4.855
85	128	3.06	3.7	53.55	1.5	100	1.125	4.412
85	126	2.08	5.72	50.15	0.5	100	0.375	5.416
85	126	2.08	5.72	45.9	1	100	0.750	6.723
85	126	2.08	5.72	53.55	1.5	100	1.125	7.096
85	126	2.08	5.72	43.18	2	100	1.500	6.256
150	219	2.8	1.91	40.85	1	60	0.600	2.922
150	219	2.8	1.91	40.85	2	60	1.200	3.136
150	219	2	1.91	43.23	1	60	0.600	3.501
150	219	2	1.91	43.23	2	60	1.200	3.531
125	212	2	1.52	30.8	0.5	63	0.315	4.038
125	212	3	1.52	30.8	0.5	63	0.315	2.528
100	130	3.08	3.09	38.69	1	60	0.300	4.462
100	130	3.08	3.09	42.4	2	60	0.600	5.692
152	381	3.44	1.96	44.8	0.75	55	0.413	2.953
152	381	3.44	1.96	44.8	0.75	55	0.413	2.780
152	381	3.44	1.96	38.1	1	55	0.550	2.936
152	381	3.44	1.96	38.1	1	55	0.550	2.987
152	381	3.44	2.63	31	1.5	55	0.825	2.573
152	381	3.44	2.63	31	1.5	55	0.825	3.402
152	381	3.44	2.63	44.9	1.5	55	0.825	3.315
152	381	3.44	2.63	44.9	1.5	55	0.825	3.281
152	381	3.44	2.63	49.2	1	80	0.800	2.987
152	381	3.44	2.63	49.2	1	80	0.800	3.782
152	381	3.44	1.96	43.3	0.75	80	0.600	3.333
152	381	3.44	1.96	43.3	0.75	80	0.600	3.281
205	610	3.5	1.96	50.8	0.75	55	0.413	2.943
205	610	3.5	1.96	50.8	0.75	55	0.413	2.719
205	610	3.5	1.96	28.7	0.75	80	0.600	2.831
205	610	3.5	1.96	28.7	0.75	80	0.600	2.775
205	610	3.5	1.52	42.3	0.75	55	0.413	2.799
205	610	3.5	1.52	29.6	0.75	80	0.600	2.159
205	610	3.5	1.52	29.6	0.75	80	0.600	1.815
205	610	3.5	1.96	44.4	1.5	55	0.825	3.495
205	610	3.5	1.96	42.8	1.5	80	1.200	3.383
125	225	2.89	3.49	90	1.25	60	0.750	5.582
150	202	2.97	1.17	21.3	0.5	55	0.275	1.551
150	202	2.97	1.17	19.6	1	55	0.550	1.848
300	437	3.09	1.5	21.3	0.5	55	0.275	1.220
300	437	3.09	1.5	19.6	1	55	0.550	1.556

Table A.2 (continued)

Beam Geometry			Longitudinal Steel	Concrete Properties	Fiber Properties			Shear Strength
$b_w(mm)$	$d(mm)$	a/d	ρ (%)	f'_c (Mpa)	V_f	l_f/d_f	F	v_u (MPa)
200	435	2.51	1.04	24.8	0.38	50	0.190	1.529
200	435	2.51	1.04	33.5	0.38	50	0.190	1.368
200	435	2.51	1.04	38.6	0.38	50	0.190	1.609
200	455	2.51	0.99	24.4	0.25	50	0.125	1.714
200	910	2.5	1.04	24.4	0.25	50	0.125	1.412
200	910	2.5	1.04	55	0.25	50	0.125	1.857
125	210	4	1.53	44.6	0.5	63	0.315	1.333
125	225	2.89	3.49	90	1.25	60	0.750	4.907
152	221	2.5	1.2	34	0.5	60	0.300	1.727
152	221	1.5	2.39	34	1	60	0.600	4.376
152	221	2.5	2.39	34	1	60	0.600	2.471
152	221	1.5	2.39	34	0.5	60	0.300	4.019
152	221	2.5	2.39	34	0.5	60	0.300	1.905
152	221	3.5	2.39	34	0.5	60	0.300	1.459
150	197	2	1.36	29.1	0.5	60	0.300	2.538
150	197	2.8	1.36	29.1	0.5	60	0.300	1.760
150	197	3.6	1.36	29.1	0.5	60	0.300	1.523
150	197	2	1.36	29.9	0.75	60	0.450	2.877
150	197	2.8	1.36	29.9	0.75	60	0.450	2.031
150	197	2.8	2.04	29.9	0.75	60	0.450	2.200
150	197	2.8	1.36	20.6	0.75	60	0.450	1.523
150	197	2.8	2.04	20.6	0.75	60	0.450	2.031
150	197	2.8	2.04	33.4	0.75	60	0.450	2.910
152	254	3.5	2.48	29	0.75	67	0.503	3.108
610	254	3.5	2.47	29	0.75	67	0.503	3.104
152	394	3.61	2.86	39	0.75	67	0.503	2.705
152	394	3.61	2.86	39	0.75	67	0.503	3.256
203	541	3.45	2.54	50	0.75	67	0.503	2.477
203	541	3.45	2.54	50	0.75	67	0.503	3.506
254	813	3.5	2.7	50	0.75	67	0.503	3.385
254	813	3.5	2.7	50	0.75	67	0.503	3.487
200	180	3.33	4.47	90.6	1	40	0.200	8.306
200	180	3.33	4.47	80.5	0.5	86	0.430	7.000
200	180	3.33	4.47	80.5	0.75	86	0.645	7.278
200	235	2.77	4.28	91.4	1	50	0.500	6.596
200	235	2.77	4.28	93.3	1	40	0.200	7.723
200	410	2.93	3.06	76.8	1	40	0.200	3.561
200	410	2.93	3.06	76.8	1	40	0.200	4.134
200	410	2.93	3.06	69.3	0.5	86	0.430	3.256
200	410	2.93	3.06	69.3	0.5	86	0.430	3.842

Table A.2 (continued)

Beam Geometry			Longitudinal Steel	Concrete Properties	Fiber Properties			Shear Strength
$b_w(mm)$	$d(mm)$	a/d	ρ (%)	f'_c (Mpa)	V_f	l_f/d_f	F	v_u (MPa)
200	410	2.93	3.06	60.2	0.75	86	0.645	4.171
200	410	2.93	3.06	75.7	0.75	86	0.645	3.598
300	570	2.98	2.87	76.8	1	40	0.200	2.673
300	570	2.98	2.87	60.2	0.75	86	0.645	3.047
200	314	3.5	3.5	132	2	75	0.750	4.029
200	314	3.5	3.5	154	2	75	0.750	5.096
200	314	3.5	3.5	146	2	75	0.750	5.717
200	314	3.5	3.5	133	1	75	0.375	4.268
200	314	3.5	3.5	143	1	75	0.375	3.201
200	314	3.5	3.5	153	1	75	0.375	4.936
55	265	2	4.31	36.49	1	100	0.750	5.489
55	265	3.43	4.31	41.902	1	100	0.750	3.979
55	265	4.91	4.31	36.9	1	100	0.750	2.882
55	265	2	2.76	38.704	1	100	0.750	4.871
55	265	3.43	2.76	33.948	1	100	0.750	3.088
150	560	1.63	2.14	54.1	0.75	60	0.450	3.298
150	560	1.63	2.14	49.9	1.5	60	0.900	3.869
150	560	1.63	2.14	54.8	0.4	60	0.240	2.441
150	560	1.63	2.14	56.5	0.6	60	0.360	2.774
150	560	1.63	2.14	46.9	0.4	60	0.240	2.952
150	560	1.63	2.14	40.8	0.6	60	0.360	2.833
120	167.5	1.43	1.32	25.7	0.5	60	0.300	2.985
120	167.5	1.43	2.82	70.5	0.5	60	0.300	8.856
120	167.5	1.43	2.82	67.3	1	60	0.600	8.408
120	167.5	1.43	2.82	67.3	1.5	60	0.900	9.254
120	167.5	1.43	2	82.4	0.5	60	0.300	7.811
120	167.5	1.43	2.82	86.1	0.5	60	0.300	7.612
200	265	3.02	1.78	47.9	0.5	50	0.250	1.717
200	265	3.02	1.78	38	0.75	50	0.375	2.000
200	265	3.02	1.78	42.2	1	50	0.500	2.811
200	310	2.55	1.13	39.8	0.375	80	0.300	2.145
200	285	2.77	3.33	39.8	0.375	80	0.300	3.895
200	260	3.46	3.55	46.4	0.25	65	0.163	2.115
200	260	3.46	3.55	43.2	0.5	65	0.325	2.308
200	260	3.46	3.55	47.6	0.75	65	0.488	2.981
200	260	1.54	1.81	40.7	0.25	65	0.163	5.404
200	260	1.54	1.81	42.4	0.75	65	0.488	5.789
200	262	2.48	1.15	39.1	0.25	65	0.163	1.584
200	262	2.48	1.15	38.6	0.75	65	0.488	2.080
200	260	2.5	1.81	39.1	0.25	65	0.163	2.096

Table A.2 (continued)

Beam Geometry			Longitudinal Steel	Concrete Properties	Fiber Properties			Shear Strength
$b_w(mm)$	$d(mm)$	a/d	ρ (%)	f'_c (Mpa)	V_f	l_f/d_f	F	v_u (MPa)
200	260	2.5	1.81	38.6	0.75	65	0.488	2.789
200	260	4.04	1.81	40.7	0.25	65	0.163	1.596
200	260	4.04	1.81	42.4	0.75	65	0.488	2.269
200	262	2.48	1.15	26.5	0.25	45	0.113	1.928
200	262	2.48	1.15	27.2	0.75	45	0.338	2.309
200	260	2.5	1.81	26.5	0.25	45	0.113	1.942
200	260	2.5	1.81	27.2	0.75	45	0.338	2.327
200	262	2.48	1.15	47.4	0.5	65	0.325	2.500
200	260	2.5	1.81	46.8	0.5	65	0.325	3.039
200	262	2.48	1.15	45.4	0.5	80	0.400	2.824
200	305	2.46	1.03	34.4	0.57	80	0.456	2.689
175	210	4.5	4.01	36.408	0.4	100	0.300	2.177
175	210	4.5	4.01	38.376	0.8	100	0.600	3.129
175	210	4.5	4.01	40.836	1.2	100	0.900	3.157
175	210	4.5	3.1	39.114	0.8	100	0.600	3.238
175	210	4.5	4.01	38.54	0.8	100	0.600	1.905
101	127	4.4	3.09	33.22	0.22	102	0.112	2.417
101	127	4.2	3.09	33.22	0.22	102	0.112	2.417
101	127	4.2	3.09	33.22	0.22	102	0.112	2.105
101	127	4.2	3.09	33.22	0.22	102	0.112	1.871
101	127	4.3	3.09	33.22	0.22	102	0.112	2.261
101	127	4.3	3.09	33.22	0.22	102	0.112	2.105
101	127	4	3.09	40.21	0.44	102	0.224	2.495
101	127	4	3.09	40.21	0.44	102	0.224	2.339
101	127	4	3.09	40.21	0.44	102	0.224	2.495
101	127	4.4	3.09	33.22	0.22	102	0.112	2.183
101	127	4.4	3.09	33.22	0.22	102	0.112	2.027
101	127	4	3.09	33.22	0.22	62	0.102	2.261
101	127	4	3.09	33.22	0.22	62	0.102	2.339
101	127	4	3.09	33.22	0.22	62	0.102	2.495
101	127	4.6	3.09	33.22	0.22	62	0.102	1.949
101	127	4.4	3.09	33.22	0.22	62	0.102	2.027
101	127	4.4	3.09	33.22	0.22	62	0.102	1.949
101	127	5	3.09	33.22	0.22	62	0.102	1.871
101	127	4.8	3.09	33.22	0.22	62	0.102	1.715
101	127	4	3.09	40.21	0.44	62	0.205	2.417
101	127	4.2	3.09	40.21	0.44	62	0.205	2.573
101	127	4.2	3.09	40.21	0.44	62	0.205	2.261
101	127	4.2	3.09	40.21	0.44	62	0.205	2.495
101	127	3.2	3.09	39.72	0.88	62	0.409	2.807

Table A.2 (continued)

Beam Geometry			Longitudinal Steel	Concrete Properties	Fiber Properties			Shear Strength
$b_w(mm)$	$d(mm)$	a/d	ρ (%)	f'_c (Mpa)	V_f	l_f/d_f	F	v_u (MPa)
101	127	3.4	3.09	39.72	0.88	62	0.409	2.651
101	127	3.4	3.09	39.72	0.88	62	0.409	2.495
101	127	3.4	3.09	39.72	0.88	62	0.409	3.196
101	127	3.4	3.09	39.72	0.88	62	0.409	3.041
101	127	1.8	3.09	39.79	1.76	62	0.818	5.925
101	127	1.2	3.09	39.79	1.76	62	0.818	11.226
101	127	1.2	3.09	39.79	1.76	62	0.818	10.837
101	127	4.8	3.09	33.22	0.22	62	0.102	1.871
101	127	4.8	3.09	33.22	0.22	62	0.102	1.793
101	127	4.8	3.09	33.22	0.22	62	0.102	1.949
100	175	2	3.59	80	0.5	100	0.250	6.800
100	175	2	3.59	80	1	100	0.500	7.371
100	175	3	3.59	80	0.5	100	0.250	3.143
100	175	3	3.59	80	1	100	0.500	4.057
100	175	4.5	3.59	80	0.5	100	0.250	2.743
100	175	4.5	3.59	80	1	100	0.500	3.429
200	300	2.5	3.08	110	0.75	75	0.563	4.767
200	300	3.5	3.08	111.5	0.75	75	0.563	3.517
200	300	4.5	3.08	110.8	0.75	75	0.563	3.567
152.4	282.575	2.5	1.99	33.06897	1	100	1.000	3.158
152.4	282.575	2.5	1.99	33.24138	1	100	1.000	3.367
152.4	282.575	2.5	1.99	33.03448	2	100	2.000	3.088
152.4	282.575	2.5	1.99	34.37931	2	100	2.000	3.205
100	165.5	3.02	3.43	39.4	0.5	60	0.300	1.813
100	165.5	3.02	3.43	39.2	1	60	0.600	3.082
100	165.5	3.02	3.43	40	1.5	60	0.900	3.202
100	165.5	3.02	3.43	35.5	2	60	1.200	2.840
100	159	3.14	4.78	58	1	60	0.600	4.591
100	159	3.14	4.78	80.1	0.5	60	0.300	4.528
100	159	3.14	4.78	88	1	60	0.600	5.094
150	219	2.8	1.91	80.04	1	55	0.550	3.470
150	219	2	1.91	80.04	1	55	0.550	4.292
100	275	2	0.55	28.4	0.5	75	0.375	1.527
125	212	3.77	1.52	59.4	0.5	55	0.275	1.623
125	212	3.77	1.52	49.6	0.5	80	0.400	1.698
125	210	3.81	2.28	49.7	0.75	55	0.413	1.676
125	210	3.81	2.28	51.5	1	55	0.550	2.210
125	210	3.81	2.28	54.5	1	55	0.550	2.248
100	140	1.07	1.12	36.08	0.5	63	0.315	5.143
100	140	1.07	1.12	36.9	0.75	63	0.473	6.143

Table A.2 (continued)

Beam Geometry			Longitudinal Steel	Concrete Properties	Fiber Properties			Shear Strength
b_w (mm)	d (mm)	a/d	ρ (%)	f'_c (Mpa)	V_f	l_f/d_f	F	v_u (MPa)
100	140	2.5	1.12	36.08	0.5	63	0.315	2.857
100	150	2.33	1.05	36.08	0.5	63	0.315	2.933
100	150	2.33	1.05	36.9	0.75	63	0.473	3.067
100	170	2.41	0.92	36.08	0.5	63	0.315	2.412
100	170	1.29	0.92	36.08	0.5	63	0.315	1.235
100	245	0.9	0.64	36.08	0.5	63	0.315	2.041
100	85.25	3.52	1.66	54.8	1	127	0.953	2.229
100	85.25	3.52	1.66	49.3	1	191	1.433	2.463
100	85.25	3.52	1.66	49.3	1	191	1.433	2.111
100	85.25	3.52	1.66	53.7	2	191	2.865	2.229
100	85.25	3.52	1.66	53.5	0.5	191	0.716	2.581
100	85.25	3.52	1.66	53.5	0.5	191	0.716	1.994
200	273	2.75	3.48	110.9	0.75	64	0.480	3.681
200	273	2.75	3.48	109.2	0.75	67	0.503	3.846
80	165	2.99	1.71	41.23	1	50	0.500	2.424
80	165	2.99	1.71	39.87	1.5	50	0.750	3.030
300	420	3.21	3.22	62.3	0.75	65	0.488	3.302
125	222	1.8	1.45	30	0.5	80	0.400	2.811
125	222	1.8	1.45	30	0.5	80	0.400	3.063
310	258	3	2.5	23	1	55	0.550	2.638
310	240	3	4.03	41	1	55	0.550	3.777
300	531	3	1.88	23	1	55	0.550	1.595
300	523	3	2.55	23	1	55	0.550	1.555
300	523	3	2.55	41	1	55	0.550	2.843
300	923	3	1.44	41	1	55	0.550	1.802
300	920	3	2.03	41	1	55	0.550	1.826
300	923	3	1.44	80	1	55	0.550	2.355
300	920	3	2.03	80	1	55	0.550	2.355
200	300	3.5	3.6	215	2	55	1.100	6.217
200	300	2	3.6	199	2	55	1.100	9.767

Curriculum Vitae

- Name:** Wassim Ben Chaabene
- Post-Secondary Education and Degrees:** National Engineering School of Tunis
Tunis, Tunisia
2015-2018 BSc (Civil Engineering)
- Western University
London, Ontario, Canada
2019-2020 MEng (Civil Engineering)
- Honors and Awards:** Dean's Honor List for outstanding undergraduate academic performance, National Engineering School of Tunis (2017)
Mitacs Globalink Scholarship (2018)
Mitacs Graduate Fellowship (2019)
- Related Work Experience:** Research and Teaching Assistant
Western University
2019-2020
- Publications**
1. **Ben Chaabene, W.**, Flah, M., and Nehdi, M. L. (2020). Machine Learning Prediction of Mechanical Properties of Concrete: Critical review. *Construction and Building Materials*, 260, 119889.
 2. **Ben Chaabene, W.**, and Nehdi, M. L. Novel Soft Computing Hybrid Model for Predicting Shear Strength and Failure Mode of SFRC Beams with Superior Accuracy. *Composites Part C*, 3, 100070.
 3. **Ben Chaabene, W.**, and Nehdi, M. L. Genetic Programming Based Symbolic Regression for Shear Capacity Prediction of SFRC Beams. *Construction and Building Materials*. Under Review.
 4. Flah, M., Nunez, I., **Ben Chaabene, W.**, and Nehdi, M. L. (2020). Machine Learning Algorithms in Civil Structural Health Monitoring: A Systematic Review. *Archives of Computational Methods in Engineering*, <https://doi.org/10.1007/s11831-020-09471-9>